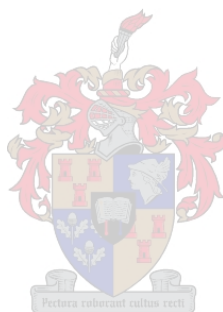


**Poly(*N*-vinylpyrrolidone) -  
Poly( $\gamma$ -benzyl-L-glutamate)  
Conjugates**

**by**

**Jaco Jacobs**

*Thesis presented in partial fulfilment of the requirements for the  
degree of Master of Science (Polymer Science)*



**Supervisor:** Prof Bert Klumperman

**Co-supervisor:** Dr Gwenaelle Pound-Lana

University of Stellenbosch

Faculty of Science

Department of Chemistry and Polymer Science

March 2012

## **DECLARATION**

By submitting this thesis/dissertation electronically, I declare that the entirety of the work contained therein is my own, original work, that I am the sole author thereof (save to the extent explicitly otherwise stated), that reproduction and publication thereof by Stellenbosch University will not infringe any third party rights and that I have not previously in its entirety or in part submitted it for obtaining any qualification.

Jaco Jacobs

March 2012

## Summary

The combination of natural and synthetic polymers allow for the synthesis of advanced hybrid copolymers. These hybrid copolymers have applications in biomedical areas, one such area being in drug delivery systems (DDS). In this study, a modular approach was used to prepare amphiphilic block copolymers with the ability to self-assemble into three dimensional structures.

Reversible addition-fragmentation chain transfer (RAFT) was the synthetic tool used to mediate the polymerization of *N*-vinylpyrrolidone. RAFT is a versatile method to prepare polymers with control over molecular weight and dispersity. A xanthate chain transfer agent (CTA) was used to obtain the hydrophilic poly(*N*-vinylpyrrolidone) (PVP) block. An aldehyde functionality could be introduced due to the lability of the xanthate moiety, the procedure of which was effectively optimized to produce quantitative conversion. A di-xanthate CTA was synthesized to produce a PVP chain which after the modification reaction, resulted in a  $\alpha,\omega$ -telechelic polymer.

A polypeptide was synthesized *via* the ring-opening polymerization of *N*-carboxyanhydrides (ROP NCA). The living and controllable ROP of NCAs is a method which results in polypeptides, but without a well-defined amino acid order. Poly( $\gamma$ -benzyl-L-glutamate) (PBLG) was synthesized with a narrow dispersity ( $\mathcal{D} = 1.10 - 1.15$ ) using conditions that promote the retention of a terminal primary amine. A protected cysteine functionality was introduced *via* the terminal amine PBLG chain-end, using peptide synthesis techniques. This resulted in the conjugation of the aldehyde functional PVP and the cysteine terminal PBLG using a covalent, non-reducible thiazolidine linkage.

The deprotection of the cysteine, more specifically the deprotection of the thiol was a non-trivial procedure. The thiol protecting acetamidomethyl (Acm) group could not be cleaved using traditional methods, but instead a modified procedure was developed to effectively remove the Acm group while inhibiting hydrolysis of the benzyl esters.

It was determined that the conjugation reaction could effectively proceed in *N,N*-dimethylformamide (DMF) at a slightly elevated temperature and so continued to prepare the amphiphilic hybrid block copolymers, PVP-*b*-PBLG. A structurally different PBLG chain, namely PBLG-*b*-Cys was conjugated to the  $\omega$ -aldehyde PVP and the conjugation efficiency was compared to our PBLG-Cys block. In the case of PBLG-*b*-Cys the *in situ* deprotection and conjugation as well as a two-step deprotection and conjugation reaction with PVP resulted in very low conjugation efficiency. The cysteine end-functional PBLG resulted in near quantitative conjugation with PVP.

The critical micelle concentration (CMC) for PVP<sub>90</sub>-*b*-PBLG<sub>54</sub> was determined to be 6  $\mu$ g/mL, using fluorescence spectroscopy. Particle sizes were determined with TEM and DLS and found to range from 25 nm to 120 nm depending on the polymer block lengths as well as hydrophobic/hydrophilic block length ratios. Furthermore, when the micelles were subjected to an increased acidic environment, the labile benzyl ester bonds were hydrolyzed. This was observed with TEM where the particle sizes increased 10-fold to form vesicular structures. Hydrolysis was further confirmed with ATR-FTIR and <sup>1</sup>H-NMR spectroscopy.

Cytotoxicity tests confirmed that the copolymer micelles had good cell compatibility at high concentrations such as 0.9 mg/mL. Investigation into drug loading using a pyrene probe confirmed the viability of using PVP-*b*-PBLG as a responsive DDS.

## OPSOMMING

Die kombinasie van natuurlike en sintetiese polimere maak dit moontlik vir die sintese van gevorderde hibried kopolimere. Hierdie kopolimere het toepassing in biomediese gebiede, een so 'n gebied is in medisinale vervoer sisteme (MVS). 'n Modulêre benadering is in hierdie studie gebruik om amfifiliese blok kopolimere te berei.

Omkeerbare addisie-fragmentasie kettingoordrag (OAF) is gebruik as die sintetiese tegniek vir die polimerisasie van *N*-vinielpirolidoon (NVP). OAF is 'n veelsydige metode om polimere te berei met beheer oor molekulêre gewig en dispersiteit ( $\bar{M}_w$ ). 'n Xantaat kettingoordrag agent (KOA) is gebruik om die hidrofiliese poli(*N*-vinielpirolidoon) (PVP) blok te sintetiseer. 'n Aldehyd endgroep was deur die terminale xantaat funksionaliteit berei, 'n proses wat geoptimeer is tot kwantitatiewe omsetting. 'n Di-xantaat KOA is gesintetiseer om, na modifikasie, 'n  $\alpha$ ,  $\omega$ -telecheliese polimeer te produseer.

Die polipeptied was gesintetiseer deur middel van 'n ringopening polimerisasie van *N*-karboksianhidriede (ROP NKA). Die lewende en beheerbare ROP van NKA is 'n metode wat lei tot polipeptiede sonder 'n gedefinieerde aminosuur volgorde. Poli( $\gamma$ -benzyl-L-glutamaat) met 'n lae dispersiteit ( $\bar{M}_w = 1.10 - 1.15$ ), is gesintetiseer deur gebruik te maak van kondisies wat die behoud van 'n terminale primêre amien bevorder. 'n Beskermdesistien-funksionaliteit is ingebou *via* die terminale amien met behulp van peptidsintese tegnieke.

Die tiol beskerming van die asetamidometiel (Asm) groep kon nie gekleef word deur gebruik te maak van tradisionele metodes nie, maar 'n nuwe proses is ontwikkel om die Asm groep te kleef sowel as om die hidrolise van die bensiel esters te inhibeer.

Die koppelings reaksie het effektief verloop in DMF by 'n effens verhoogde temperatuur en sodoende is die amfifiliese hibried blok-kopolimere, PVP-*b*-PBLG berei. Twee verskillende PBLG kettings is gekoppel aan die  $\omega$ -aldehyd PVP en die koppeling doeltreffendheid is vergelyk. Daar is bevind dat net die sistien end-funksionele PBLG tot kwantitatiewe konjugasie kon lei.

Die kritiese misel konsentrasie is bepaal vir PVP<sub>90</sub>-*b*-PBLG<sub>54</sub> as 6 µg/mL met behulp van fluoressensie spektroskopie. Die deeltjie-groottes is bepaal met TEM en DLS en wissel van 25 nm tot 120 nm, afhangende van die polimeer bloklengtes sowel as hidrofobiese / hidrofiliese blok lengte verhoudings. Die miselle is blootgestel aan 'n verhoogde suur omgewing, wat tot die hidrolise van die bensiel ester groepe gelei het. TEM het getoon dat die deeltjie-groottes met 10-voud vergroot het tot vesikulêre strukture. Hidrolise is verder bevestig met ATR-FTIR en <sup>1</sup>H-KMR spektroskopie.

Sitotoksiese toetse het bevestig dat die miselle geen of min toksisiteit toon teenoor eukariotiese selle nie, selfs teen 'n hoë konsentrasies soos 0.9 mg/ml. Die medisinale behoud vermoë is met behulp van piren bevestig en dus ook die potensiaal van PVP-*b*-PBLG as 'n moontlike MVS.

## ACKNOWLEDGEMENTS

I would like to thank my supervisor, Prof. Bert Klumperman as well as my co-supervisor, Dr. Gwenaelle Pound-Lana for their guidance and encouragement over the last few years.

I would like to thank all the staff at the Department of Chemistry and Polymer Science who have been instrumental in my project, in particular Calvin Maart, Jim Motshweni, Deon Koen, Erinda Cooper and Aneli Fourie.

I would like to thank Elsa Malherbe for NMR analysis, and Francious Cummings for the TEM analysis.

I would like to thank the National Research Foundation of South Africa for funding.

Special thanks to Eric van den Dungen for the invaluable discussions and all the advice you freely supplied.

Thanks to all the free radical research members, past and present members: Paul, Celeste, William, Welmarie, Khotso, Osama, Ahmed, Nathalie, Rueben, Nellie, Waled, Hamilton, Lizl, Sandile, Mpho, Barry, Njabu.

I really appreciate all the assistance, discussions and friendships we have made.

Furthermore, to friends and family – thank you.

## Table of Contents

<b>Declaration</b>	.....	<b>ii</b>
<b>Summary</b>	.....	<b>iii</b>
<b>Opsomming</b>	.....	<b>v</b>
<b>Acknowledgements</b>	.....	<b>vii</b>
<b>List of Figures</b>	.....	<b>xiv</b>
<b>List of Schemes</b>	.....	<b>xviii</b>
<b>List of Tables</b>	.....	<b>xx</b>
<b>List of Abbreviations</b>	.....	<b>xxi</b>
<b>List of Symbols</b>	.....	<b>xxiv</b>
<b>Chapter 1: General Introduction and Objectives</b>		
<i>Prologue</i>	.....	<b>1</b>
<b>1.1 Introduction</b>	.....	<b>1</b>
<b>1.2 Objectives</b>	.....	<b>1</b>
<b>1.3 Layout of thesis</b>	.....	<b>2</b>
1.3.1 Chapter 1: General Introduction and Objectives	.....	<b>2</b>
1.3.2 Chapter 2: Historical and Theoretical background	.....	<b>2</b>
1.3.3 Chapter 3: PVP Synthesis and Modification reactions	.....	<b>2</b>
1.3.4 Chapter 4: PBLG Synthesis and Modification reactions	.....	<b>2</b>
1.3.5 Chapter 5: PVP and PBLG hybrid block copolymers	.....	<b>3</b>
1.3.6 Chapter 6: Conclusions and Outlook	.....	<b>3</b>
<b>1.4 References</b>	.....	<b>3</b>



**Chapter 2: Historical and Theoretical background**

<i>Controlled Radical Polymerizations</i> .....	5
<b>2.1 Introduction</b>	<b>5</b>
2.1.1 Terminology .....	6
<b>2.2 RAFT mediated polymerization</b> .....	<b>7</b>
2.2.1 The RAFT mechanism .....	8
2.2.2 Choice of RAFT agent .....	10
2.2.2.1 The R group .....	10
2.2.2.2 The Z group .....	11
<b>2.3 Polymerization of NVP</b> .....	<b>12</b>
2.3.1 ATRP .....	13
2.3.2 Organostibine mediated LRP .....	14
2.3.3 RAFT .....	15
<b>2.4 Polypeptides via living ring-opening polymerizations of N-carboxyanhydrides</b> .....	<b>18</b>
2.4.1 N-Carboxyanhydride ring opening polymerization (NCA ROP) .....	18
2.4.2 NCA ROP Mechanisms .....	19
2.4.3 Polypeptide implementation .....	22
2.4.4 Poly(benzyl-L-glutamate) via NCA ROP .....	23
<b>2.5 Self-assembly of amphiphilic block copolymers</b> .....	<b>24</b>
2.5.1 Polymeric micelles .....	24
2.5.2 The EPR effect .....	25
<b>2.6 References</b> .....	<b>27</b>

**Chapter 3: PVP Synthesis and Modification reactions**

<i>RAFT mediated polymerization of N-vinylpyrrolidone and end-group modification of xanthate end-functional PVP</i> .....	33
<b>3.1 Introduction</b> .....	<b>33</b>
<b>3.2 Experimental</b> .....	<b>35</b>

## Index

3.2.1	Materials .....	35
3.2.2	RAFT CTA synthesis .....	36
3.2.2.1	Fluorescent tagged RAFT CTA, X21 .....	36
3.2.2.2	Difunctional RAFT CTA, X16 .....	37
3.2.2.3	Synthesis of N-(2-(1H-indol-3-yl)ethyl)-2- bromopropanamide .....	38
3.2.2.4	Synthesis of S-(1-((2-(1H-indol-3-yl)ethyl)amino)-1- oxopropan-2-yl) O-ethyl carbonodithioate .....	38
3.2.2.5	Synthesis of diethyl 2,5- bis((ethoxycarbonothioyl)thio)hexanedioate .....	39
3.2.3	General polymerization procedure .....	39
3.2.3.1	X21-mediated homopolymerization of N-vinyl pyrrolidone .....	41
<b>3.3</b>	<b>End-functional PVP .....</b>	<b>42</b>
3.3.1	Preparation of hydroxyl end-functional PVP .....	42
3.3.2	Preparation of aldehyde end-functional PVP .....	42
<b>3.4</b>	<b>Analysis .....</b>	<b>42</b>
3.4.1	NMR .....	42
3.4.2	SEC .....	42
3.4.3	ATR-FTIR .....	43
3.4.4	MALDI-Tof-MS .....	43
<b>3.5</b>	<b>Results and discussion .....</b>	<b>44</b>
3.5.1	Chain-end analysis .....	44
3.5.1.1	<sup>1</sup> H-NMR analysis .....	44
<b>3.6</b>	<b>End-group modification of xanthate end-functional PVP .....</b>	<b>48</b>
3.6.1	Chain end analysis .....	48
3.6.1.1	<sup>1</sup> H- and <sup>13</sup> C-NMR analysis .....	48
3.6.2	Optimization of ω-aldehyde end-group synthesis .....	51
<b>3.7</b>	<b>Conclusion .....</b>	<b>55</b>

<b>3.8</b>	<b>References:</b> .....	<b>56</b>
<b>Chapter 4: PBLG Synthesis and Modification reactions</b>		
	<i>Living N-carboxyanhydride (NCA) Ring Opening Polymerization of <math>\gamma</math>-benzyl-L-glutamate via the Normal Amine Mechanism (NAM)</i> .....	<b>57</b>
<b>4.1</b>	<b>Introduction</b> .....	<b>57</b>
<b>4.2</b>	<b>Experimental</b> .....	<b>59</b>
4.2.1	Materials .....	59
4.2.2	NCA of $\gamma$ -Benzyl-L-glutamate (BLG) .....	59
4.2.2.1	Synthesis of BLG .....	60
4.2.2.2	Synthesis of NCA of BLG .....	61
4.2.3	Polymerization system .....	61
4.2.3.1	Experimental procedure for ROP of BLG NCA .....	62
4.2.4	Peptide coupling reaction.....	63
4.2.4.1	Synthesis of Fmoc-cys(Acm) end-functional PBLG .....	64
4.2.4.2	Deprotection of primary amine - Fmoc group removal .....	64
4.2.4.3	Simultaneous thiol deprotection and oxidation - Acm group removal .....	64
<b>4.3</b>	<b>Analysis</b> .....	<b>65</b>
4.3.1	NMR Spectroscopy .....	65
4.3.2	SEC .....	65
4.3.3	MALDI-ToF-MS .....	65
<b>4.4</b>	<b>Results and discussion</b> .....	<b>66</b>
4.4.1	ROP of BLG NCA .....	66
4.4.1.1	<sup>1</sup> H-NMR analysis.....	66
4.4.1.2	MALDI-ToF-MS.....	68
4.4.2	Peptide coupling reaction.....	69
4.4.2.1	Synthesis of PBLG-Fmoc-Cys(Acm) .....	70
4.4.2.3	Synthesis of PBLG-Cys .....	74

<b>4.5</b>	<b>Conclusions</b> .....	<b>76</b>
<b>4.6</b>	<b>References</b> .....	<b>77</b>
<b>Chapter 5: PVP and PBLG hybrid block copolymers</b>		
	<i>Biohybrid poly(N-vinylpyrrolidone)-b-poly(<math>\gamma</math>-benzyl-L-glutamate) copolymers via thiazolidine chemistry</i> .....	<b>79</b>
<b>5.1</b>	<b>Introduction</b> .....	<b>79</b>
5.1.1	Biohybrid amphiphilic block copolymers .....	79
<b>5.2</b>	<b>Experimental details</b> .....	<b>82</b>
5.2.1	Materials .....	82
5.2.2	General reaction procedure for thiazolidine formation .....	82
5.2.2.1	Synthesis of cysteine containing PBLG .....	82
5.2.2.2	Synthesis of cysteine containing PBLG .....	82
5.2.2.3	Synthesis of PVP- <i>b</i> -PBLG amphiphilic block copolymers.....	83
5.2.3	Preparation of polymeric micelles .....	84
5.2.4	Determination of the critical micelle concentration (CMC) .....	84
5.2.5	Preparation of pyrene-loaded micelles.....	85
5.2.6	Cell viability study .....	85
<b>5.3</b>	<b>Analysis</b> .....	<b>86</b>
5.3.1	NMR spectroscopy .....	86
5.3.2	SEC .....	86
5.3.3	ATR-FTIR spectroscopy .....	86
5.3.4	Fluorescence spectroscopy .....	86
5.3.5	UV-Vis spectroscopy.....	87
5.3.6	Transmission electron microscopy (TEM).....	87
5.3.7	Dynamic Light Scattering (DLS).....	87
<b>5.4</b>	<b>Reaction of <math>\omega</math>-aldehyde end functional PVP with cysteamine</b> .....	<b>88</b>
<b>5.4</b>	<b>Results and discussion</b> .....	<b>88</b>
5.4.1	Chain-end analysis .....	88

## Index

<b>5.5</b>	<b>PVP-<i>b</i>-PBLG copolymer synthesis and characterization.....</b>	<b>93</b>
5.5.1	Conjugation of $\omega$ -aldehyde PVP and PBLG cysteine. ....	93
5.5.2	Conjugation of $\omega$ -aldehyde PVP and P(BLG <sub>40</sub> - <i>b</i> -tBMLC <sub>3</sub> ).....	93
5.5.2.1	In situ deprotection and conjugation. ....	93
5.5.2.2	Conjugation reactions with deprotected P(BLG <sub>40</sub> - <i>b</i> - tBMLC <sub>3</sub> ) (using the two-step approach).....	96
5.5.3	Conjugation of $\omega$ -aldehyde PVP and PBLG-Cys .....	97
5.5.3	Secondary structure identification.....	100
5.5.4	CMC of PVP- <i>b</i> -PBGL.....	101
5.5.5	Particle size and morphology determination with TEM and DLS.....	102
5.5.6	Effect of pH on particle size .....	105
5.5.7	Cell viability.....	110
5.5.8	Pyrene loading of micelles .....	112
<b>5.6</b>	<b>Conclusions .....</b>	<b>113</b>
<b>5.7</b>	<b>References .....</b>	<b>114</b>
<b>Chapter 6: Conclusions and Outlook</b>		
	<i>Epilogue</i> .....	116
<b>6.1</b>	<b>Introduction.....</b>	<b>116</b>
<b>6.2</b>	<b>Outlook.....</b>	<b>118</b>
<b>6.3</b>	<b>References.....</b>	<b>118</b>

## List of Figures

Figure 2.1	General structures for commonly used RAFT agents.....	7
Figure 2.2	Guidelines for selection of RAFT agents for various polymerizations. The addition rates decrease and fragmentation rates increase from left to right.....	11
Figure 2.3	Organostibine mediators for the LRP of PVP.....	14
Figure 2.4	Structures of RAFT CTAs used for the LRP of PVP.....	17
Figure 2.5	RAFT CTAs used to mediate the LRP of NVP and Vac.....	17
Figure 2.6	The different components of a micelle after the self-assembly of the amphiphilic block copolymers.....	25
Figure 2.7	Passive targeting of micelles by the EPR effect, utilizing the compromised endothelial cells of tumor blood vessels. Nanoparticles take advantage of this leaky vasculature to accumulate into the tumor tissues while the absence of effective lymphatic drainage contributes to this retention.....	26
Figure 3.1	RAFT CTA for LRP of NVP with fluorescent moiety (X21).....	36
Figure 3.2	<sup>1</sup> H-NMR spectrum of PVP-X21 in CDCl <sub>3</sub> prepared via the bulk polymerization of NVP at 60 °C.....	44
Figure 3.3	<sup>1</sup> H-NMR spectrum of PVP-X16 in CDCl <sub>3</sub> prepared via the bulk polymerization of NVP at 60 °C.....	47
Figure 3.4	<sup>1</sup> H-NMR spectra of PVP in CDCl <sub>3</sub> before and after being heated in aqueous solution (pH = 4.5) at 40 °C for 20 hours.....	49
Figure 3.5	<sup>1</sup> H-NMR spectrum of PVP in CDCl <sub>3</sub> after being hydrolyzed and subsequently heated for 20 hours at 120 °C under vacuum.....	50
Figure 3.6	<sup>13</sup> C-NMR spectrum of aldehyde end functional PVP in CDCl <sub>3</sub> . The insert indicates the characteristic signal for aldehyde functionality at 201 ppm.....	50

## Index

Figure 3.7	<sup>1</sup> H-NMR spectra of PVP-X21 (CDCl <sub>3</sub> ) after hydrolysis under varying aqueous conditions. The pH of the aqueous solutions was 3 (top), 2 (middle) and 1 (bottom) respectively.....	51
Figure 3.8	<sup>1</sup> H-NMR spectrum of PVP-X21 (CDCl <sub>3</sub> ) after hydrolysis at 50 °C (top spectra) and 60 °C (bottom spectra) respectively.....	54
Figure 4.1	Possible end-group configurations found in the NCA ROP of PBLG. Structure 5 is due to cyclization of the the terminal γ-benzyl-L-glutamate unit on the chain.....	62
Figure 4.2	<sup>1</sup> H-NMR spectrum of PBLG synthesized via the ROP of BLG NCA. .....	66
Figure 4.3	MALDI-ToF-MS of PBLG prepared by the ROP of PBLG NCA at 0 °C for 3 days under high vacuum.....	69
Figure 4.4	MALDI-ToF-MS of PBLG after the coupling reaction with Fmoc-Cys(Acm) group.....	71
Figure 4.5	<sup>1</sup> H-NMR spectra showing PBLG before deprotection (top) and after deprotection (bottom) of the amine (via the removal of the Fmoc group).....	72
Figure 4.6	SEC traces indicating the extent of Acm deprotection and subsequent oxidation of PBLG. The black trace is fully protected, the red trace partially deprotected (I <sub>2</sub> /[Ox]) and the blue trace fully deprotected (TFA).....	75
Figure 5.1	Graphical representation of the hydrophilic PVP block conjugated to the hydrophobic PBLG block via a thiazolidine linkage.....	80
Figure 5.2	The two different cysteine end-functional PBLG chains incorporated in the study i.e. PBLG-Cys (1) and PBLG- <i>b</i> -Cys (2).....	80
Figure 5.3	MALDI-ToF-MS spectrum of ω-thiazolidine PVP prepared via the reaction of cysteamine with ω-aldehyde PVP.....	91
Figure 5.4	Comparison of SEC traces which include the PVP- <i>b</i> -PBG copolymer (blue) and the starting materials which include PBLG (black) and ω-aldehyde PVP (red).....	94

## Index

Figure 5.5	SEC trace of (PVP- <i>b</i> -Cys- <i>b</i> -PBLG) before (dashed line) and after dialysis (solid line). The structural assignments of the peaks are presented in Table 5.3.....	95
Figure 5.6	SEC trace indicating the bimodality of the conjugation reaction with PVP-CHO and the PBLG- <i>b</i> -Cys copolymer (2).....	97
Figure 5.7	SEC trace of PVP <sub>90</sub> - <i>b</i> -PBLG <sub>54</sub> indicating quantitative conjugation of the PVP and PBLG chains.....	98
Figure 5.8	Schematic diagram depicting the self-assembly concept of PBLG- <i>b</i> -PVP- <i>b</i> -PBLG into a flower-like conformation.....	98
Figure 5.9	A typical ATR-FTIR spectrum for a PVP- <i>b</i> -PBLG copolymer is shown. The amide I band and amide II band is shown which is indicative of $\alpha$ -helical conformation.....	100
Figure 5.10	The CMC determination for PVP <sub>90</sub> - <i>b</i> -PBLG <sub>54</sub> using fluorescence spectroscopy with Nile Red as probe.....	101
Figure 5.11	TEM images indicating particle sizes of PVP <sub>90</sub> - <i>b</i> -PBLG <sub>41</sub> (A), PVP <sub>90</sub> - <i>b</i> -PBLG <sub>54</sub> (B), PVP <sub>27</sub> - <i>b</i> -PBLG <sub>54</sub> (C), PVP <sub>225</sub> - <i>b</i> -PBLG <sub>54</sub> (D) and PBLG <sub>54</sub> - <i>b</i> -PVP <sub>62</sub> - <i>b</i> -PBLG <sub>54</sub> (E).....	103
Figure 5.12	Particle size distribution by number for PVP <sub>27</sub> - <i>b</i> -PBLG <sub>54</sub> as determined by DLS. The micelles were subjected to a buffer system of pH 7.2 and pH 5.4 for 48 hours.....	106
Figure 5.13	Particle size distribution by number for PBLG <sub>54</sub> - <i>b</i> -PVP <sub>62</sub> - <i>b</i> -PBLG <sub>54</sub> as determined by DLS. The micelles were subjected to a buffer system of pH 7.2 and pH 5.4 for 48 hours.....	106
Figure 5.14	TEM images of PVP <sub>27</sub> - <i>b</i> -PBLG <sub>59</sub> before (A) and after (B) being subjected to a sodium acetate buffer system (pH 5.4) for 7 days....	107
Figure 5.15	TEM images of PBLG <sub>59</sub> - <i>b</i> -PVP <sub>101</sub> - <i>b</i> -PBLG <sub>59</sub> before (A) and after (B) subjected subjected to a sodium acetate buffer system (pH 5.4) for 7 days.....	107
Figure 5.16	ATR FT-IR spectrum comparing PVP- <i>b</i> -PBLG before (black) and after (red) exposure to pH 5.4 environment for 7 days.....	108



## Index

- Figure 5.17  $^1\text{H-NMR}$  spectra comparing PVP-*b*-PBLG in  $\text{CDCl}_3$  before (bottom) and after (top) hydrolysis of the benzyl ester groups. The middle  $^1\text{H-NMR}$  spectrum is the copolymer after hydrolysis in DMSO- $d_6$ ...109
- Figure 5.18 Copolymer cytotoxicity test results for a known membrane permeabilizer to indicate positive cell death.....111
- Figure 5.19 Copolymer cytotoxicity test results for PVP<sub>90</sub>-*b*-PBLG<sub>54</sub> at a concentration of 0.9 mg/mL.....112

## List of Schemes

Scheme 2.1	The general mechanism of a nitroxide mediated polymerization (NMP)	6
Scheme 2.2	Mechanistic basis of atom transfer radical polymerization (ATRP)	6
Scheme 2.3	Mechanism of RAFT-mediated polymerization	9
Scheme 2.4	General scheme for the polymerization of NVP	12
Scheme 2.5	Degenerative Transfer Mechanism of Organostibine-Mediated Living Radical Polymerization (SBRP)	14
Scheme 2.6	Zwitterionic canonical forms of xanthates and dithiocarbamates	16
Scheme 2.7	In situ formation of S-(cyano)isopropyl xanthate	17
Scheme 2.8	The normal amine mechanism (NAM)	20
Scheme 2.9	The activated monomer mechanism (AMM)	20
Scheme 2.10	NCA ROP of Poly( $\gamma$ -benzyl-L-glutamate)	23
Scheme 3.1	Modification of PVP xanthate chain-ends into hydroxyl and aldehyde end-groups	35
Scheme 3.2	Synthesis of fluorescent tagged RAFT CTA, X21 (1)	37
Scheme 3.3	Synthesis of the difunctional RAFT CTA, X16 (7)	37
Scheme 3.4	General polymerization procedure for NVP at 60 °C with AIBN as the initiator. X21 and X16 are used as the CTAs for the top and bottom reaction respectively	40
Scheme 4.1	Synthesis of NCA of $\gamma$ -benzyl-L-glutamate (BLG)	60
Scheme 4.2	ROP of NCA of $\gamma$ -benzyl-L-glutamate	61
Scheme 4.3	Coupling reaction resulting in a PBLG polypeptide with the protected, terminal cysteine functionality	63
Scheme 4.4	Deprotection steps of the Fmoc-cys(Acm) end-functional PBLG resulting in the terminal cysteine moiety	70

## Index

Scheme 4.5	Equilibrium of DBF and piperidine after Fmoc deprotection.....	72
Scheme 5.1	The mechanism for thiazolidine formation is depicted. This proceeds via the reaction of a 1,2-aminothiol and an aldehyde.....	81
Scheme 5.2	One-pot deprotection of P(BLG <sub>40</sub> - <i>b</i> -tBMLC <sub>3</sub> ) and conjugation with $\omega$ -aldehyde PVP.....	83
Scheme 5.3	General reaction of cysteamine and the $\omega$ -aldehyde end-functional PVP for the formation of the thiazolidine linkage.....	88
Scheme 5.4	Hydrolysis of the labile benzyl ester groups resulting in a random copolypeptide comprising of $\gamma$ -glutamic acid and $\gamma$ -benzyl glutamate repeat units.....	108

## List of Tables

Table 3.1	General characterization results for the PVPX21 homopolymer.....	46
Table 3.2	General characterization results for the PVPX16 homopolymer.....	48
Table 3.3	Comparison of the end group conversion after the hydrolysis and subsequent thermolysis of xanthate end functional PVP as a function of pH.....	52
Table 3.4	Comparison of the end group conversion after hydrolysis at different temperatures and subsequent thermolysis of the xanthate end functional PVP.....	53
Table 4.1	SEC results for the NCA polymerization of PBLG.....	67
Table 4.2	Structural assignments for the MALDI-ToF-MS spectra in figures 5.3 and 5.4.....	73
Table 5.1	Summary of the varying conditions tested for the thiazolidine formation. ....	90
Table 5.2	Structural assignments for the MALDI-ToF-MS spectrum of the thiazolidine end-functional chains in Figure 5.5. ....	92
Table 5.3	Identification of possible structures with SEC after dialysis of the in situ deprotection of PBLG- <i>b</i> -Cys and conjugation with $\omega$ -aldehyde functional PVP.....	95
Table 5.4	Summary of reaction conditions and results after the conjugation of PBLG (1) and PBLG (2) with $\omega$ -aldehyde functional PVP.....	99
Table 5.5	TEM and DLS results for the self-assembled PVP- <i>b</i> -PBLG copolymers. ....	104
Table 5.6	DLS (Number distribution) and TEM results for the self-assembled PVP- <i>b</i> -PBLG copolymers after being subjected to aqueous conditions of pH 5.4 and pH 7.2 for 48 hours.....	105

## **List of Abbreviations**

Acm	Acetamidomethyl
AIBN	2,2'-azobisisobutyronitrile
AMM	Activated monomer mechanism
ATR-FTIR	Attenuated total reflectance - Fourier transform infrared
ATRP	Atom transfer radical polymerization
<i>t</i> Boc	<i>tert</i> -butyloxycarbonyl
CRP	Controlled/Living radical polymerization
CTA	Chain transfer agent
Cys	Cysteine
DCM	Dichloromethane
DDI	Distilled Deionized (water)
DLS	Dynamic light scattering
DMAc	N,N-dimethylacetamide
DMF	Dimethylformamide
DMSO	Dimethylsulfoxide
DP	Degree of polymerization
EPR	Enhanced permeability and retention
Fmoc	9-fluorenylmethoxycarbonyl
FRP	Free radical polymerization
Glu	Glutamic acid
HOBT	1-Hydroxybenzotriazole
HPLC	High Performance Liquid Chromatography

## Index

HV	High vacuum
IR	Infrared spectroscopy
Lys	Lysine
MALDI-ToF-MS	Matrix Assisted Laser Desorption Ionization Time of Flight Mass Spectroscopy
$M_n$	number average molecular weight
$M_p$	peak average molecular weight
NAM	Normal amine mechanism
NCA	N-carboxyanhydride
NMP	Nitroxide mediated polymerization
NMR	Nuclear magnetic resonance
NVP	N-vinylpyrrolidone
PDI	Polydispersity Index
PBocLL- <i>b</i> -PLP	Poly-(Boc-L-lysine)- <i>b</i> -poly(L-proline)
PBLG- <i>b</i> -PLP	Poly( $\gamma$ -benzyl-L-glutamate)- <i>b</i> -poly(L-proline)
PBLG- <i>b</i> -tBMLC	Poly( $\gamma$ -benzyl-L-glutamate)- <i>b</i> - <i>tert</i> -butylmercapto-L-cysteine
PEG	Poly(ethylene glycol)
PI- <i>b</i> -Plys	Polyisoprene- <i>b</i> -poly(L-lysine)
PLP	Poly(L-proline)
PLP- <i>b</i> -PEO	Poly(L-proline)- <i>b</i> -poly(ethylene oxide)
PLP- <i>b</i> -PEO- <i>b</i> -PLP	Poly-(L-proline)- <i>b</i> -poly(ethylene oxide)- <i>b</i> -poly(L-proline)
PI- <i>b</i> -PZLys	Polyisoprene- <i>b</i> -poly( $\epsilon$ -benzyloxycarbonyl-L-lysine)
PS- <i>b</i> -PBLG	Polystyrene- <i>b</i> - poly( $\gamma$ -benzyl-L-glutamate)
PS- <i>b</i> -PZLys	Polystyrene- <i>b</i> - poly( $\epsilon$ -benzyloxycarbonyl-L-lysine)

## Index

p-TSA	p-Toluenesulfonic acid
PVP	Poly( <i>N</i> -vinylpyrrolidone)
PVP-CHO	$\omega$ -aldehyde Poly( <i>N</i> -vinylpyrrolidone)
PVP-OH	$\omega$ -hydroxyl Poly( <i>N</i> -vinylpyrrolidone)
RES	Reticuloendothelial System
RAFT	Reversible addition-fragmentation chain-transfer
ROP	Ring-opening polymerization
SEC	Size exclusion chromatography
TEA	Triethylamine
TEM	Transmission electron microscopy
TFA	Trifluoroacetic acid
THF	Tetrahydrofuran
TLC	Thin layer chromatography
TMS	Tetramethylsilane
UV	Ultraviolet

## List of Symbols

$\alpha$	conversion
$\Delta$	Heat
$\int$	Integrated fraction
$[I]_0$	Initial initiator concentration
$[M]_0$	Initial monomer concentration
$\mathcal{D}$	Dispersity
$DP_n$	Number average degree of polymerization
$k_{\text{deact}}$	Rate constant of deactivation
$k_i$	Rate constant of initiation
$k_p$	Rate constant of propagation
$k_t$	Rate constant of termination
$k_{\text{tr}}$	Rate constant of transfer
$M_{n,\text{theo}}$	Theoretical molar mass
$M_{\text{rCTA}}$	Molecular weight of the CTA
$M_{\text{rmonomer}}$	Molecular weight of the monomer



## Prologue

### 1.1 Introduction

Smart polymers have the ability to undergo physical and/or chemical changes in response to small changes in their environment. Scientists have been studying natural polymers in living systems to try and mimic their structural as well as physiological roles. These synthetic smart polymers have promising applications in the biomedical field as delivery vehicle for therapeutic agents. Polymeric materials are being formulated to respond to biological triggers which are able to induce predictable conformational changes.<sup>1</sup>

Currently, the most sought after application of these smart polymers in biomedicine is targeted drug release. This implies the efficient control of drug retention until the delivery system has reached the desired target and then the subsequent release via a chemical or physiological trigger.<sup>2</sup>

These smart polymers typically have well-defined functional groups either situated at the chain-ends or as pendant groups. These functional groups allow for a broader range of applications which is achieved by suitably engineering these synthetic polymers. The applicability of these synthetic polymers in biomedicine include polymer-drug conjugates,<sup>3</sup> polymer-protein bioconjugates<sup>4,5</sup> and polymeric micelles which incorporate water-insoluble drugs via physical or chemical encapsulation.<sup>6</sup> These bioconjugates incorporate polypeptides, which have the ability to act like polyelectrolytes and thus bear weakly acidic or basic groups in their structure. This allows the chain to reversibly accept or release protons in response to changes in the environmental pH. This combinatorial science is able to effectively enhance polymer therapeutics.

### 1.2 Objectives

The aim of this project was to synthesize hybrid amphiphilic block copolymers which could self-assemble into three-dimensional structures in aqueous solution. The hydrophilic polymer of choice is poly(*N*-vinylpyrrolidone) (PVP), chosen due to its excellent biocompatibility. Furthermore, the synthetic tool to be used is reversible addition-fragmentation chain-transfer (RAFT) mediated polymerization which allows for the introduction of functionalities at the  $\omega$ - and  $\alpha$ -chain-end.

## Chapter 1: General Introduction and Objectives

Poly( $\gamma$ -benzyl-L-glutamate) (PBLG) will be incorporated as the hydrophobic block. The polypeptide undergoes secondary conformational changes in certain solvent conditions, making for an interesting polymer system. A cysteine functionality will be introduced via peptide chemistry to conjugate the polypeptide and an  $\omega$ -aldehyde functional PVP via a thiazolidine linkage.

The self-assembly characteristics of the hybrid amphiphilic block copolymer will be characterized along with the toxicity and possible drug loading ability. This will be done to assess the conjugate's potential as a drug delivery vehicle.

The details of this work are briefly outlined below.

### 1.3 Layout of thesis

#### 1.3.1 Chapter 1: General Introduction and Objectives

This chapter gives a brief introduction on the importance of functional polymers and their incorporation into biomedical fields. The study's objectives and a short outline of the rest of the work is described.

#### 1.3.2 Chapter 2: Historical and Theoretical background

Chapter 2 introduces the historical and theoretical aspects on the chemistry of living/controlled radical polymerization (LRP). LRP techniques are introduced with emphasis on RAFT-mediated polymerization. The ring-opening polymerization (ROP) of *N*-carboxyanhydrides (NCAs) as these are the synthetic tools used in this work. The synthesis of PVP and PBLG is specifically discussed using these respective techniques.

#### 1.3.3 Chapter 3: PVP Synthesis and Modification reactions

In this chapter the RAFT-mediated polymerization of *N*-vinylpyrrolidone (NVP) is described. The synthesis of PVP with a mono- and difunctional xanthate chain transfer agent (CTA) is described along with optimized modification reactions to produce mono- and dialdehyde end-functional PVP. Characterization methods used include size exclusion chromatography (SEC), nuclear magnetic resonance (NMR) spectroscopy and matrix-assisted laser desorption ionization time-of-flight mass spectrometry (MALDI-ToF-MS).

### 1.3.4 Chapter 4: PBLG Synthesis and Modification reactions

Chapter 4 describes the synthesis of amine terminal PBLG via the ROP of NCAs. Conditions which promote the living polymerization via the normal amine mechanism are applied which decrease possible side-reactions.<sup>7</sup> A protected cysteine functionality is introduced via the terminal amine on PBLG and subsequent deprotection steps are described. The thiol-protecting acetamidomethyl group is removed using a modified procedure that inhibits the hydrolysis of the ester bonds.<sup>8,9</sup>

### 1.3.5 Chapter 5: PVP and PBLG hybrid block copolymers

Chapter 5 gives a brief description of polymer therapeutics and ways in which they are exploited. A model study is described to find suitable conditions for the conjugation reaction of the cysteine-terminal PBLG and  $\omega$ -aldehyde PVP. Two structurally different cysteine-functional PBLG chains are incorporated in the synthesis of the hybrid copolymers and their conjugation efficiency is evaluated. Characterization on the hybrid copolymers is done using SEC, NMR spectroscopy, transmission electron microscopy (TEM) and dynamic light scattering (DLS). Further analysis of the nanoparticles includes the determination of the critical micelle concentration (CMC), drug loading viability and cytotoxicity tests.

### 1.3.6 Chapter 6: Conclusions and Outlook

This chapter gives a short overview of the conclusions gathered from this study. It also describes the challenges encountered during this project and necessary future work.

## 1.4 References

- (1) Börner, H. G.; Kühnle, H.; Hentschel, J. *Journal of Polymer Science Part A: Polymer Chemistry*, **48**, 1-14.
- (2) Ganta, S.; Devalapally, H.; Shahiwala, A.; Amiji, M. *J. Controlled Release* **2008**, *126*, 187-204.
- (3) Pasut, G.; Veronese, F. M. *Prog. Polym. Sci.* **2007**, *32*, 933-961.
- (4) Heredia, K. L.; Maynard, H. D. *Org. Biomol. Chem.* **2007**, *5*, 45-53.

Chapter 1: General Introduction and Objectives

- (5) Nicolas, J.; Mantovani, G.; Haddleton, D. M. *Macromol. Rapid Commun.* **2007**, *28*, 1083-1111.
- (6) Croy, S. R.; Kwon, G. S. *Curr. Pharm. Des.* **2006**, *12*, 4669-4684.
- (7) Habraken, G. J. M.; Wilsens, K. H. R. M.; Koning, C. E.; Heise, A. *Polymer Chemistry*, *2*, 1322-1330.
- (8) Guo, J.; Huang, Y.; Jing, X.; Chen, X. *Polymer* **2009**, *50*, 2847-2855.
- (9) Cuthbertson, A. O., NO); Amersham Health AS (Oslo, NO): United States, 2005.

## Controlled Radical Polymerizations

### 2.1 Introduction

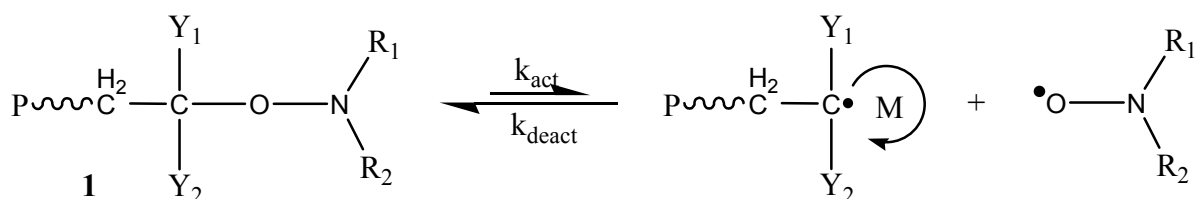
Commercially, free radical polymerization is the preferred synthesis method for a large variety of high molecular weight polymers. This is due to its inherent compatibility with a wide range of monomers, solvents and reaction conditions, which inadvertently allows for a robust polymerization technique.<sup>1</sup> In conventional free radical polymerization, this tolerance does, however, come with the price of limited control as far as architecture, topology and molecular weight distribution is concerned.

Due to the drawbacks of conventional free radical polymerization, a large body of work has been done over the last decade to develop techniques which allow for the synthesis of a diverse range of macromolecules with well defined architectures, functionalities and control over the degree of polymerization while still retaining their end-groups. The techniques developed are described as living/controlled radical polymerizations (LRP).<sup>2,3</sup> Living polymerizations are seen as systems where the polymer chain can propagate in the presence of monomer but does not undergo termination or chain transfer reactions, although in reality this is not the case.

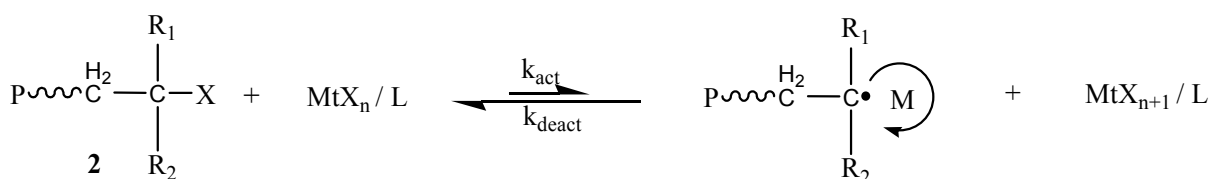
The effectiveness of LRP techniques is due to their ability to combine the benefits of living anionic polymerization i.e. designed molecular architecture with the versatility and robustness of free radical polymerization. These have the advantage of being able to produce polymers *via* a process which controls the chain length and the chain length distribution (characterized by the dispersity ( $\mathcal{D}$ )) while synthesizing polymers which have predictable and reproducible chain-end functionalities.

The key concept of LRP is the establishment of a reversible dynamic equilibrium between a low concentration of active species ( $P^{\bullet}$ ), which are able to propagate and a high concentration of dormant species ( $P-X$ ) which are not able to propagate (Scheme 2.1). For a system to have a “living character” it is necessary that the equilibrium lies towards the dormant species, this minimizes the concentration of active radicals present at any one moment thereby reducing possible radical-radical reactions, which inadvertently terminate growing chains. The consequence of this is that all the chains are grow simultaneously thus giving the technique its “living” character.

The most commonly used LRP techniques as noted by various LRP reviews are NMP<sup>4,5</sup> (*nitroxide mediated polymerization*), ATRP<sup>5</sup> (*atom transfer radical polymerization*) and RAFT<sup>6, 7,8</sup> (*reversible addition-fragmentation chain transfer*) mediated polymerization. The mechanism of NMP and ATRP differs vastly from that of RAFT mediated polymerizations as the former obtain the living character (of the system) by reversibly capping the growing radical chains with stable nitroxide radicals and halogens respectively to obtain the dormant species (**1** and **2**) (see Scheme 2.1 and 2.2).



Scheme 2.1 The general mechanism of a nitroxide mediated polymerization (NMP).



Scheme 2.2 Mechanistic basis of atom transfer radical polymerization (ATRP).

RAFT<sup>9</sup> mediated polymerization and a similar method, MADIX<sup>10,11</sup> (*macromolecular design via interchange of xanthates*) were introduced roughly at the same time in 1998 by the CSIRO group and the Rhodia research group respectively. Both these processes have the same reversible transfer mechanism and will both be referred to by the general term of RAFT mediated polymerization.

### 2.1.1 Terminology

For the purpose of this report, the term living radical polymerization is used to describe the synthetic techniques used to synthesize polymer. This is done with the knowledge of the controversy surrounding the general use of the term 'living' or 'controlled' when describing radical polymerizations.<sup>12,13</sup> According to the International Union of Pure and Applied Chemistry (IUPAC), the term 'living

polymerization' refers to a "chain polymerization in which chain termination and irreversible chain transfer are absent" with the terms "immortal", "controlled/living", "pseudo-living", and "quasi-living" being discouraged.<sup>14</sup> With this in mind, an IUPAC task force has coined a general term for systems in which an equilibrium between dormant and active chains exists (NMP, ATRP and RAFT), namely reversible deactivation radical polymerization (RDRP).<sup>1</sup> Thus, we use the term LRP as it relates to the process in which termination is significantly decreased from the RAFT system and hence these macromolecules possess the ability of further growth with the addition of more monomer.

## 2.2 RAFT mediated polymerization

RAFT mediated polymerization will be the LRP technique discussed the most comprehensively. It is arguably the best synthetic tool available for obtaining the living characteristics necessary in radical polymerizations to obtain optimum control over the molecular weight distribution (MWD) with the added advantage of controlled chain ends. It is a facile technique that can be conducted under numerous reaction conditions, compatible with a wide range of monomers and tolerant to various functional groups.

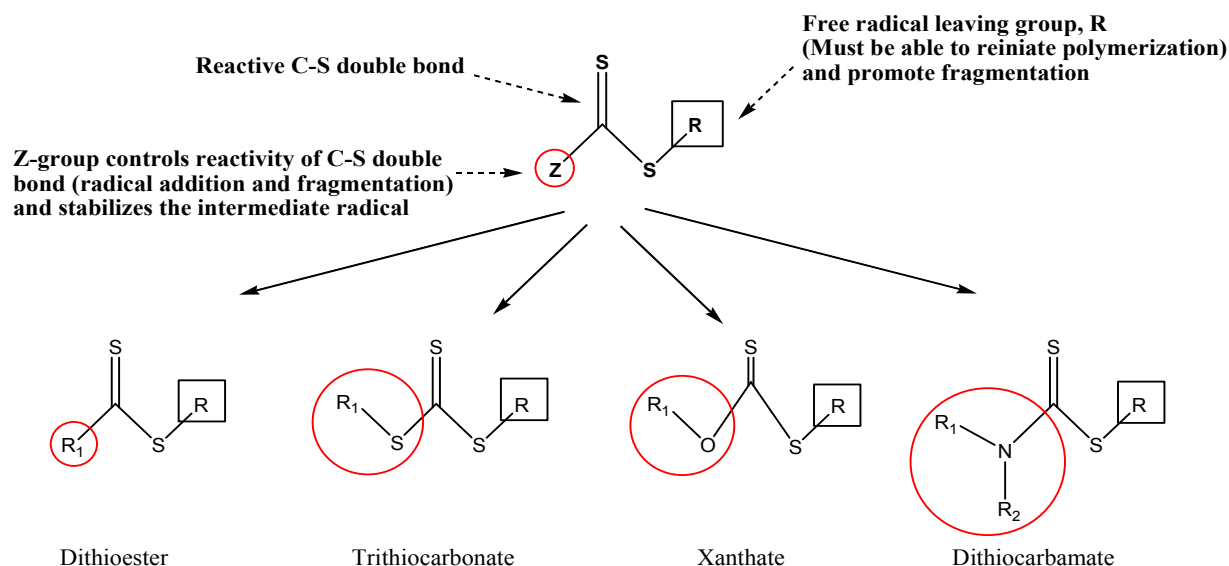


Figure 2.1

General structures for commonly used RAFT agents.

RAFT mediated polymerization is a degenerative process which acts *via* a two-step addition-fragmentation mechanism. It has the major advantage of being arguably the most versatile LRP technique thus far. In addition it has the inherent feature of being able to produce polymer with reactive/functional moieties at both the  $\alpha$ - and  $\omega$ -chain end. This is achieved *via* the RAFT agent's R- and Z-groups (Figure 2.1), which inadvertently allows for the introduction of functionalities at the chain ends. The R-group is found at the  $\alpha$ -chain end while the Z-group ends up at the  $\omega$ -chain end of the polymer, attached as a reactive thiocarbonyl thio moiety. It is possible to design a RAFT agent for each specific monomer. The R- and Z-groups, *i.e.* the re-initiating and activating groups respectively, can mediate the polymerization to the extent of obtaining excellent control over chain-end functionalities and offering further modification possibilities.

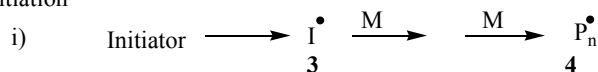
### 2.2.1 The RAFT mechanism

The basic fundamentals of free radical polymerization apply to the RAFT process where the rate of radical termination ( $R_t$ ) is related to the square of the radical concentration ( $R_t \propto [P_n \bullet]^2$ ) and the rate of propagation is directly proportional to the radical concentration ( $R_p \propto [P_n \bullet]$ ). Thus to eliminate (decrease) termination and allow for a 'living' character, the radical concentration needs to be kept low. This is achieved *via* the addition of a controlling agent into the polymerization medium, which is able to create a rapid equilibrium between the active propagating radicals and the dormant polymeric thiocarbonyl thio compound (Scheme 2.3, **ii** and **iv**). This dynamic equilibrium ensures an equal probability for all the chains to grow resulting in narrowly dispersed polymers.

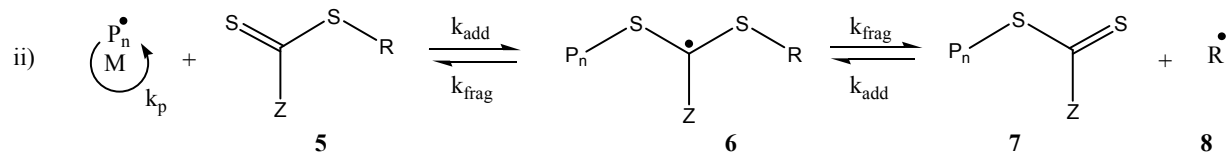


## Chapter 2: Historical and Theoretical background

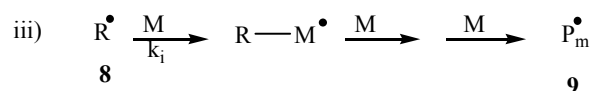
Initiation



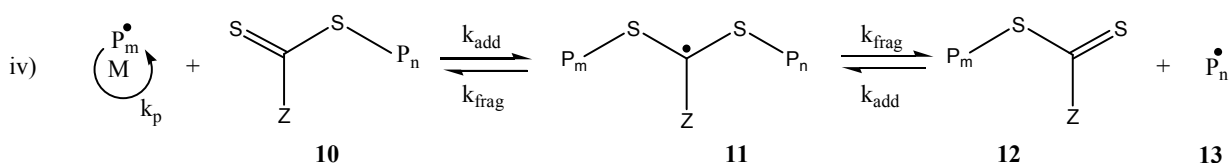
Reversible chain transfer (propagation)



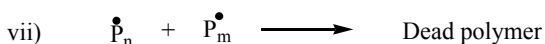
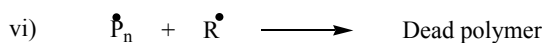
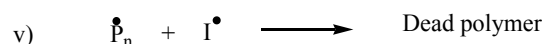
Reinitiation



Chain equilibrium (propagation)



Termination



## Scheme 2.3 Mechanism of RAFT-mediated polymerization.

Initiation is identical to conventional free radical polymerization where radicals (**3**) are generated by decomposition of a free radical initiator, typically an azo type molecule such as AIBN. The initial transfer reaction between the active species (**4**) and the chain transfer agent (CTA) (**5**) leads to the addition to the reactive C=S bond of the chain transfer agent to produce a carbon centered intermediate radical (**6**). This species may undergo a  $\beta$ -scission reaction which can either yield the reactants back, or release the R-group as a radical fragment (**8**) and leave the polymeric chain capped with the initial active species thus forming the reversible, dormant species (**7**) (this stage is commonly referred to as the pre-equilibrium, Equation ii).

The released R• radical (**8**) can initiate a new chain by adding to the monomer or it can add back to the CTA producing the carbon centered intermediate radical (**6**).

The main equilibrium (**v**) takes place solely between propagating chains (active species) and macro-CTAs (dormant species end-capped with the CTA, **10**), resulting in a rapid exchange of the CTA cap. The propagating radical chains rapidly exchange between the two dormant forms (**10**) and (**12**) and their actively propagating forms.

By using a minimal amount of initiator (only free-radical source, typically added at a concentration 0.1 to 0.2 times the RAFT agent concentration), termination reactions are minimized due to the resulting low concentration of the active species. Rapid exchange ensures that each chain has the same probability of growth, which is essential as all chains must be initiated early in the polymerization reaction for a narrow MWD.

### 2.2.2 Choice of RAFT agent

The structure of the RAFT agent is very important to the success of the RAFT process as the stability of the intermediate radical can be modified by selecting a particular Z- and to a lesser extent the R group. Subsequently, RAFT CTAs can only sufficiently control the polymerization of a certain type of monomer. In a comprehensive review by Moad *et al.*,<sup>15</sup> thiocarbonyl thio compounds that are used as RAFT agents in combination with certain monomer classes are reviewed and the efficient combination of CTA and monomer are given. These CTAs include dithioesters (Z = alkyl or aryl), trithiocarbonates (Z = thiol compound), dithiocarbamate (Z = dialkylamino) and xanthates (Z = alkoxy).

#### 2.2.2.1 The R group

After the initialization step, the subsequently formed oligomeric radicals react with the RAFT agent to form the intermediate radical (**6**). The R-group (leaving group) re-initiates the polymerization which, ideally with fast consumption of the RAFT agent and subsequent fragmentation, will result in most of the chains being initiated at the commencement of polymerization. The R-group should fragment at least as quickly as the polymer chains from the stabilized radical intermediate. This rapid interchange in the chain transfer step ensures that the concentration of growing radical chains is kept lower than that of the stabilized radical intermediates, thereby limiting termination reactions.

The R-group is expected to have less effect on the kinetics of the reaction after initiation, as, after the addition of only one or two monomer units, the R-group does no longer influence the reactivity of the propagating polymer radical.

### 2.2.2.2 The Z group

The role of the Z-group is to control the stability of the intermediate radical by activating or deactivating the C=S double bond and thereby affecting the reactivity towards the incoming radical. The interplay between the reactivity of the incoming radical and the leaving ability of the R-group directly affects the concentration of the intermediate radicals and thus the extent to which these are involved in termination reactions.

Furthermore, the nature of the monomer has a great influence as these can be classified into two groups which effectively rate the activity of the monomer, *i.e.* “more activated” monomers (MAMs) such as styrene, methyl acrylate and methyl methacrylate compared to the “less activated” monomers (LAMs) which would then include vinyl acetate, *N*-vinylpyrrolidone, and *N*-vinylcarbazole. Generally RAFT agents suitable for the one type of monomer are ineffective for the other type as it results in retardation and/or inhibition during the polymerization process (Fig 2.2).<sup>16</sup>

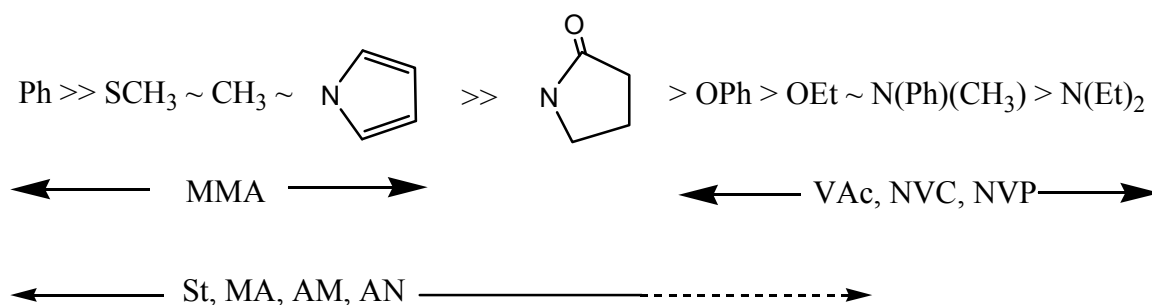
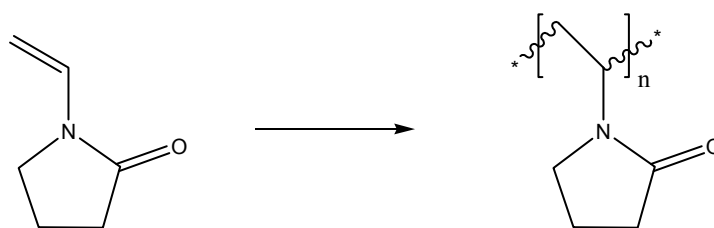


Figure 2.2 Guidelines for selection of RAFT agents for various polymerizations. The addition rates decrease and fragmentation rates increase from left to right.<sup>1</sup>

Thus, it is essential to select an appropriate RAFT agent. Poor transfer efficiency,<sup>17</sup> slow reinitiation rate<sup>18</sup> and a slow rate of fragmentation<sup>19</sup> have been proposed as the main causes of lack of control when doing RAFT mediated polymerizations.

### 2.3 Polymerization of NVP

Poly(N-vinyl pyrrolidone) (PVP) is a promising water-soluble polymer where its amphiphilic and non-biodegradable character makes it ideal as a synthetic biocompatible alternative. The repeating unit of PVP (Scheme 2.4) includes a polar cyclic amide group (lactam), which allows for hydrogen bonding as well as a non-polar backbone in the form of the methylene and methine groups. This allows for the solubilisation of PVP in an aqueous medium as well as in numerous organic solvents.<sup>20</sup>



Scheme 2.4 General scheme for the polymerization of NVP.

Due to the hydrophilic, non-toxic nature of the polymer it shows promise as a possible polymeric modifier, specifically in the biomedical area, which needs to be investigated. The initial medical applicability of PVP was during the Second World War, where it was used as a synthetic blood plasma extender but due to its stable nature (non-biodegradable) the high molecular weight polymer collected in the reticuloendothelial system (RES). The molecular weight of the polymer must fall below the threshold value for the renal system to clear the specific molecule (< 30 kDa).<sup>20</sup>

The promise of PVP holds in the pharmaceutical industry, where the bioconjugation of polymers to bio-active proteins have shown significant improvement in the therapeutical effectiveness of the bioconjugate as compared to the native protein.<sup>21,22</sup>

Covalently bonding proteins to polymers and specifically to poly(ethylene glycol) (PEG) to generate PEG-peptide conjugates has been done extensively to the point of being coined PEGylation. PVP has been identified as a possible polymeric modifier as it showed an increased mean residence time (MRT) in circulation after *in vivo* injection, as well as minimal tissue distribution when compared to other possible water-soluble polymeric carriers like PEG, polyacrylamide (PAAm), polydimethylacrylamide (PDAAm), polyvinyl alcohol (PVA), and dextran.

Furthermore, PVP conjugated with TNF- $\alpha$  (natural human tumor necrosis factor-alpha) showed an increase in the general circulation lifetime as compared to PEG-TNF- $\alpha$  and the native TNF- $\alpha$ , as well as better localization of the conjugated drug in the blood, thus showing the viability of PVP as a possible polymeric drug carrier.<sup>23</sup>

Due to the positive results that PVP has shown as a polymeric modifier for polymer-protein conjugates when compared to PEG,<sup>23</sup> *i.e.* very low toxicity, good biocompatibility and the high complexation ability,<sup>24,25</sup> the next step would entail further investigation of PVP in diverse drug delivery systems (DDS) as literature on this is fairly limited when compared to that of PEG.

Until recently, the synthesis of NVP was the major problem for its use as a possible alternative to other water-soluble polymeric modifiers as control over the molar mass dispersity and chain-end functionalities was not sufficient. The problem lies with the inability of NVP to form stabilized radicals thus resulting in propagating radicals which are prone to side-reactions. This is very similar to vinyl acetate, where the propagating radical (**8** and **13**) is a poor homolytic leaving group and subsequently, the intermediate radical adducts (**6** and **11**) are more stable than the intended fragmented chains. Subsequently, conventional living polymerization methods were fairly limited in their control. This was seen when ionic mechanisms only resulted in the formation of oligomers,<sup>20</sup> thus limiting polymerization techniques to free radical mechanisms. NVP can be polymerized in bulk with azo initiating compounds or in solution in an organic or aqueous media while initiating with azo- or peroxide initiators.<sup>20</sup> For the purpose of using polymers and thus PVP in DDS, it is necessary that the well defined polymers are synthesized with narrow distributions as different molecular weights can lead to different toxicities and pharmacokinetics.<sup>26</sup> Consequently, the best way to achieve this is *via* controlled/living radical polymerization strategies.

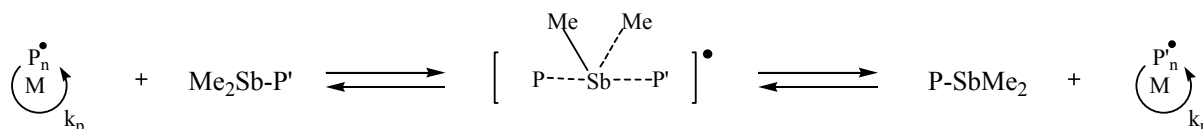
### 2.3.1 ATRP

In the past decade, various reports were published that explored ways to control the polymerization of NVP *via* LRP pathways. These included ATRP where the Matyjaszewski group<sup>27</sup> reported the polymerization of NVP using Me<sub>4</sub> Cyclam as a ligand to produce PVP of  $\bar{D} = 1.15$ , but limited chain-end functionalities while Meng *et al.*<sup>28</sup> have more recently reported the controlled synthesis of PVP and its

copolymers *via* Me<sub>6</sub>Cyclam as the ligand, producing polymers with narrow distributions,  $\mathcal{D} = 1.2 - 1.38$ .

### 2.3.2 Organostibine mediated LRP

Organostibine mediated LRP is analogous to RAFT and MADIX where the control of molecular weight is obtained *via* a degenerative transfer mechanism (Scheme 2.5).



Scheme 2.5 Degenerative Transfer Mechanism of Organostibine-Mediated Living Radical Polymerization (SBRP).

Ray *et al.*<sup>29</sup> reported the synthesis of high molecular weight PVP ( $M_n \sim 100\,000$  g/mol) with excellent control ( $\mathcal{D} < 1.3$ ) using organostibines as mediators (Fig 2.3).

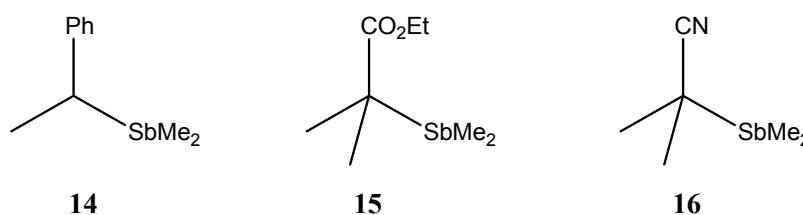


Figure 2.2 Organostibine mediators for the LRP of PVP.

Excellent control over PVP was reported ( $\mathcal{D} \sim 1.1$ ) when molecular weights were sufficiently low ( $M_n < 15\,000$  g/mol) but control decreased as the targeted molecular weight of PVP was increased. This was said to be due to head-to-head insertions taking place, which resulted in an organostibine PVP chain, which was unable to produce a propagating radical, thus eliminating the possibility of degenerative transfer taking place.

Yamago<sup>30</sup> documented a comprehensive report on the synthesis of controlled polymer synthesis *via* controlled/living degenerative transfer polymerization methods. These include organotellurium-, organostibine- and organobismuthine-mediated LRP (TERP, SBRP, and BIRP, respectively). These allow for the polymerization of NVP with  $M_n$  values ranging from 3100 - 83 500 g/mol and narrow MWDs ( $\mathcal{D} \sim 1.06 - 1.29$ ). Successive addition of monomer (and subsequent isolation of the product) allowed

them to synthesize di- and triblock copolymers. The control obtained after these second- and third generation monomer additions indicate the robust and versatile nature of these degenerative transfer polymerization techniques.

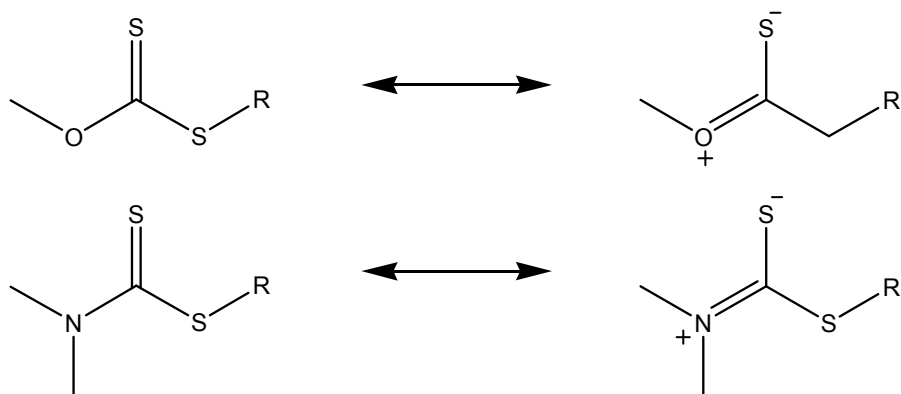
As far as control over the MWD of PVP is concerned, TERP, SBRP, and BIRP have the ability to compete and even surpass<sup>31</sup> the control one obtains when using RAFT, but its shortcoming is mainly in the ability to form a wide range of well defined end-group structures, which is exactly where RAFT has its strength.

### 2.3.3 RAFT

RAFT is one of the most versatile and robust methods for synthesizing high molecular weight polymer from a wide range of monomers. The control over the molecular weight distribution is achieved *via* the correct choice of chain transfer agent which is dependent on the activity of the monomer.

In the case of vinyl monomers, which are typically known as LAMs<sup>1,32</sup> the control of the radical polymerization is generally more difficult. The most popular classes of thiocarbonyl thio RAFT CTAs such as dithioesters and trithiocarbonates are generally ineffective when it come to the polymerization of vinyl monomers and more specifically NVP.<sup>33,34</sup> These RAFT agents have an inhibiting effect on NVP, which is generally a consequence of the stability of the intermediate radical adduct resulting in slow fragmentation of **6** and **11** (Equation ii and iv).

Thus, the choice of the RAFT agent for the fast propagating NVP is limited to less active RAFT agents. In general, the CTA's reactivity decreases in the series dithiobenzoates > trithiocarbonates > xanthates > dithiocarbamates. Subsequently, the choices of CTA is limited to the xanthates and dithiocarbamates, where these RAFT agents each have a lone pair of electrons on the oxygen or nitrogen which is adjacent to the thiocarbonyl group. These heteroatoms conjugate with the C=S bond, thus reducing its double bond character and, hence, reducing its affinity for radical addition (Scheme 2.6).



Scheme 2.6 Zwitterionic canonical forms of xanthates and dithiocarbamates.

Postma *et al.*<sup>35</sup> describe the polymerization of NVP using phthalimidomethyl trithiocarbonates and – xanthates. The polymerization with the trithiocarbonate (Figure 2.4, **17**) did not obtain the desired control ( $\bar{D} \sim 1.48-1.6$ ) while also showing an initial inhibition period. The S - phthalimidomethyl xanthate (Figure 2.4, **18**) however showed no inhibition period and good control over the lower molecular weight polymers ( $< 10\ 000\ \text{g/mol}$ ,  $\bar{D} \sim 1.16-1.27$ ). Wan *et al.*<sup>34</sup> reported the MADIX-mediated polymerization of NVP in the presence of fluoroalcohols. They found that the syndiotacticity of the polymer was dependent on the amount of fluoroalcohol which they attributed to the hydrogen-bonding between the fluoroalcohol and monomer/propagating radical. Two O-ethyl xanthates with a 1-phenylethyl (Figure 2.4, **19**) and benzyl R-group (Figure 2.4, **20**) were compared. Even under varying condition, the RAFT CTA with the 1-phenylethyl R-group gave the best control over the MWD. This is most probably due to the ability of the secondary carbon to form an intermediate radical which fragments faster when compared to the primary benzylic carbon, which results in a poor leaving group for NVP.



## Chapter 2: Historical and Theoretical background

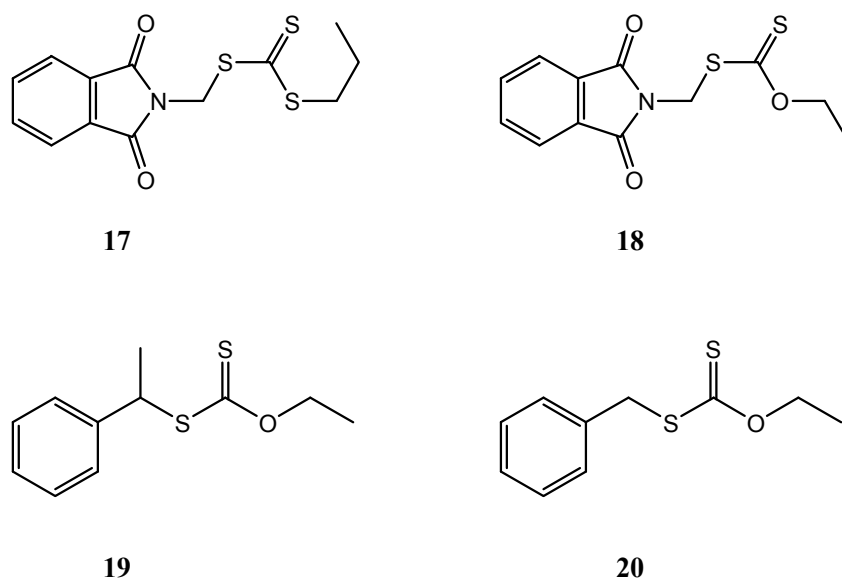
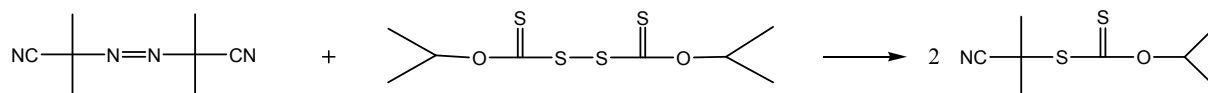


Figure 2.3 Structures of RAFT CTAs used for the LRP of PVP.

Recently, Yan *et al.*<sup>32</sup> reported on the investigation of different reaction conditions for the universal MADIX-mediated polymerization of LAMs, which included vinyl acetate, *N*-vinylcarbazole and *N*-vinylpyrrolidone. The polymer synthesis entails the *in situ* formation of *S*-(cyano)isopropyl xanthate as CTA *via* the reaction of a xanthate precursor, isopropylxanthic disulfide (DIP) and AIBN (Scheme 2.7).



Scheme 2.7 *In situ* formation of *S*-(cyano)isopropyl xanthate.

The polymerization proceeded with an induction time of 280 minutes for NVP, which is partly due to the time it takes for the *in situ* formation of the CTA, which needs to mediate the polymerization, as well as the possibility of a pre-equilibrium stage (Equation ii) which inhibits the polymerization (due to the slow consumption of the initial xanthate). Good control over the MWD was found for polymer below 30 000 g/mol with  $\mathcal{D} < 1.3$ . The living character of the system was shown *via* the chain extension of a preformed polymer which essentially acts as a macro-CTA. The macro-CTA, 10 600 g/mol ( $\mathcal{D} \sim 1.26$ ) was successfully extended to 22 600 g/mol ( $\mathcal{D} \sim 1.71$ ) where the increase in the  $\mathcal{D}$  was due to the presence of dead polymer in combination with the initial macro-CTA. The chain extension proved the capability of DIP to act as a suitable CTA with the ability to polymerize under living conditions.

In our group, Pound *et al.* have done a significant amount of research regarding the polymerization of poorly stabilized monomers *via* RAFT-mediated polymerizations and more specifically the xanthate-mediated polymerization of NVP.<sup>36-38</sup> *In situ* <sup>1</sup>H-NMR spectroscopy was used to probe the efficacy of xanthate CTAs<sup>36</sup> where it was shown that VAc and NVP exhibit selective initialization with specific xanthate CTAs. In the case of NVP, selective initialization, *i.e.* no significant polymerization until all the CTA is converted to a single monomer adduct, was observed when using **21** to polymerize NVP. This is then in comparison to **22** and **23** where hybrid behaviour was found, which led to chain propagation before all the CTA was converted into a single monomer adduct (Figure 2.5). In the case of **23**, it was said to be due to the enhanced leaving group ability of the monomer-derived radical when compared to that of the tertiary butyl R-group.

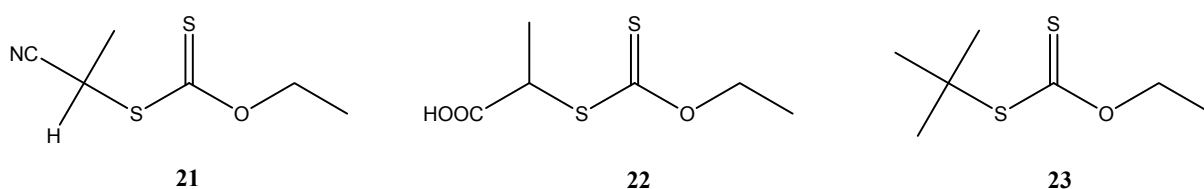


Figure 2.4 RAFT CTAs used to mediate the LRP of NVP and Vac.

## 2.4 Polypeptides *via* living ring-opening polymerizations of *N*-carboxyanhydrides

Peptides and proteins play significant roles in our everyday lives. They are built from  $\alpha$ -amino acids, connected *via* amide bonds. Unfortunately, the synthesis of natural polypeptides (proteins) with well-defined amino acid sequences, are severely limited to low molecular weight polypeptides of minimal quantities. This is due to the synthesis method namely *via* solid-phase peptide synthesis (SPPS) *i.e.* a one-by-one amino acid addition *via* a solid-phase support.<sup>39,40</sup>

### 2.4.1 *N*-Carboxyanhydride ring opening polymerization (NCA ROP)

There is however another method, which allows for the synthesis of high molecular weight peptides without a specific amino acid sequence. This is achieved *via* the ring-opening polymerization (ROP) of  $\alpha$ -amino *N*-carboxyanhydrides (NCAs). The ROP of NCAs resembles a living polymerization system, but traditionally this was not the case as termination reactions plagued the possibility of obtaining any control over the targeted molecular weight or the distributions.<sup>41</sup> It was not until recently that

Deming *et al.*<sup>42</sup> reported the first successful synthesis of well-defined high molecular weight polypeptides *via* the ROP of NCAs.

The necessity for structural control over the synthetic polypeptides is evident in the importance it plays for their naturally found counterparts. It is the homogeneity in the sequences of these  $\alpha$ -amino acids, which eventually determines their primary structure and essentially needs to be a reproducible process when produced synthetically.

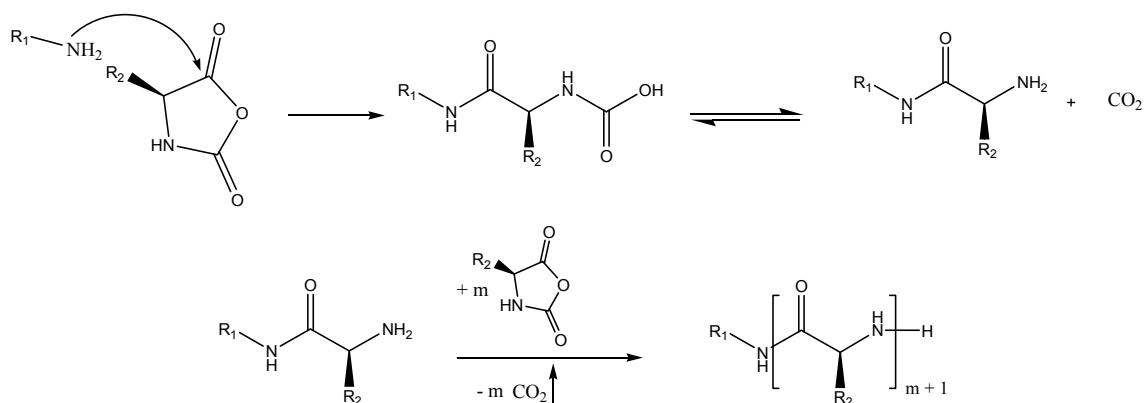
When utilizing the robustness of the ROP of NCAs, the possibilities are unlimited as one can essentially obtain a synthesis procedure with all the advantages of a living system while combining it with a wide range of natural and synthetic  $\alpha$ -amino acids, each with their own unique properties.

The added advantage over traditional synthetic polymers is their inherent biodegradability as well as the ability to form stable secondary structures in solution due to cooperative hydrogen bonding. Thus, the living nature of ROP of NCAs has led to a wide range of achievable architectures *via* the use of functional polypeptides,<sup>37,43,44</sup> multiblock copolypeptides<sup>42,45,46</sup> along with the added possibility for self-assembly. This self-assembling character is not only due to the rigid conformations ( $\alpha$ -helices and  $\beta$  sheets) between polypeptide chains but also due to the hydrophobic, electrostatic and dipolar interactions.<sup>46-48</sup>

#### 2.4.2 NCA ROP Mechanisms

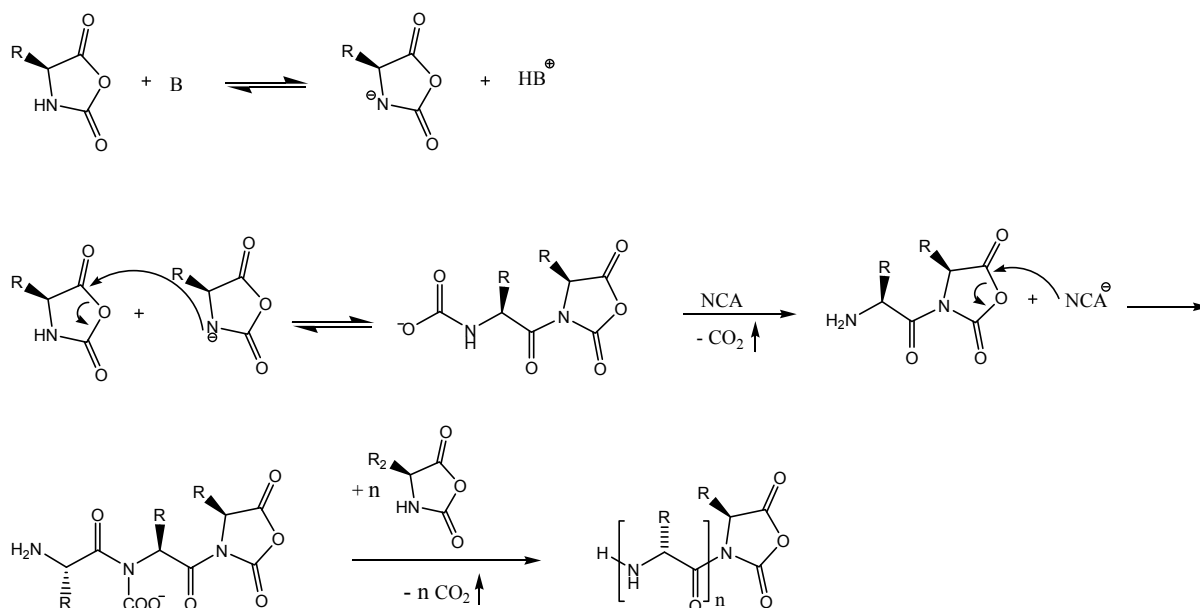
The ROP of NCAs has two likely mechanisms depending on the type of initiator used.<sup>41,47,49</sup> The normal amine mechanism (NAM) entails that the initiator is a nucleophile with a mobile hydrogen atom. These include (primary and secondary) amines, alcohols and water, where the nucleophilic attack of the initiator results in a carbamic acid intermediate which, after decarboxylation results in a terminal amino group. It is the formed primary amine that continues the propagation and allows for the formation of the eventual polypeptide (Scheme 2.8). Low dispersities can be engineered *via* the correct choice of initiator as seen with primary amines, where the latter's reactivity exceeds that of the  $\omega$ -amines of the propagating chains, resulting in the situation where  $k_i > k_p$  thus allowing all the chains to start growing simultaneously.<sup>41,49</sup>

## Chapter 2: Historical and Theoretical background



Scheme 2.8 The normal amine mechanism (NAM).

In the case where the initiator acts like a base instead of a nucleophile and abstracts a proton from the NCA, it is referred to as the activated monomer mechanism (AMM). Here an NCA anion forms due to the abstraction of a proton from the nitrogen atom of the monomer, which then attacks the carbonyl group in the 5-position (Scheme 2.9). Subsequently, this method is limited to NCAs with an unsubstituted nitrogen atom in the ring.



Scheme 2.9 The activated monomer mechanism (AMM).

The differences in the two different mechanisms are seen when one compares achievable molecular weights as well as the possible control one can obtain. This is said to be due to the higher propagation rate of the anion which leads to higher molecular weight for AMM, but higher dispersities are expected due to  $k_i < k_p$ .<sup>50</sup>

Recently, Lu *et al.* have shown the control one can obtain when exploiting this fact as they synthesized poly(benzyl-L-glutamate (PBLG) with high molecular weight but a low  $\bar{D}$  using the secondary amine, *N*-trimethylsilyl amine. Thus allowing the functionalization at the C-terminus, while still obtaining the control one expects of primary amines. The polymerization propagates *via* a trimethylsilyl carbamate (TMS-CBM) group which is unable to extract the proton of the nitrogen thus restricting the polymerization to the normal amine mechanism. Control of  $\bar{D} = 1.1$  is reported for PBLG (28 500 g/mol) using the selected initiators.<sup>37</sup>

Although optimization of the reaction is possible *via* the choice of initiator, it is also possible to follow a more facile route by optimizing the NAM conditions and thereby trying to reduce possible side reactions as well as accelerating reaction rates. This includes lowering the temperature<sup>45,51</sup> varying the solvent<sup>52</sup> or possibly working at higher vacuum,<sup>53,54</sup> whereby the two greatest influences are arguably temperature and vacuum.

Lowering the temperature essentially increases the stability of the carbamic acid intermediate, which after decarboxylation, forms the primary amine and subsequently propagates the polymerization.<sup>41</sup> Kricheldorf *et al.*<sup>52</sup> have shown that some solvents can induce polymerization of  $\alpha$ -amino acids resulting in cyclic polypeptides while working at high vacuum results in the removal of CO<sub>2</sub>. This results in acceleration of the reaction as well as in minimization of possible side reactions that CO<sub>2</sub> can have with the solvent.<sup>41,54</sup>

As mentioned before, the term 'living system' is used in the sense of the control achieved ( $\bar{D} < 1.2$ ) as well as the ability to reinitiate polymer chains in the presence of more monomer. Using this term loosely, Kricheldorf<sup>49</sup> described the ROP of NCAs as 'living polypeptides' when using primary amines as the initiator. This is due to the fast initiation rate for small, unhindered amines, and thus the excellent control one can achieve as well as the ease of tailoring the degree of polymerization *via* the correct choice of the monomer/initiator molar ratio ( $[NCA]/[I]$ ).

This all has allowed for a wider scope of possible implementation of polypeptides as the incorporation of other living polymerization techniques in combination with NCA ROP allow for the efficient tailoring of composition and topology.<sup>55-57</sup>

### 2.4.3 Polypeptide implementation

Due to the biological importance of polypeptides and the previous discussion on the living nature of the NCA ROP, it is evident that an array of applications is possible. This is especially true for their use in the biomedical field where the combination of natural- and synthetically prepared polymers allow for special biohybrid materials.

Even though the polypeptides synthesized *via* NCA ROP do not have the amino acid sequences necessary for certain enzymatic processes, their ability to form secondary structures does however allow them to self-organize. It is this self-assembling ability along with their inherent biodegradability which makes them so favorable for drug delivery purposes.

Lecommandoux *et al.*<sup>58</sup> reported the synthesis of polymer/peptide conjugates, PS-*b*-PBLG and PS-*b*-PZLys. It is noted that under ambient conditions, the peptide segments revert to their  $\alpha$ -helical secondary structure resulting in a rod-coil block copolymer, while certain stimuli such as temperature, segment lengths and chemical composition induce a transition to the  $\beta$ -sheet secondary structure.

Further investigation was done by Babin<sup>59</sup> on the self-assembly of rod-coil block copolymers, PI-*b*-PZLys and PI-*b*-PLys, in the aqueous and solid state. The stimuli responsive nature of micelles in water is investigated, where pH and ionic strength are varied to induce transitions in the polypeptide's secondary structure. In doing so, they could attribute the dimensional changes of the micelles to the  $\alpha$ -helix and  $\beta$ -sheet structure transitions.

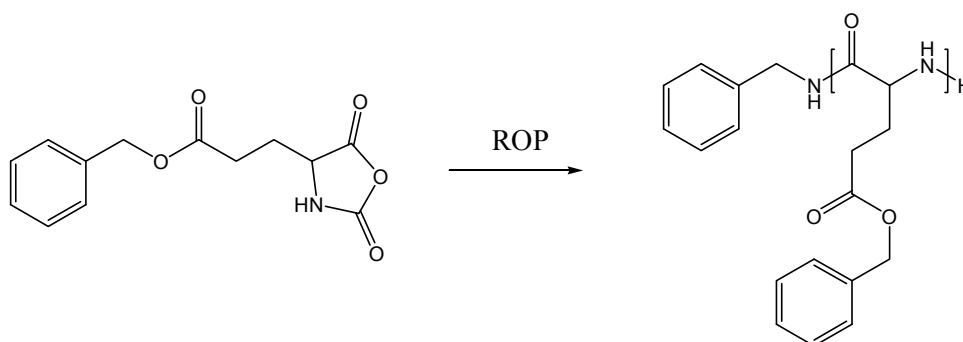
Recently, Gkikas *et al.*<sup>60</sup> have reported the synthesis of poly(L-proline), a polypeptide with a cyclised  $\alpha$ -amino group, which allowed for a trans conformation (PLP 2) and subsequently a hydrophilic, helical polypeptide independent of temperature and pH. High molecular weight PLP was previously plagued by the inability to effectively synthesize the pure monomer, a problem they claim to have overcome whilst producing poly(L-proline) based materials like PLP-*b*-PEO, PLP-*b*-PEO-*b*-PLP, PBLG-*b*-PLP and PBocLL-*b*-PLP.

In the case of polypeptides, most of the structures formed *via* self-assembly are due to the fact that they are essentially polyelectrolytes. Thus, at certain pH values they are charged molecular chains with a secondary structure that will always favour certain dimensional conformations leading to these self-assembling structures. This,

in combination with amphiphilic block copolypeptides or amphiphilic polymer-protein conjugates are the driving force for the formation of vesicles,<sup>61-63</sup> aggregates,<sup>61</sup> micelles<sup>64,65</sup> and organogels.<sup>57</sup>

#### 2.4.4 Poly( $\gamma$ -benzyl-L-glutamate) *via* NCA ROP

Poly( $\gamma$ -benzyl-L-glutamate) (PBLG) is a hydrophobic polypeptide synthesized *via* the ROP of the  $\gamma$ -benzyl-L-glutamate NCA (Scheme 2.10). It has good solubility in strong polar solvents like DMF, THF, DMSO and DMAc where it exists in a highly ordered  $\alpha$ -helical conformation, held intact *via* intramolecular hydrogen bonds. The interest in PBLG lies in the ability to alter the solubility of the polypeptide *via* the selective removal of the benzyl groups. This effectively means that the polypeptide can be hydrolyzed to allow increased solubility in aqueous conditions or *via* ester exchange reactions to introduce various functionalities on the backbone<sup>44</sup> or graft synthetic polymers to produce amphiphilic graft copolymers.<sup>66,67</sup>



Scheme 2.10 NCA ROP of Poly( $\gamma$ -benzyl-L-glutamate).

Furthermore, its hydrophobic character,  $\alpha$ -helical conformation as well as the inherent biological advantages it has over normal synthetic polymers makes it ideal for biomedical applications. In the past, there were limited applications due to the difficulty in synthesizing narrowly dispersed, well-defined polypeptides. However, as explained in section 2.4.3, a lot of work has been done to overcome these problems and essentially allow their potential to be unlocked. In the case of PBLG, Habraken *et al.*<sup>54,68</sup> have shown the influence of temperature and pressure on the control over the polymerization and they optimized conditions to minimize possible side reactions while still retaining the active chain-ends.

## 2.5 Self-assembly of amphiphilic block copolymers

The self-assembling properties of conjugates which incorporate water-soluble polymeric modifiers include polymer-drug conjugates,<sup>69</sup> polymer-protein bioconjugates<sup>70,71</sup> and amphiphilic block copolymers. The latter of which are able to transport hydrophobic drugs using physical or chemical encapsulation.<sup>72</sup>

The main purpose of this combinatorial science is to increase the therapeutic effectiveness of water-insoluble drugs by increasing the residence time of the drug delivery vehicle in the desired environment. This (could) result(s) in better targeting as well as an improvement in the solubilization of the drug either *via* complexation or encapsulation.

### 2.5.1 Polymeric micelles

Polymeric micelles are self-assembled, three-dimensional structures, typically formed from AB type amphiphilic block copolymers. The hydrophobic (apolar) and hydrophilic (polar) segments of a chain generally have a large solubility difference thereby promoting the self-assembly into core-shell type nanostructures. These nanoscopic structures form in two distinct layers as an inner core and an outer shell (Fig 2.6). The outer shell forms as the hydrophilic, hydrated layer which encompasses the inner core of polymer chains associated *via* cohesive interactions which include ionic interaction, hydrophobic interaction and hydrogen bonding.<sup>73</sup>

The micellization process starts when the concentration of the block copolymers are greater than a certain threshold concentration known as the critical micelle concentration (CMC), which will be dependent on e.g. the solvent, temperature and type of block copolymers.

The solubilization and entrapment of poorly soluble drugs into the micellar core are either due to chemical conjugation or physical entrapment. Chemical conjugation has the advantage of higher drug loading as well as sustained release of the drug. Linkages which allow for enzymatic cleavage or hydrolysis are usually necessary as the incorporated drug will mostly be inactive when conjugated to the polymer chains of the hydrophobic inner core.<sup>74,75</sup> The extent of physical entrapment is largely dependent on the compatibility of the hydrophobic drug with the polymer chains that form the inner micellar core. The advantage of this method is that the effectiveness of the drug is not altered, as is usually the case with chemical conjugation. Generally,



the drug release mechanism is simpler, *i.e.* the drug will either diffuse out of the core or will be released upon dissociation of the micelles when the concentration becomes lower than the CMC.

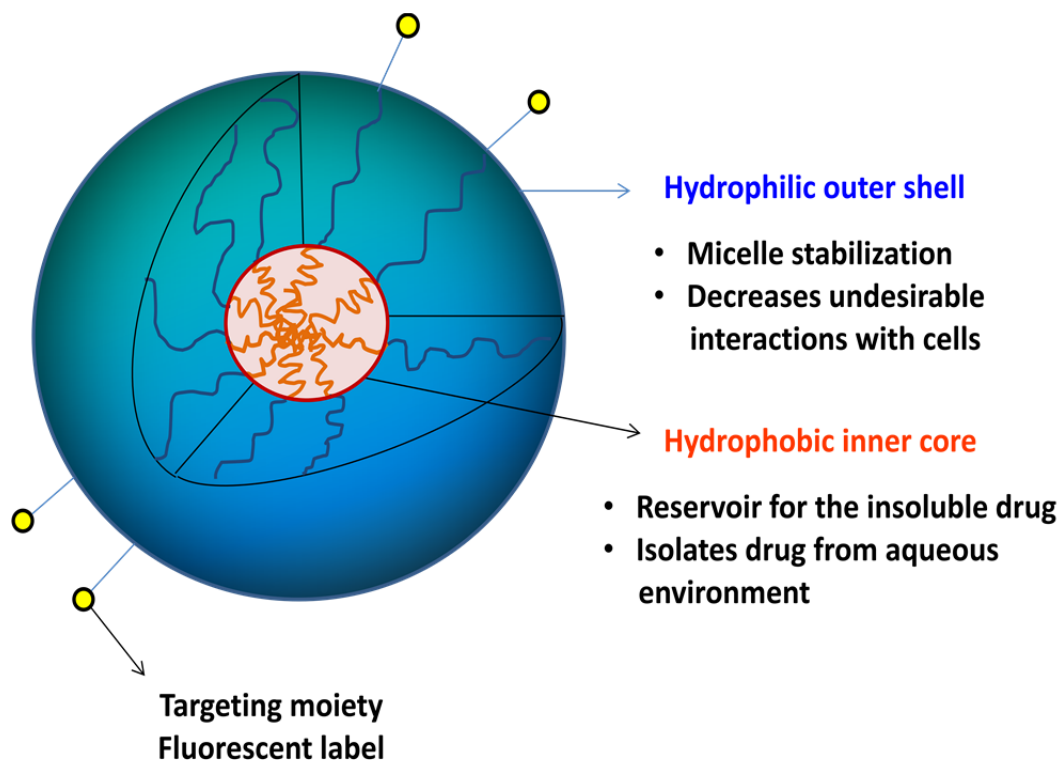


Figure 2.5 The different components of a micelle after the self-assembly of the amphiphilic block copolymers.

### 2.5.2 The EPR effect

The major advantage of using macromolecular DDS is the *enhanced permeability and retention* (EPR) effect as first reported by Matsumura and Maeda in 1986.<sup>76</sup> A lot of research has been done by Maeda *et al.* on the EPR effect<sup>77-79</sup> as well as on ways to exploit the EPR effect with polymeric drugs and subsequently optimizing the efficiency of tumor-targeted DDS.

The enhanced permeability and retention effect is found in solid tumors where the endothelium of blood vessels is damaged and cause an increased permeability through the compromised physical barrier (Fig. 2.8). It is this vascular permeability that ensures the tumor of a constant supply of nutrients and oxygen. Furthermore, the absence of effective drainage from tumors allows macromolecules (MW > 40 kDa) to permeate through the tumor vessels and accumulate in the tumor tissues.<sup>11-14</sup> This is in contrast with lower molecular weight compounds which are cleared from

the plasma and excreted *via* the renal system thus eliminating any potential treatment that native anti-cancer drugs could achieve.

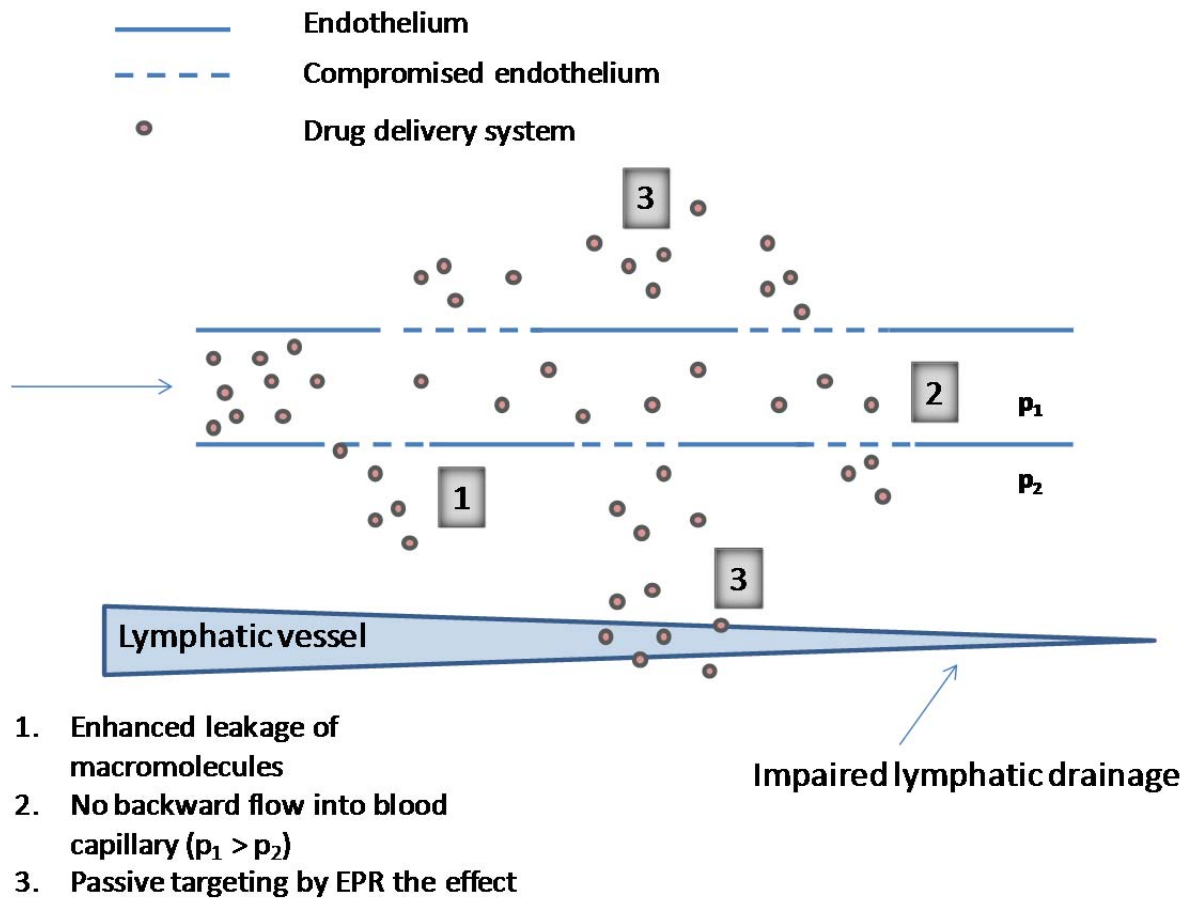


Figure 2.6 Passive targeting of micelles by the EPR effect, utilizing the compromised endothelial cells of tumor blood vessels. Nanoparticles take advantage of this leaky vasculature to accumulate into the tumor tissues while the absence of effective lymphatic drainage contributes to this retention.

The EPR effect provides a means to develop polymeric micelles as nanovehicles in these DDS. Anti-cancer drugs can be incorporated inside the micellar core where their diameter can be engineered in the range of 20-100 nm to stop penetration through normal (healthy) blood vessel walls. This essentially minimizes drug related side effects as the EPR effect promotes greater tumor selectivity, thereby reducing the drug distribution in the body. Currently, various polymeric micelle systems are undergoing clinical trials, which may be cleared for clinical use in the near future.<sup>80,81</sup>

## 2.6 References

- (1) Moad, G.; Rizzardo, E.; Thang, S. H. *Acc. Chem. Res.* **2008**, *41*, 1133-1142.
- (2) Julien, N.; Giuseppe, M.; David, M. H. *Macromol. Rapid Commun.* **2007**, *28*, 1083-1111.
- (3) Braunecker, W. A.; Matyjaszewski, K. *Prog. Polym. Sci.* **2007**, *32*, 93-146.
- (4) Hawker, C. J.; Bosman, A. W.; Harth, E. *Chem. Rev. (Washington, DC, U. S.)* **2001**, *101*, 3661-3688.
- (5) Xia, J.; Matyjaszewski, K. *Macromolecules* **1997**, *30*, 7692-7696.
- (6) Barner-Kowollik, C.; Buback, M.; Charleux, B.; Coote, M. L.; Drache, M.; Fukuda, T.; Goto, A.; Klumperman, B.; Lowe, A. B.; McLeary, J. B.; Moad, G.; Monteiro, M. J.; Sanderson, R. D.; Tonge, M. P.; Vana, P. *J. Polym. Sci., Part A: Polym. Chem.* **2006**, *44*, 5809-5831.
- (7) Moad, G.; Rizzardo, E.; Thang, S. H. *Aust. J. Chem.* **2005**, *58*, 379-410.
- (8) Moad, G.; Rizzardo, E.; Thang, S. H. *Aust. J. Chem.* **2009**, *62*, 1402-1472.
- (9) Le, T. P. M., G.; Rizzardo, E.; Thang, S. H. *PCT Int. Appl. WO.* **98/01478** **1998**.
- (10) Rhodia Chimie: Corpart, P. C., D.; Biadatti, T.; Zard, S.Z.; Michelet, D.; *PCT Int. Appl. WO.* **9858974** **1998**.
- (11) Perrier, S.; Takolpuckdee, P. *J. Polym. Sci., Part A: Polym. Chem.* **2005**, *43*, 5347-5393.
- (12) Darling, T. R.; Davis, T. P.; Fryd, M.; Gridnev, A. A.; Haddleton, D. M.; Ittel, S. D.; Matheson, R. R.; Moad, G.; Rizzardo, E. *J. Polym. Sci., Part A: Polym. Chem.* **2000**, *38*, 1706-1708.

## Chapter 2: Historical and Theoretical background

- (13) Penczek, S. *J. Polym. Sci., Part A: Polym. Chem.* **2002**, *40*, 1665-1676.
- (14) Penczek, S.; Moad, G. *Pure Appl. Chem.* **2008**, *80*, 2163(31).
- (15) Moad, G.; Rizzardo, E.; Thang, S. H. *Polymer* **2008**, *49*, 1079-1131.
- (16) Benaglia, M.; Chiefari, J.; Chong, Y. K.; Moad, G.; Rizzardo, E.; Thang, S. H. *J. Am. Chem. Soc.* **2009**, *131*, 6914-6915.
- (17) Destarac, M.; Brochon, C.; Catala, J.-M.; Wilczewska, A.; Zard, S. Z. *Macromol. Chem. Phys.* **2002**, *203*, 2281-2289.
- (18) McLeary, J. B.; McKenzie, J. M.; Tonge, M. P.; Sanderson, R. D.; Klumperman, B. *Chem. Commun. (Cambridge, U. K.)* **2004**, 1950-1951.
- (19) Vana, P.; Davis, T. P.; Barner-Kowollik, C. *Macromol. Theory Simul.* **2002**, *11*, 823-835.
- (20) Haaf, F.; Sanner, A.; Straub, F. *Polym. J. (Tokyo, Jpn.)* **1985**, *17*, 143-152.
- (21) Pasut, G.; Veronese, F. M. *Prog. Polym. Sci.*, *32*, 933-961.
- (22) Duncan, R.; Ringsdorf, H.; Satchi-Fainaro, R. *J. Drug Targeting* **2006**, *14*, 337-341.
- (23) Kaneda, Y.; Tsutsumi, Y.; Yoshioka, Y.; Kamada, H.; Yamamoto, Y.; Kodaira, H.; Tsunoda, S.-i.; Okamoto, T.; Mukai, Y.; Shibata, H.; Nakagawa, S.; Mayumi, T. *Biomaterials* **2004**, *25*, 3259-3266.
- (24) D'Souza, A. J. M.; Schowen, R. L.; Topp, E. M. *J. Controlled Release* **2004**, *94*, 91-100.
- (25) Luo, L.; Ranger, M.; Lessard, D. G.; Le Garrec, D. e.; Gori, S.; Leroux, J.-C.; Rimmer, S.; Smith, D. *Macromolecules* **2004**, *37*, 4008-4013.
- (26) Godwin, A.; Hartenstein, M.; Müller, A. H. E.; Brocchini, S. *Angew. Chem., Int. Ed.* **2001**, *40*, 594-597.

## Chapter 2: Historical and Theoretical background

- (27) Matyjaszewski, K.; Beers, K. L.; Kern, A.; Gaynor, S. G. *J. Polym. Sci., Part A: Polym. Chem.* **1998**, *36*, 823-830.
- (28) Lu, X.; Gong, S.; Meng, L.; Li, C.; Yang, S.; Zhang, L. *Polymer* **2007**, *48*, 2835-2842.
- (29) Ray, B.; Kotani, M.; Yamago, S. *Macromolecules* **2006**, *39*, 5259-5265.
- (30) Yamago, S. *Chem. Rev. (Washington, DC, U. S.)* **2009**, *109*, 5051-5068.
- (31) Yusa, S.-i.; Yamago, S.; Sugahara, M.; Morikawa, S.; Yamamoto, T.; Morishima, Y. *Macromolecules* **2007**, *40*, 5907-5915.
- (32) Yan, Y.; Zhang, W.; Qiu, Y.; Zhang, Z.; Zhu, J.; Cheng, Z.; Zhang, W.; Zhu, X. *J. Polym. Sci., Part A: Polym. Chem.*, *48*, 5206-5214.
- (33) Bilalis, P.; Pitsikalis, M.; Hadjichristidis, N. *J. Polym. Sci., Part A: Polym. Chem.* **2006**, *44*, 659-665.
- (34) Wan, D.; Satoh, K.; Kamigaito, M.; Okamoto, Y. *Macromolecules* **2005**, *38*, 10397-10405.
- (35) Postma, A.; Davis, T. P.; Li, G.; Moad, G.; O'Shea, M. S. *Macromolecules* **2006**, *39*, 5307-5318.
- (36) Pound, G.; McLeary, J. B.; McKenzie, J. M.; Lange, R. F. M.; Klumperman, B. *Macromolecules* **2006**, *39*, 7796-7797.
- (37) Pound, G.; Eksteen, Z.; Pfukwa, R.; McKenzie, J. M.; Lange, R. F. M.; Klumperman, B. *J. Polym. Sci., Part A: Polym. Chem.* **2008**, *46*, 6575-6593.
- (38) Pound-Lana, G.; Klumperman, B. In *Controlled/Living Radical Polymerization: Progress in RAFT, DT, NMP & OMRP*; American Chemical Society: 2009; Vol. 1024, p 167-179.
- (39) Marsden, H. R.; Handgraaf, J.-W.; Nudelman, F.; Sommerdijk, N. A. J. M.; Kros, A. *J. Am. Chem. Soc.*, *132*, 2370-2377.
- (40) Merrifield, B. *Science* **1986**, *232*, 341-347.

## Chapter 2: Historical and Theoretical background

- (41) Hadjichristidis, N.; Iatrou, H.; Pitsikalis, M.; Sakellariou, G. *Chem. Rev. (Washington, DC, U. S.)* **2009**, *109*, 5528-5578.
- (42) Deming, T. J. *Nature* **1997**, *390*, 386.
- (43) Tang, H.; Zhang, D. *Biomacromolecules*, *11*, 1585-1592.
- (44) Guo, J.; Huang, Y.; Jing, X.; Chen, X. *Polymer* **2009**, *50*, 2847-2855.
- (45) Vayaboury, W.; Giani, O.; Cottet, H.; Deratani, A.; Schué, F. *Macromol. Rapid Commun.* **2004**, *25*, 1221-1224.
- (46) Gibson, M. I.; Cameron, N. R. *J. Polym. Sci., Part A: Polym. Chem.* **2009**, *47*, 2882-2891.
- (47) Deming, T. J. *J. Polym. Sci., Part A: Polym. Chem.* **2000**, *38*, 3011-3018.
- (48) Papadopoulos, P.; Floudas, G.; Klok, H. A.; Schnell, I.; Pakula, T. *Biomacromolecules* **2003**, *5*, 81-91.
- (49) Kricheldorf, H. R. *Angew. Chem., Int. Ed.* **2006**, *45*, 5752-5784.
- (50) Peggion, E.; Cosani, A.; Mattucci, A. M.; Scoffone, E. *Biopolymers* **1964**, *2*, 69-78.
- (51) Vayaboury, W.; Giani, O.; Cottet, H.; Bonaric, S.; Schué, F. *Macromol. Chem. Phys.* **2008**, *209*, 1628-1637.
- (52) Kricheldorf, H. R.; von Lossow, C.; Schwarz, G. *Macromolecules* **2005**, *38*, 5513-5518.
- (53) Pickel, D. L.; Politakos, N.; Avgeropoulos, A.; Messman, J. M. *Macromolecules* **2009**, *42*, 7781-7788.
- (54) Habraken, G. J. M.; Wilsens, K. H. R. M.; Koning, C. E.; Heise, A. *Polymer Chemistry*, *2*, 1322-1330.
- (55) Audouin, F.; Knoop, R. J. I.; Huang, J.; Heise, A. *J. Polym. Sci., Part A: Polym. Chem.*, *48*, 4602-4610.

## Chapter 2: Historical and Theoretical background

- (56) Knoop, R. J. I.; Habraken, G. J. M.; Gogibus, N.; Steig, S.; Menzel, H.; Koning, C. E.; Heise, A. *J. Polym. Sci., Part A: Polym. Chem.* **2008**, *46*, 3068-3077.
- (57) Gibson, M. I.; Cameron, N. R. *Angew. Chem., Int. Ed.* **2008**, *47*, 5160-5162.
- (58) Lecommandoux, S.; Achard, M.-F.; Langenwalter, J. F.; Klok, H.-A. *Macromolecules* **2001**, *34*, 9100-9111.
- (59) Babin, J.; Rodriguez-Hernandez, J.; Lecommandoux, S.; Klok, H.-A.; Achard, M.-F. *Faraday Discuss.* **2005**, *128*, 179-192.
- (60) Gkikas, M.; Iatrou, H.; Thomaidis, N. S.; Alexandridis, P.; Hadjichristidis, N. *Biomacromolecules*,
- (61) Holowka, E. P.; Pochan, D. J.; Deming, T. J. *J. Am. Chem. Soc.* **2005**, *127*, 12423-12428.
- (62) Iatrou, H.; Frielinghaus, H.; Hanski, S.; Ferderigos, N.; Ruokolainen, J.; Ikkala, O.; Richter, D.; Mays, J.; Hadjichristidis, N. *Biomacromolecules* **2007**, *8*, 2173-2181.
- (63) Sun, J.; Chen, X.; Deng, C.; Yu, H.; Xie, Z.; Jing, X. *Langmuir* **2007**, *23*, 8308-8315.
- (64) Osada, K.; Christie, R. J.; Kataoka, K. *Journal of The Royal Society Interface* **2009**, *6*, S325-S339.
- (65) Heffernan, M.; Murthy, N. *Annals of Biomedical Engineering* **2009**, *37*, 1993-2002.
- (66) Tang, D.; Lin, J.; Lin, S.; Zhang, S.; Chen, T.; Tian, X. *Macromol. Rapid Commun.* **2004**, *25*, 1241-1246.
- (67) Yi, J.; Zhou, X.; Hu, G.; Wang, B. *Polymer Science Series B*, *52*, 35-40.
- (68) Habraken, G. J. M.; Peeters, M.; Dietz, C. H. J. T.; Koning, C. E.; Heise, A. *Polymer Chem.* , *1*, 514-524.
- (69) Pasut, G.; Veronese, F. M. *Prog. Polym. Sci.* **2007**, *32*, 933-961.

## Chapter 2: Historical and Theoretical background

- (70) Heredia, K. L.; Maynard, H. D. *Org. Biomol. Chem.* **2007**, *5*, 45-53.
- (71) Nicolas, J.; Mantovani, G.; Haddleton, D. M. *Macromol. Rapid Commun.* **2007**, *28*, 1083-1111.
- (72) Croy, S. R.; Kwon, G. S. *Curr. Pharm. Des.* **2006**, *12*, 4669-4684.
- (73) Yokoyama, M.; Satoh, A.; Sakurai, Y.; Okano, T.; Matsumura, Y.; Kakizoe, T.; Kataoka, K. *J. Controlled Release* **1998**, *55*, 219-229.
- (74) Kwon, G.; Naito, M.; Yokoyama, M.; Okano, T.; Sakurai, Y.; Kataoka, K. *J. Controlled Release* **1997**, *48*, 195-201.
- (75) Kataoka, K.; Harada, A.; Nagasaki, Y. *Adv. Drug Delivery Rev.* **2001**, *47*, 113-131.
- (76) Matsumura, Y.; Maeda, H. *Cancer Res.* **1986**, *46*, 6387-6392.
- (77) Maeda, H.; Wu, J.; Sawa, T.; Matsumura, Y.; Hori, K. *J. Controlled Release* **2000**, *65*, 271-284.
- (78) Maeda, H. *Advances in Enzyme Regulation* **2001**, *41*, 189-207.
- (79) Maeda, H.; Bharate, G. Y.; Daruwalla, J. *Eur. J. Pharm. Biopharm.* **2009**, *71*, 409-419.
- (80) Duncan, R. *Nat. Rev. Drug Discovery* **2003**, *2*, 347.
- (81) Matsumura, Y.; Kataoka, K. *Cancer Sci.* **2009**, *100*, 572-579.



## **RAFT mediated polymerization of *N*-vinylpyrrolidone and end-group modification of xanthate end-functional PVP**

### **3.1 Introduction**

In this chapter the experimental conditions for the homopolymerization of NVP are discussed along with the characterization methods used to determine molecular weight, dispersity ( $\mathcal{D}$ ) and end-group functionality. Furthermore, the conditions are optimized for end-group modifications of the homopolymer along with characterization of the introduced chain-end functionalities.

As discussed in chapter two, certain problems arise when trying to polymerize *N*-vinylpyrrolidone (NVP) into well-defined, narrowly dispersed PVP. This is mostly due to the reactivity of the propagating radical which readily forms the intermediate radical adduct and thus needs a destabilizing factor to promote fragmentation. Yan and Postma<sup>1,2</sup> have shown that xanthate-mediated polymerization ensures the best control over the polymerization of NVP. Essentially this is due to the relatively low reactivity of the thiocarbonyl (C=S) bond, where the double bond's affinity for radical addition is suppressed by the presence of the lone pair of electrons on the adjacent oxygen atom (Scheme 2.6), which allows for the efficient addition of poorly stabilized propagating radicals. Upon radical addition, the increase of the electron density at the radical centre results in the destabilization of the intermediate radical adduct. The lone pair of electrons induct towards the adduct radical which destabilizes it and leads to fragmentation. The destabilization leads to a more dynamic equilibrium effectively increasing the control one can obtain.<sup>3,4</sup>

Furthermore, the choice of the R-group can be optimized for characterization purposes, *i.e.* act as a tag or reference to allow for a facile method of quantifying or identifying polymeric chains. It is however necessary that the R-group still acts as an efficient leaving group for the specific monomer to successfully reinitiate the polymerization.

The synthesis of well-defined end-functional polymers is necessary to ensure effective and quantitative conjugation of the homopolymer poly(*N*-vinylpyrrolidone) (PVP) to a hydrophobic polypeptide for the eventual purpose of forming amphiphilic block copolymers. Bioinert polymers such as PVP hold special interest in the biomedical field and more so in drug delivery systems (DDS) due to its water-soluble,

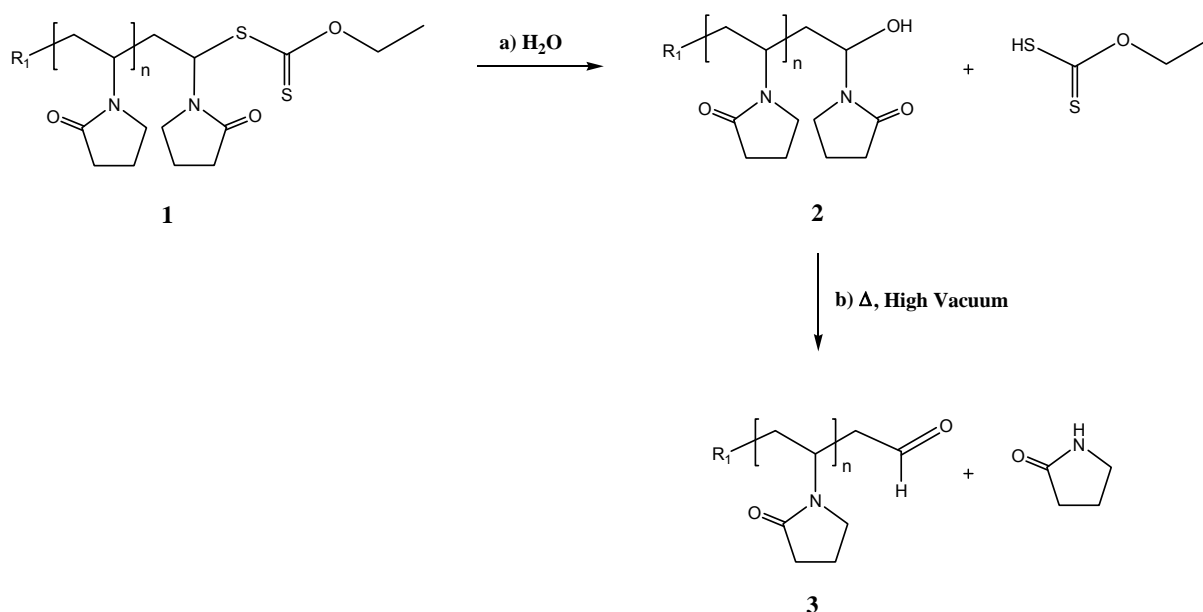
non-ionic and non-toxic nature.<sup>5</sup> The difficulty in synthesizing polymers with adequate end-functionalities for further conjugation or chain extension has in general been overcome in recent years due to the multitude of synthetic tools available.<sup>6</sup>

More specifically, in the present case the use of reversible addition-fragmentation chain transfer (RAFT) mediated polymerization allows for the post-polymerization modification of polymers. This is due to the presence of the labile thiocarbonyl thio moiety. Previously, it has been shown that the thiocarbonyl thio moiety can be converted to a free thiol in the presence of a primary or secondary amine, *i.e. via* aminolysis.<sup>7</sup> Qui *et al.*<sup>8</sup> have reported the synthesis of  $\alpha$ ,  $\omega$ -hydroxy telechelic polymers *via* a facile one pot reaction. A difunctional RAFT agent was used to mediate the polymerization whereby aminolysis and Michael addition of a hydroxyl containing acrylate were performed sequentially to obtain a telechelic polymer chain.

When using xanthates as the RAFT CTA for the polymerization of NVP, one has the benefit to modify the  $\omega$  end-group under moderate conditions. This includes the formation of thiol-terminated PVP by cleaving the thiocarbonyl thio moiety resulting in reversible disulfide linkages, readily cleaved using DTT.<sup>9</sup> Pound *et al.*<sup>10</sup> have shown that the xanthate functionality can be completely removed *via* post-polymerization modification of the using a facile hydrolysis technique resulting in aldehyde end-functional PVP. This allows for easy conjugation to polypeptides to produce non-reducible polymer-protein conjugates

The formation of aldehyde end-groups during conventional free radical polymerization of NVP with hydrogen peroxide was reported as a side product.<sup>11</sup> Pound *et al.*<sup>10</sup> have shown that it is possible to obtain an aldehyde end-functionality from the thiocarbonyl thio end-group to near quantitative conversion. Quantification with <sup>1</sup>H-NMR spectroscopy proved that the conversion to end-functional aldehyde corresponds to 90% of the chain-ends. The aldehyde formation is depicted in Scheme 3.1.

## Chapter 3: PVP Synthesis and Modification reactions



Scheme 3.1 Modification of PVP xanthate chain-ends into hydroxyl and aldehyde end-groups.

Optimization of the conditions for the synthesis of the  $\omega$ -aldehyde end-functional PVP was conducted to see whether it is possible to improve the fraction of functional chain-ends finally obtained.

### 3.2 Experimental

#### 3.2.1 Materials

Potassium *O*-ethyl xanthate (95 %, Merck), diethyl *meso*-2,5-dibromo adipate (98 %, Sigma-Aldrich), tryptamine (> 99%, Sigma-Aldrich), 2-bromopropionyl bromide (97%, Fluka), sodium hydroxide (Saarchem), triethylamine ( $\geq 98$  %, Fluka) and magnesium sulphate (anhydrous) (Merck) were used as received.

Tetrahydrofuran (THF) (dried Seccosolv™), diethyl ether (dried, Seccosolv™), *n*-pentane (for synthesis) and triethylamine (for synthesis) were all purchased from Merck and used as is. Chloroform (KIMIX, CP-grade, 99.5 %.), dichloromethane (DCM, KIMIX, CP-grade, 99.5 %.) and ethanol (KIMIX, CP-grade, 99.5 %) were dried over molecular sieves (4 Å, 1.6 mm pellet). Hydrochloric acid (HCl, 37 %) and ethyl acetate (anhydrous, 99.8 %) were purchased from Sigma-Aldrich and used without further purification.

2,2-Azobis(isobutronitrile) (AIBN) was recrystallized twice from methanol. Phosphate buffered saline tablets (Merck) were used to make up a PBS solution. Distillation of NVP was performed under reduced pressure ( $< 1$  mbar) at  $74$  °C.

### 3.2.2 RAFT CTA synthesis

#### 3.2.2.1 Fluorescent tagged RAFT CTA, X21 (1)

The RAFT CTA, X21 was predominantly used to synthesize the PVP homopolymer for the purpose of our study as it incorporates a fluorescent tag at the  $\alpha$ -chain-end which allows for simpler characterization and quantification of any PVP chain conjugated to an enzyme or polypeptide (Figure 3.1).

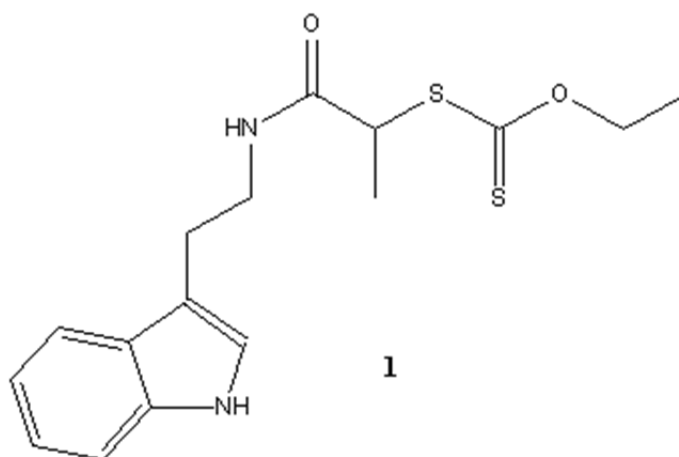
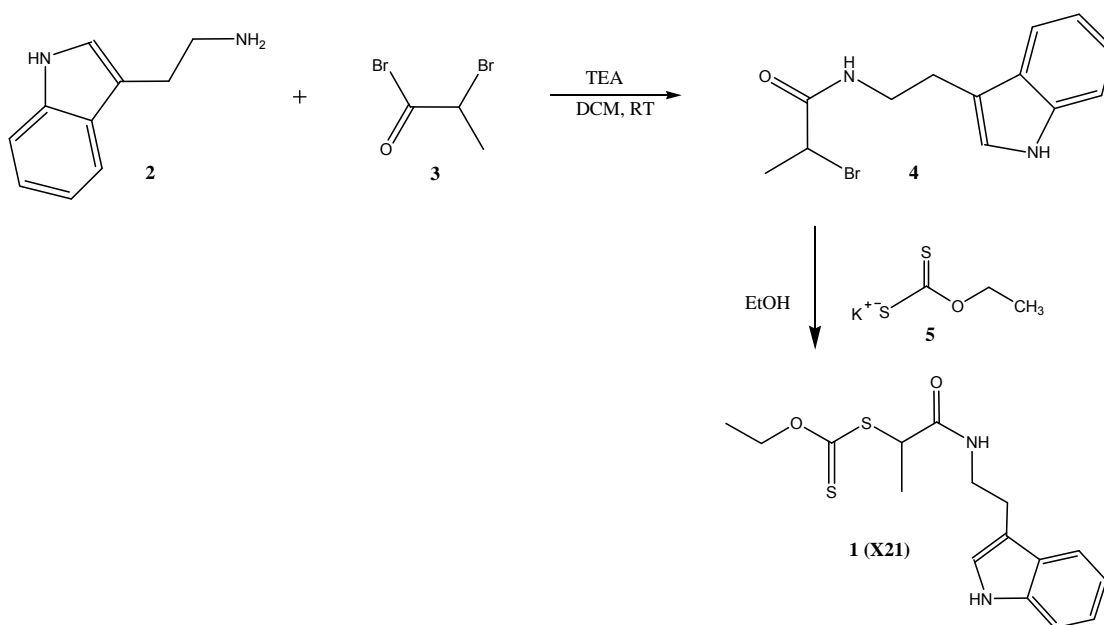


Figure 3.1 RAFT CTA for LRP of NVP with fluorescent moiety (X21).

The RAFT agent is an *O*-ethyl xanthate with a tryptamine-based R-group. This allows for a PVP homopolymer, which can be excited at 283 nm and emits at 350 nm. In general, increased steric bulk of the R-group is likely to increase its leaving ability but also have a negative effect on the reinitiating capability due to steric hindrance.

The xanthate was prepared in good yields with an optimized method based on a procedure previously used in our group (Scheme 3.2). It is a two-step reaction with purification done *via* a simple crystallization step for the fluorescent functional alkylating agent (4), before reacting it with the *O*-ethyl xanthate salt to produce the RAFT CTA (1), which was subsequently purified *via* column chromatography.

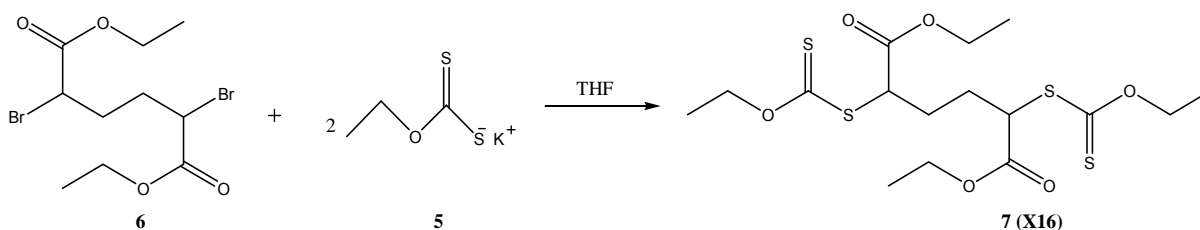
## Chapter 3: PVP Synthesis and Modification reactions



Scheme 3.2 Synthesis of fluorescent tagged RAFT CTA, X21 (1).

## 3.2.2.2 Difunctional RAFT CTA, X16 (7)

For the purpose of engineering triblock copolymers, RAFT CTA X16 (7) was synthesized that could then be used to mediate the polymerization of NVP, resulting in a difunctional PVP homopolymer. Xanthate 7 (Scheme 3.2) was readily prepared in a one-pot reaction, with minimal purification required. Due to the commercial availability of both the xanthate salt (5) and the dihalide alkylating agent (6) the reaction is a simple nucleophilic substitution reaction which produces 7 in yields > 75%.



Scheme 3.3 Synthesis of the difunctional RAFT CTA, X16 (7).

### 3.2.2.3 Synthesis of *N*-(2-(1*H*-indol-3-yl)ethyl)-2-bromopropanamide (4)

Tryptamine (2.013 g, 12.56 mmol) and triethylamine (1.904 g, 18.81 mmol) were dissolved in dichloromethane (20 mL) in a round bottom flask. The flask was cooled with an ice bath while 2-bromopropionyl bromide (2.413 g, 11.18 mmol) was dissolved in dichloromethane (DCM) (10 mL) and added dropwise *via* a dropping funnel over approximately 10 min to the tryptamine solution. After the complete addition of the bromide solution, the ice bath was removed and the solution left stirring at room temperature for 16 hours. The reaction was stopped and a dark brown solution with a white precipitate ( $\text{Et}_3\text{N}^+\text{HBr}^-$ ) had formed, which was filtered off. Diethyl ether (200 mL) was added to the filtrate, which resulted in a heterogeneous solution, this cleared to an orange solution after an initial wash with 50 mL 1M HCl. The solution was then washed with a further 50 mL 1M HCl, 1M aqueous NaOH (50 mL) and finally with distilled water (50 mL) after which the solution was dried over anhydrous magnesium sulphate. The solvent was removed *via* rotary evaporation under high vacuum, resulting in a crystalline orange solid, which was subsequently redissolved in ethyl acetate and recrystallized from DCM. The product was left in the refrigerator overnight to ensure complete recrystallization. Yield: 2.53 g, 8.57 mmol, 68%.

$^1\text{H}$  NMR (300 MHz,  $\text{CDCl}_3$ ,  $\delta$ , ppm): 8.26 (s, 1H, -CHNH), 7.60 (m, 1H, ArH), 7.37 (m, 1H, ArH), 7.26 – 7.08 (m, 2H, ArH), 7.02 (t, 1H, -CHNH), 6.46 (s, 1H, -CO<sub>2</sub>NH), 4.30 (m, 1H, -CH(CH<sub>3</sub>)Br), 3.60 (m, 2H, -NHCH<sub>2</sub>), 2.99 (t, 2H, -NHCH<sub>2</sub>CH<sub>2</sub>), 1.82 (d, 3H, -CH<sub>3</sub>(CH)Br).

### 3.2.2.4 Synthesis of *S*-(1-((2-(1*H*-indol-3-yl)ethyl)amino)-1-oxopropan-2-yl) *O*-ethyl carbonodithioate (1)

The alkylating agent (4, 2.50 g, 8.47 mmol) was dissolved in 25 mL of dry ethanol and potassium *O*-ethyl xanthate (1.81 g, 11.23 mmol) was added and left stirring for 30 hours. A white precipitate was filtered off and the filtrate concentrated *via* rotary evaporation under vacuum. The viscous solution was diluted with 250 mL of diethyl ether. A white precipitate formed, but was removed after washing with water (4x50 mL) as it dissolved in the aqueous phase. The organic phase was dried over anhydrous magnesium sulphate and the solvent evaporated by rotary evaporation

under high vacuum. 2.91 g of a highly viscous orange product was obtained and purified *via* column chromatography using an initial solvent system of ethyl acetate: pentane in a 60:40 *v/v* ratio, while gradually increasing the percentage of ethyl acetate. The solvent was then evaporated under high vacuum, which resulted in 2.18 g of an orange yellow product, which was identified as the final product *via*  $^1\text{H-NMR}$  spectroscopy. Yield = 2.18 g, 6.48 mmol, 76%.

$^1\text{H NMR}$  (300 MHz,  $\text{CDCl}_3$ ,  $\delta$ , ppm): 8.18 (s, 1H, -CHNH), 7.60 (m, 1H, ArH), 7.37 (m, 1H, ArH), 7.24 – 7.07 (m, 2H, ArH), 7.01 (d, 1H, -CHNH), 6.39 (s, 1H, -CO<sub>2</sub>NH), 4.50 (m, 2H, (-OCH<sub>2</sub>CH<sub>3</sub>)), 4.30 (m, 1H, -CH(CH<sub>3</sub>)S), 3.60 (m, 2H, -NHCH<sub>2</sub>), 2.97 (t, 2H, -NHCH<sub>2</sub>CH<sub>2</sub>), 1.50 (m, 3H, -CH<sub>3</sub>(CH)S), 1.33 (t, 3H, -CHCH<sub>3</sub>).

### 3.2.2.5 Synthesis of diethyl 2,5-bis((ethoxycarbonothioyl)thio)hexanedioate (7)

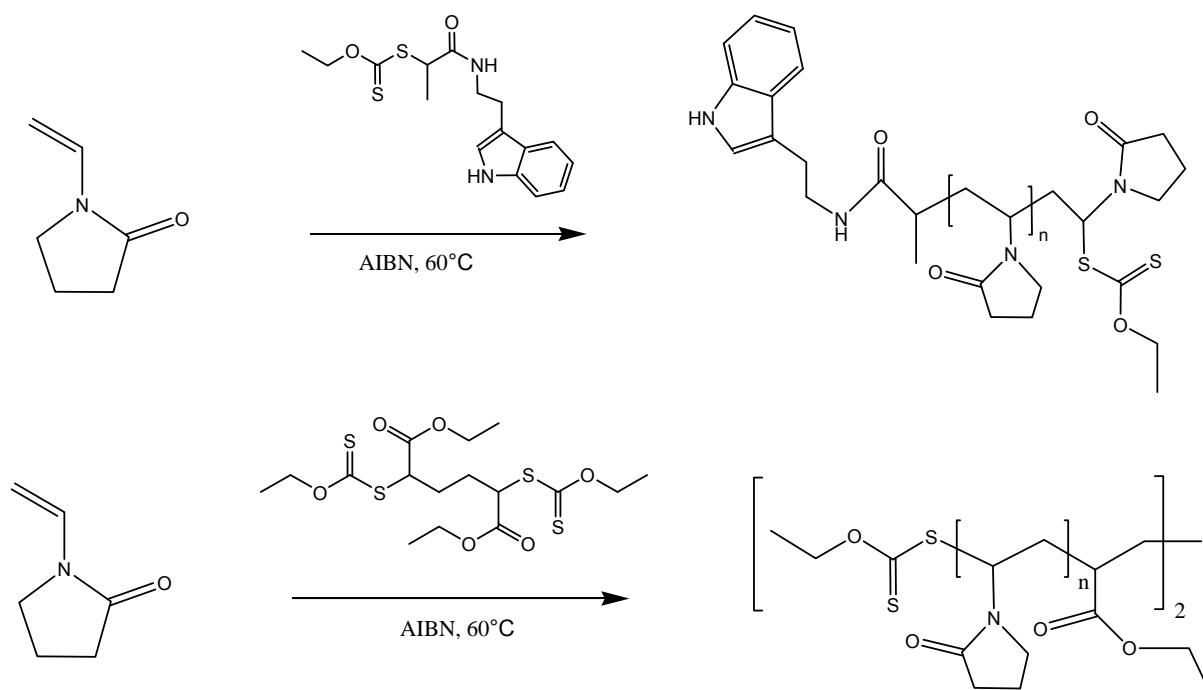
Diethyl 2,5 dibromoadipate (2.05 g, 5.5 mmol) was added to 30 mL THF in a 100 mL round bottom flask at 0 °C. Potassium *O*-ethyl xanthate (2.11 g, 13.2 mmol) was added to the reaction flask, closed off and the reaction allowed to proceed for 22 hours at room temperature. A precipitate was filtered off and the product concentrated after which it was diluted with 300 mL diethyl ether. The ethereal phase was washed with NaCl solution (2 x 100 mL) and distilled water (3 x 50 mL). The organic phase was dried over anhydrous magnesium sulphate. The solvent was removed *via* rotary evaporation and placed under high vacuum for further purification. The product crystallized out completely when left in the refrigerator overnight and  $^1\text{H-NMR}$  spectra showed a clean difunctional RAFT agent with no further purification necessary. 1.91 g of the product was obtained (Yield = 78%).

$^1\text{H NMR}$  (300 MHz,  $\text{CDCl}_3$ ,  $\delta$ , ppm): 4.64 (q, 4H, -(CO)OCH<sub>2</sub>CH<sub>3</sub>), 4.44 – 4.33 (m, 2H, CH), 4.21 (q, 4H, -(CS)OCH<sub>2</sub>CH<sub>3</sub>), 2.23 – 1.90 (m, 4H, CH<sub>2</sub>), 1.42 (t, 6H, -(CO)OCH<sub>2</sub>CH<sub>3</sub>), 1.29 (t, 6H, -(CS)OCH<sub>2</sub>CH<sub>3</sub>).

### 3.2.3 General polymerization procedure

The general procedure for the RAFT-mediated LRP of NVP using X21 and X16 as the RAFT CTAs are described (Scheme 3.4).

## Chapter 3: PVP Synthesis and Modification reactions



**Scheme 3.4** General polymerization procedure for NVP at 60°C with AIBN as the initiator. X21 and X16 are used as the CTAs for the top and bottom reaction respectively.

The polymerizations of NVP using CTAs X16 and X21 were carried out in pear-shaped 50 mL Schlenk flasks. The reaction mixtures were thoroughly degassed *via* successive freeze-pump-thaw cycles, backfilled with argon and subsequently sealed before immersing the flask into a preheated oil bath. The polymerization was typically left to proceed for five times the half-life of the initiator, which in the case for AIBN at 60 °C is roughly 6 - 7 hours or until the reaction mixture was very viscous and hampered stirring. The molar ratio of the RAFT CTA to initiator was kept at approximately 5:1. Isolation of the product was done by precipitation in diethyl ether as the non-solvent using the ratio of polymer: solvent: non-solvent (*i.e.* polymer: dichloromethane: diethyl ether) as 1:5:50. The molar ratio of monomer to RAFT CTA was calculated from Equation 3.1.1 and adjusted with the knowledge that a typical NVP bulk polymerization only achieves roughly 50% conversion before stirring is hampered and the high viscosity adversely affects the dispersity,  $\bar{D}$ . For example, when PVP with a molecular weight of 10 000 g/mol was targeted (*i.e.*  $DP_{\text{target}, 50\%} \sim 10\,000/111.1 = 90$ ), the ratio of  $[\text{monomer}]/[\text{RAFT CTA}]$  was adjusted to 180, this adjusted target was calculated with Equation 3.1.2.



Theoretical molecular weights ( $M_n^{\text{Theo}}$ ) were calculated using Equation 3.1.1,

$$M_n^{\text{Theo}} = \frac{[\text{monomer}]_0}{[\text{CTA}]_0} \times \text{conversion} \times Mr(\text{monomer}) + Mr(\text{CTA}) \quad 3.1.1$$

The targeted molecular weight was calculated with Equation 3.1.2 on the basis of a 50% conversion,

$$M_n^{50\%} = \frac{[\text{NVP}]_0}{[\text{CTA}]_0} \times 0.5 \times Mr(\text{NVP}) + Mr(\text{CTA}) \quad 3.1.2$$

$[\text{NVP}]_0$  ~ initial monomer concentration

$[\text{CTA}]_0$  ~ initial chain transfer agent concentration

$Mr(\text{NVP})$  ~ Molecular weight of monomer

$Mr(\text{CTA})$  ~ Molecular weight of chain transfer agent

### 3.2.3.1 X21-mediated homopolymerization of *N*-vinyl pyrrolidone

A typical polymerization of NVP proceeded as follows:

NVP (8 g,  $7.2 \times 10^{-2}$  mol), the CTA X21 (0.298 g,  $8.86 \times 10^{-4}$  mol) and AIBN (0.0291 g,  $1.77 \times 10^{-4}$  mol) were placed in a Schlenk flask and degassed *via* four freeze-pump-thaw cycles. Ultrahigh purity argon was introduced into the flask, the flask was sealed and immersed into a preheated oil bath thermostated at 60 °C. The reaction mixture was left under magnetic stirring for a 7 hour period during which the reaction mixture's viscosity increased greatly to the extent that stirring was difficult. The reaction was stopped by removing the flask from the oil bath, opening it and cooling it in an ice bath. The product, PVP, was then isolated by precipitation in diethyl ether twice and dried in a desiccator under reduced pressure. The amount of PVP recovered was 3.90 g with a conversion of 48%.

Samples were precipitated twice to remove as much monomer as possible, which typically results in sample loss, as low molecular weight chains may be lost on repeated precipitation steps resulting in an underestimation of conversion. Furthermore, some unreacted monomer is still evident in the final product as seen *via*  $^1\text{H-NMR}$  spectroscopy (Figure 3.2), which accounts for a certain weight percentage of the final product. Thus, this weight percentage of NVP was calculated and taken into account when calculating the conversion of the precipitated samples.

The experimental molecular weights were calculated *via*  $^1\text{H-NMR}$  spectroscopy as well as compared to results obtained *via* SEC, which was used to determine the  $\bar{M}$  of the homopolymer.

### 3.3 End-functional PVP

The general hydrolysis and thermolysis reaction conditions are described for the preparation of the aldehyde end-functional PVP.

#### 3.3.1 Preparation of hydroxyl end-functional PVP (2)

PVP- $X_{21}$  (3.5 g) was dissolved in distilled water (70 mL) and the solution (pH = 4.5, tested using pH-fix) was heated at 40 °C for 20 h. The solution was purified by dialysis against distilled water using SnakeSkin® pleated dialysis tubing (Pierce, molecular weight cut-off = 3500 g·mol<sup>-1</sup> dextran equivalents) for 24 h at room temperature. The solution was initially replaced three times every two hours and then every nine hours. The polymer with hydroxyl end-group (PVP-OH) was recovered by freeze-drying. 2.68 g of the product was isolated and identified *via*  $^1\text{H-NMR}$  spectroscopy.

#### 3.3.2 Preparation of aldehyde end-functional PVP (3)

PVP-OH (2.60 g, white flakes) was placed in a vacuum oven and heated at 120 °C (~1 mbar) for 20 h to yield PVP with aldehyde end-group (PVP-CHO) as identified by  $^1\text{H-}$  and  $^{13}\text{C-NMR}$  spectroscopy.

### 3.4 Analysis

#### 3.4.1 NMR

$^1\text{H}$  NMR and  $^{13}\text{C}$  NMR spectra were acquired with a Varian VXR-Unity (300 MHz) spectrometer in  $\text{CDCl}_3$  (unless specified otherwise). All chemical shifts are reported in parts per million (ppm) with tetramethylsilane (TMS) as an internal reference.

#### 3.4.2 Size exclusion chromatography (SEC)

SEC analysis at Stellenbosch University was carried out on a DMAc system using a flow rate of 1.0 mL/min. The instrument setup consisted of a Shimadzu, LC-10AD pump, a column system fitted with a 50x8 mm guard column in series with three

300x8 mm, 10  $\mu\text{m}$  particle size GRAM columns (2 x 3000Å and 100Å) obtained from PSS, a Waters 2487 dual wavelength UV detector and a Waters 2414 differential refractive index (DRI) detector all in series. 100  $\mu\text{L}$  injection volumes are sampled individually with the oven temperature of the column and DRI detector kept at 40 °C. The solvent was stabilized with 0.05% BHT (w/v) and 0.03% LiCl (w/v). Furthermore, samples were filtered through a 0.45  $\mu\text{m}$  GHP filter to prevent any impurities entering the system. Calibration was done using PMMA standard sets (Polymer Laboratories) ranging from 600 to  $1.2 \times 10^5$  g/mol. Data acquisition was done using Millennium<sup>32</sup> software, version 4.

### 3.4.3 ATR-FTIR

IR spectra were recorded using a Thermo-Nicolette iS10 FTIR with a ZnSe ATR attachment and a LC-transform attachment. This allowed the examination of samples in solid or liquid state without prior sample preparation. Spectra were recorded in the range of 500-4000  $\text{cm}^{-1}$ . Resolution was set to 8  $\text{cm}^{-1}$ , and 32 scans per sample. Omnic spectra software (version 8.1) was used for all data acquisition and processing.

### 3.4.4 MALDI-ToF-MS

MALDI-ToF-MS analysis was carried out on a Voyager-DE STR from Applied Biosystems. The laser frequency was 20 Hz, wavelength of 337 nm and a voltage of 25 kV. The matrix used was trans-2-[3-(4-tert-butylphenyl)-2-methyl-2-propenylidene]malononitrile (DCTB) (40 mg/mL). Potassium trifluoroacetic acid (KTFA) was added as cationic ionization agent (5 mg/mL). The sample was dissolved in HFIP (1 mg/mL). The matrix, cationization agent and sample solutions were added (5:1:5) and placed on the target plate and left to dry.

### 3.5 Results and discussion

#### 3.5.1 Chain-end analysis

3.5.1.1  $^1\text{H-NMR}$  analysis The configurational assignment of the PVP homopolymer, prepared *via* RAFT-mediated polymerization, was identified using  $^1\text{H-NMR}$  spectroscopy (Figure 3.2). This allowed for the qualitative and quantitative analysis of the homopolymer by characterizing chain-end functionality, conversion and molecular weight.

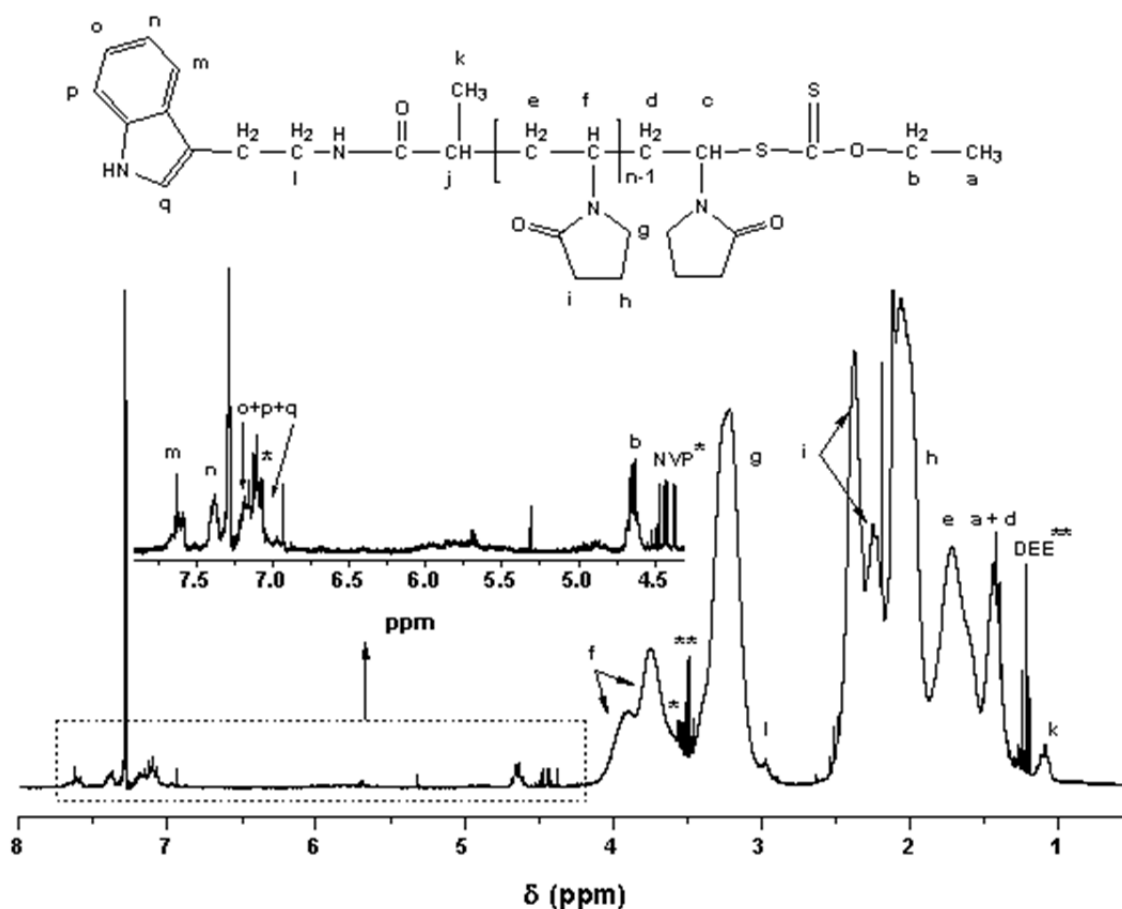


Figure 3.2  $^1\text{H-NMR}$  spectrum of PVP-X21 in  $\text{CDCl}_3$  prepared *via* the bulk polymerization of NVP at  $60^\circ\text{C}$  (NVP = \*, DEE = \*\*).

Figure 3.2 represents a typical  $^1\text{H-NMR}$  spectrum of PVP in  $\text{CDCl}_3$ . The main chain resonance peaks are easily identified as the characteristic broad signals, 4.1 – 3.0 ppm (**f** and **g**) and 2.6 – 1.4 ppm (**h**, **i**, **e**).<sup>12</sup> The most downfield of the characteristic peaks (4.1 – 3.1 ppm) represent the methine proton in the polymer backbone as well

as the methylene proton next to the nitrogen atom in the pyrrolidone ring while the more upfield (2.6 – 1.4 ppm) peaks are due to a combination of the methylene protons in the polymer backbone and in the pyrrolidone ring.

Apart from these characteristic signals, the resolution of the other resonance peaks is largely dependent on their concentration. Therefore, for end-group analysis, it is necessary to synthesize relatively low molecular weight polymer for easier end-group identification. However, there are still low molecular weight solvent and monomer peaks present, which should be taken into account when doing quantification as they overlap with the polymer signals. NVP and diethyl ether signals are identified by the single and double asterisks respectively.

Arguably the most useful signal for quantification is **b**, found at 4.6 ppm, which is due to the methylene protons of the xanthate at the  $\omega$ -chain-end of the polymer. Generally, these are the peaks used when determining the molecular weight of the polymer as these end-group signals are the most distinguishable when working with xanthate-mediated RAFT polymerizations.

#### 3.5.1.1.1 Homopolymerization *via* RAFT CTA X21

The number-average molecular weight ( $M_n$ ) can be calculated by setting the integration value of **b** to two as a reference signal (signifying the two protons as shown in Figure 3.2) and by then multiplying the subsequent integration value of **f** + **g**, *i.e.* that of the polymer backbone and ring, by the molar mass of the repeat unit. The combined signal of **f** + **g** is due to three protons on the repeat unit along with some solvent peaks that need to be taken into account when calculating  $M_n$ . The solvent peaks are due to the presence of a two-proton signal of diethyl ether (DEE) at 3.48 ppm as well as the overlapping two-proton signal of residual NVP.

The corrections are made by subtracting the appropriate integration value from the combined signal of **f** + **g**. For DEE, this is done by adjusting the signal value at 1.21 ppm (the three proton signal) to the appropriate two-proton value while the correction used to compensate for the presence of residual monomer, found at 4.30 ppm can be used directly as both integration values are due to two protons.

$$M_n^{NMR} = \left( (f + g) - \frac{2}{3}(DEE^{**}) - NVP^* \right) / 3 \times 111.14 \text{ g/mol} \quad 3.2$$

The R-group protons of the RAFT agent are found on the  $\alpha$ -chain end of the homopolymer. The aromatic protons (**m**, **n**, **o**, **p** and **q**) are all found downfield, 6.9 – 7.7 ppm while only the methylene protons,  $-\text{CH}_2$  (**l**), nearest to the nitrogen can be identified as the predominantly overlapped signal at 3.0 ppm.

A summary of the general characterization results of the PVP<sub>X21</sub> homopolymer is given in table 3.1.

**Table 3.1** General characterization results for the PVP<sub>X21</sub> homopolymer.

<sup>a</sup> DP <sub>adjusted</sub>	<sup>b</sup> M <sub>n</sub> <sup>50%</sup> (g/mol)	<sup>c</sup> Conversion (%)	<sup>d</sup> M <sub>n</sub> <sup>Calc</sup> (g/mol)	M <sub>n</sub> <sup>1H-NMR</sup> (g/mol)	M <sub>n</sub> <sup>SEC</sup> (g/mol)	<sup>e</sup> D	<sup>f</sup> Chain end functionality
90	5000	48	4 800	5 300	5 200	1.28	1.07:2
180	10 000	54	10 800	9 400	9 200	1.32	1.09:2
450	25 000	46	23 000	31 000	23 600	1.33	-
900	50 000	43	43 000	56 200	46 000	1.39	-

<sup>a</sup>Adjusted DP necessary to achieve the target M<sub>n</sub> at 50% conversion.

<sup>b</sup>M<sub>n</sub> values expected at 50% conversions as calculated using eq. 3.1.2

<sup>c</sup>Conversions were determined by weighing purified and dried polymer (= yield {g}) and then calculated as yield{g}/([NVP + AIBN + X21] {g}) × 100%; yield for dried polymer was adjusted on the amount of NVP present as calculated *via* <sup>1</sup>H-NMR.

<sup>d</sup>M<sub>n</sub> values calculated *via*: <sup>b</sup>Conv × DP<sub>adjusted</sub> × 111.1 g/mol

<sup>e</sup>D calculated from SEC results as M<sub>w</sub>/M<sub>n</sub>

<sup>f</sup>Chain-end functionality was determined as the ratio of the  $\alpha$  chain end (7.38 ppm, **1H**) :  $\omega$  chain end (4.62 ppm, **2H**)

The chain-end functionality was determined by calculating the ratio of  $\alpha$ - and  $\omega$ -chain end-groups. This was achieved *via* <sup>1</sup>H-NMR spectroscopy by comparing the integrated signals of  $\alpha$  and  $\omega$  chain-end protons. The ratio was obtained by comparing the integration values of a one-proton  $\alpha$ -chain-end signal (7.38 ppm) and a two-proton  $\omega$ -chain-end signal (4.62 ppm). The chain-end retention was limited to the lower molecular weight polymers as the decrease in concentration of end-groups limited the integration accuracy. It is, however, evident that for both the M<sub>n</sub> 5 000 g/mol and M<sub>n</sub> 10 000 g/mol, there are more  $\alpha$ -chain-ends present. This is due to the lability of the xanthate group and the ease with which side reactions can occur at the  $\omega$ -chain-end using the xanthate CTA. Fragmentation of the xanthate group leads to an unsaturated chain-end, which can be considered as no longer reactive.<sup>13</sup> The dead chain-ends should however be taken into account when quantification is done after further modification reactions involving the  $\omega$ -chain-end functionality.

The dispersity determined *via* SEC indicates sufficient control for bulk polymerization of NVP, which is notoriously difficult to obtain. The dispersity is greatly affected by conversion in the bulk polymerization of NVP as viscosity effects reduce the amount of control one can obtain. Tailing is, however, present to a small extent in the SEC traces, which can be attributed to radical-radical coupling, disproportionation as well as xanthate degradation, which all produce “dead” chains. In general, the dispersity indicates good control was maintained throughout the polymerization ( $\mathcal{D} < 1.4$ ).

### 3.5.1.1.2 Homopolymerization *via* RAFT CTA X16

The  $M_n$  of PVP synthesized using X16 as the CTA was calculated in much the same way as for X21 (Figure 3.3). This was done by using the methylene protons of the xanthate as reference, while keeping in mind that the xanthate moieties are present at both chain ends and thus referenced to four protons.

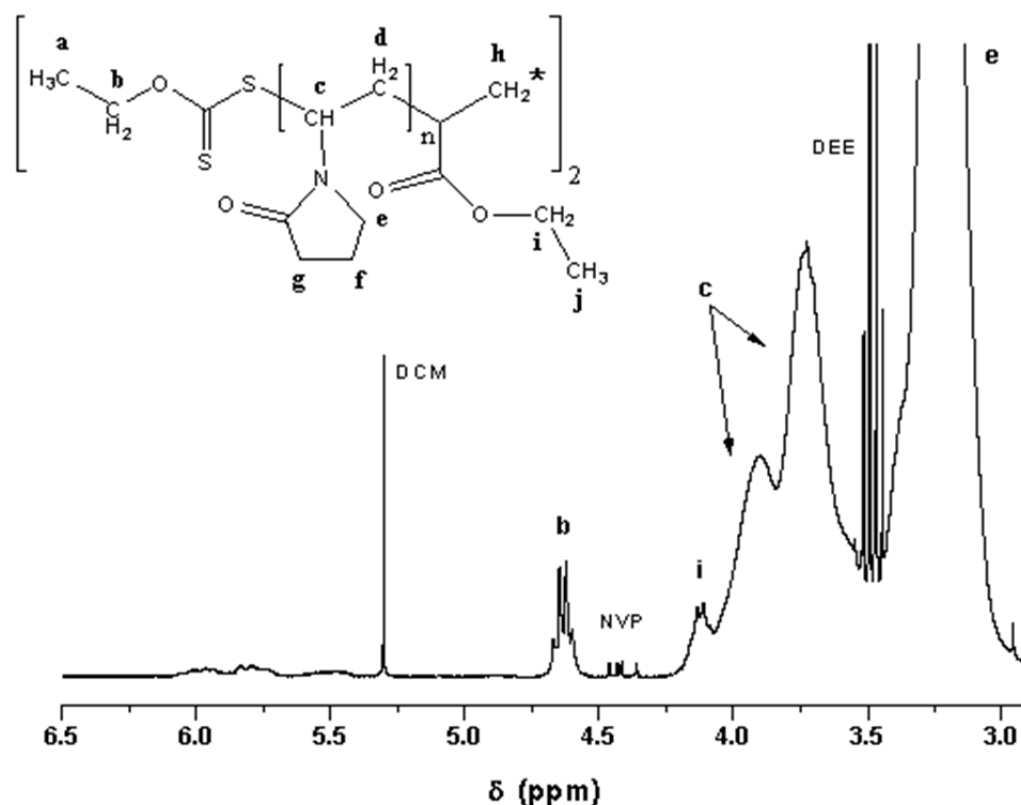


Figure 3.3

$^1\text{H-NMR}$  spectrum of PVP-X16 in  $\text{CDCl}_3$  prepared *via* the bulk polymerization of NVP at  $60^\circ\text{C}$ .

The three-proton peak due to the repeat unit, **c + e**, has another overlapping signal along with the DEE and NVP signals which need to be taken into account when calculating  $M_n$ . The signal at 4.2 ppm, **i**, is due to methylene protons on the R-group of the CTA which contributes 4 protons to the combined signal and thus needs to be subtracted along with the DEE and NVP signals (see Equation 3.3).

$$M_n^{NMR} = \left( (c + e) - \frac{2}{3}(DEE^{**}) - NVP^* - 4 \right) / 3 \times 111.14 \text{ g/mol} \quad 3.3$$

For the initial study, only one block length of the bifunctional PVP homopolymer was synthesized (Table 3.2).

**Table 3.2** General characterization results for the PVP<sub>x16</sub> homopolymer.

<sup>a</sup> DP <sub>adjusted</sub>	<sup>b</sup> M <sub>n</sub> <sup>50%</sup> (g/mol)	M <sub>n</sub> <sup>1H-NMR</sup> (g/mol)	M <sub>n</sub> <sup>SEC</sup> (g/mol)	<sup>c</sup> D
270	15 000	10 200	6900	1.22

<sup>a</sup>Adjusted DP necessary to achieve the target  $M_n$  at 50% conversion.

<sup>b</sup> $M_n$  values expected at 50% conversions as targeted using eq. 3.1.2.

<sup>c</sup>D calculated from SEC results as  $M_w/M_n$ .

The larger discrepancy in the SEC and <sup>1</sup>H-NMR value as compared to Table 3.1 is due to the difficulty in accurately determining  $M_n$  with <sup>1</sup>H-NMR spectroscopy. This discrepancy is increased due to the symmetrical nature of the polymer with no other reference signals other than the methylene protons of the xanthate moiety (**i**).

### 3.6 End-group modification of xanthate end-functional PVP

#### 3.6.1 Chain end analysis

##### 3.6.1.1 <sup>1</sup>H- and <sup>13</sup>C-NMR analysis

<sup>1</sup>H- and <sup>13</sup>C-NMR spectroscopy were used to qualitatively verify the successful end-group modification of the xanthate-functionalized PVP homopolymer as well as to quantitatively determine the extent of the end-group conversion.

The technique for hydrolysis of xanthate end-groups as pioneered by Pound *et al.*<sup>10</sup> was applied to produce hydroxyl end-functional PVP as a control for quantification purposes. This included dissolution of the O-ethyl xanthate functional PVP in aqueous solution (pH 4.5), preheating to 40 °C and incubation in an oil bath for 20 hours. The resulting solution was dialyzed and the product isolated *via* freeze-drying.



$^1\text{H-NMR}$  spectroscopy confirmed the conversion of the xanthate to the hydroxyl functionality. The hydroxyl functionality appears as a broad peak in the range of  $\delta = 5.2 - 5.5$  ppm (**B**) along with the disappearance of the xanthate's two-proton methylene signal, **A** (Figure 3.4).

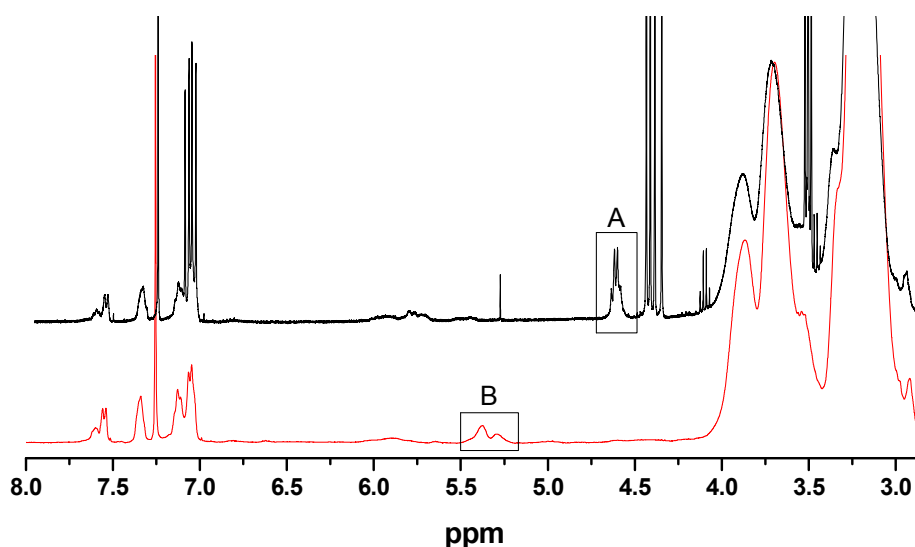


Figure 3.4  $^1\text{H-NMR}$  spectra of PVP in  $\text{CDCl}_3$  before and after being heated in aqueous solution ( $\text{pH} = 4.5$ ) at  $40^\circ\text{C}$  for 20 hours.

After hydrolysis of the xanthate end-groups, the resulting polymer was heated at  $120^\circ\text{C}$  for 20 hours under vacuum. The final product was aldehyde functionalized PVP, peak **C** in Figure 3.5. The conversion of the end-group to the aldehyde accounted for 77% of the initial xanthate end-groups when referenced to the methyl protons found at the  $\alpha$ -chain-end, signal **D** ( $\delta = 1.07$  ppm) (the assumption was made that every chain was initiated *via* RAFT polymerization and therefore has an aromatic  $\alpha$ -chain-end) (Figure 3.5). It should be stressed that quantification with polymers is very difficult due to the broadness of polymeric peaks. Thus, the conversion values of the end-group modification reactions are accurate when comparisons are made between the polymer chains, but not as an absolute value.

The aldehyde functionality was further verified using  $^{13}\text{C-NMR}$  spectroscopy. The signal at 201 ppm is characteristic for aldehyde functionalities. The insert shows the

poor resolution of the signal, common for polymeric signals (Figure 3.6).

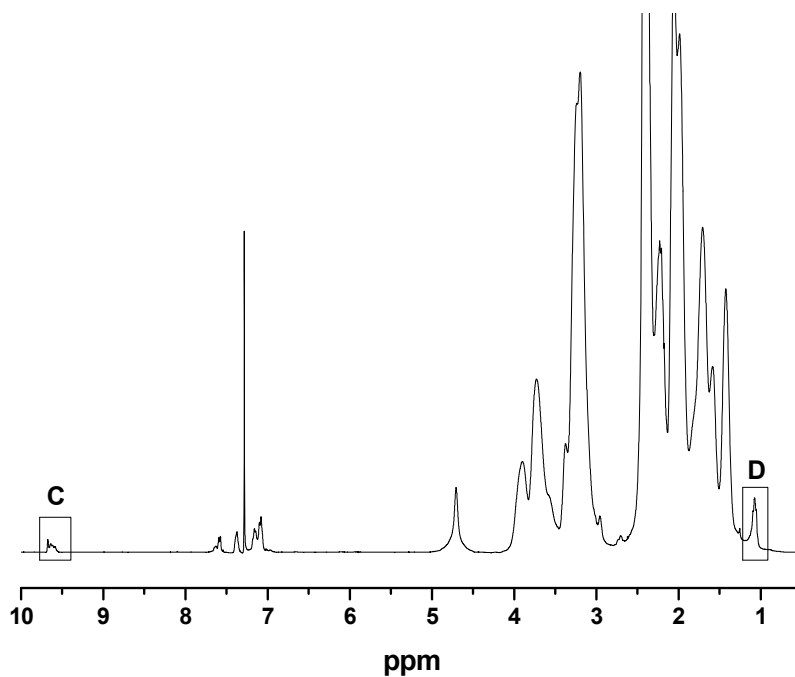


Figure 3.5  $^1\text{H}$ -NMR spectrum of PVP in  $\text{CDCl}_3$  after being hydrolyzed and subsequently heated for 20 hours at  $120^\circ\text{C}$  under vacuum.

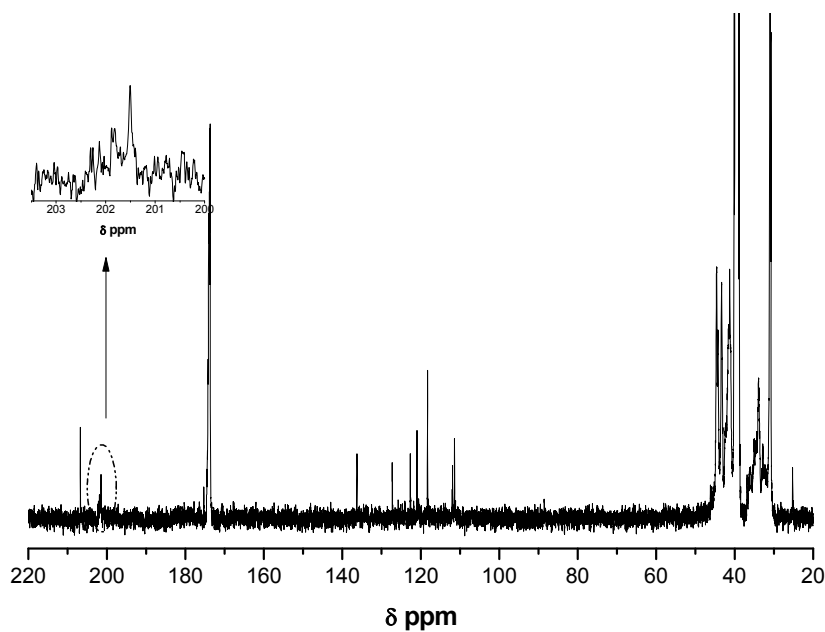


Figure 3.6  $^{13}\text{C}$ -NMR spectrum of aldehyde end functional PVP in  $\text{CDCl}_3$ . The insert indicates the characteristic signal for aldehyde functionality at 201 ppm.

### 3.6.2 Optimization of $\omega$ -aldehyde end-group synthesis

The hydrolytic stability of the thiocarbonyl thio moiety from the RAFT agent is known to be pH-dependent.<sup>14</sup> The influence of pH was investigated by varying the aqueous conditions during the initial hydrolysis step. Conditions were investigated to optimize the conversion of xanthate end-groups to aldehyde end-groups as well as decrease the fraction of unsaturated chain-ends formed during the end-group modification.

The pH range varied between 1 – 3 (Figure 3.7) and compared to the previous work of Pound *et al.*<sup>10</sup> done at pH 4.5. The solutions for pH = 2 – 3 were prepared using formic acid (90%) while the pH = 1 solution was prepared using an aqueous HCl solution (32%).

No synthetic pathway has been reported in literature (other than the work done in our group) which directly converts the xanthate to an aldehyde. It was however reported during the free radical polymerization of NVP initiated *via* aqueous hydrogen peroxide.<sup>11</sup>

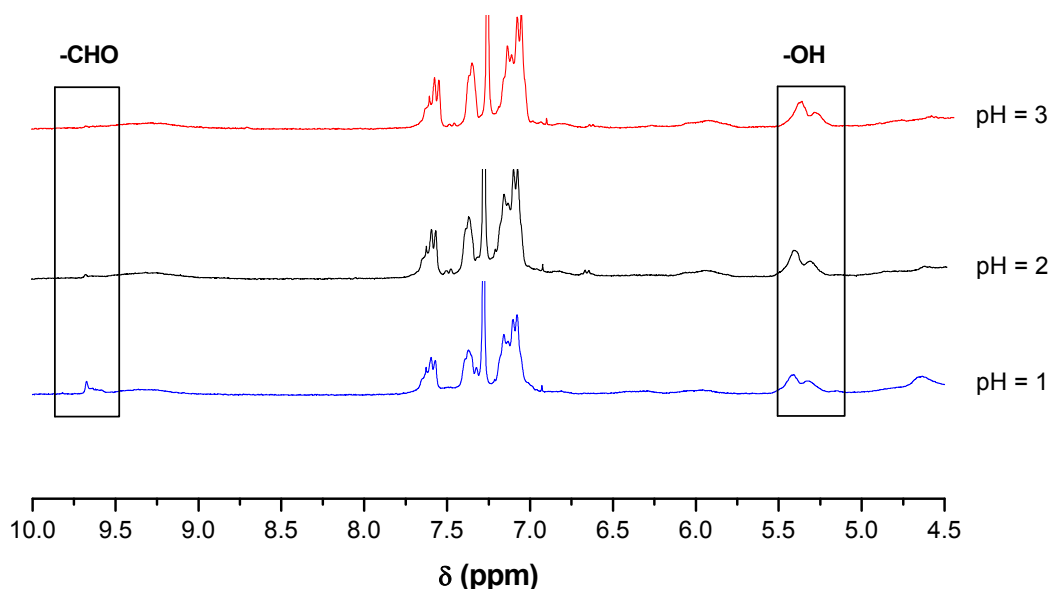


Figure 3.7  $^1\text{H-NMR}$  spectra of PVP-X2 ( $\text{CDCl}_3$ ) after hydrolysis under varying aqueous conditions. The pH of the aqueous solutions was 3 (top), 2 (middle) and 1 (bottom) respectively.

The investigation into the effect of pH clearly indicates the reliance of the mechanism on the pH of the acidic environment. This is seen in Figure 3.7, where the bottom  $^1\text{H-NMR}$  spectrum (hydrolyzed in the aqueous solution at pH 1) shows the presence of  $\omega$ -hydroxyl end-functional PVP ( $\delta = 5.18\text{-}5.55$  ppm) as well as  $\omega$ -aldehyde PVP ( $\delta = 9.66$  ppm) in a one step reaction.

The hydrolysis of the xanthate moiety was considered a precursor step for the eventual formation of the  $\omega$ -aldehyde functional PVP, after which thermolysis was the final step to ensure near quantitative conversion (Scheme 3.1). The presence of the aldehyde functionality was an indication that at lower pH a higher conversion can be obtained and the eventual heating of the polymer under vacuum should then result in closer to quantitative end-group conversion. Table 3.3 shows comparative results for the reactions done in the aqueous pH range of 1 – 4.5. Quantification was done with  $^1\text{H-NMR}$  spectroscopy by comparing the methyl peak ( $\delta = 1.07$  ppm, **D**, Figure 3.5) with either the aldehyde or hydroxyl signals. This allowed for the direct calculation of the molecular weight of PVP and to determine the conversion of the end-groups after the respective hydrolysis and thermolysis steps.

**Table 3.3** Comparison of the end-group conversion after the hydrolysis and subsequent thermolysis of xanthate end-functional PVP to the aldehyde functionality, as a function of pH.

	After hydrolysis		After thermolysis
	End group		End group
pH	$\int$ hydroxyl <sup>a</sup>	$\int$ aldehyde <sup>a</sup>	$\int$ aldehyde <sup>a</sup>
4.5	0.88	-	0.77
3.0	1.01	-	0.80
2.0	1.08	-	0.81
1.0	0.92	0.11	0.94

<sup>a</sup>Integrated fraction of end-group functionalities determined via  $^1\text{H-NMR}$ .

Table 3.3 indicates the decrease of hydroxyl end-groups present after hydrolysis in an increasingly acidic environment. This is in conjunction with the presence of aldehyde functionalities when hydrolyzed under the most acidic condition, namely pH = 1. Table 3.3 indicates an improvement of the aldehyde formation when hydrolyzed at pH 1. The conversion of the xanthate to the aldehyde functionality is enhanced when there is a smaller fraction of hydroxyl groups present prior to the thermolysis step. The thermolysis step entailed heating the polymer at 120 °C for 20 hours.

The difficulty in accurately determining quantitative results with  $^1\text{H}$ -spectroscopy is evident in table 3.3, where the integration values sometimes exceed 100%. These values were used as is, to effectively compare the different conditions as the reference signal itself and the method of integration was kept constant.

The thermal and acidic lability of the xanthate group allows one to try and achieve a one-step conversion to the aldehyde functionality. This was attempted by increasing the temperature at which the initial hydrolysis step takes place (Table 3.4).

**Table 3.4** Comparison of the end group conversion after hydrolysis at different temperatures and subsequent thermolysis of the xanthate end-functional PVP.

		After hydrolysis		After thermolysis
		End-group type		End-group type
pH	Temperature (°C)	∫ hydroxyl <sup>a</sup>	∫ aldehyde <sup>a</sup>	∫ aldehyde <sup>a</sup>
1	50	0.44	0.55	0.98
1	60	-	0.95	1.02

<sup>a</sup>Integrated fraction of end-group functionalities determined via  $^1\text{H}$ -NMR.

The combination of the low pH and increased hydrolysis temperature seems to further enhance the conversion of the xanthate to the aldehyde functionality even before thermolysis.  $^1\text{H}$ -NMR spectra however showed some new signals which seem to indicate some side reactions did possibly take place under the harsher conditions (Figure 3.8).

This allows one to postulate that the mechanism is dependent on the following factors which greatly determine whether the eventual conversion is near quantitative. Firstly, the lability of the xanthate is dependent on the acidity of the aqueous solution, which is evident in the integration values after hydrolysis. The thermal lability of the xanthate can also be exploited during the hydrolysis step to increase the aldehyde conversion. Secondly, the final conversion to the aldehyde is significantly increased when there was aldehyde already present prior to thermolysis. This emphasizes the importance of hydrolyzing the xanthate moiety prior to thermolysis as this inhibits the irreversible formation of unsaturated chain-ends.

The formation of the hydroxyl and subsequent aldehyde functionality from the xanthate moiety has only been reported when used to polymerize NVP. This

suggests that the terminal pyrrolidone substituent next to the hydroxyl functionality plays an integral role in the formation of these types of end-groups.

It is important to grasp that when the modification reactions are attempted, less than 100% of the chains have the  $\omega$ -xanthate functionality as unsaturated chain-ends are present after polymerization (section 3.5.1.1.1). This was taken into account when referring to quantitative conversion.

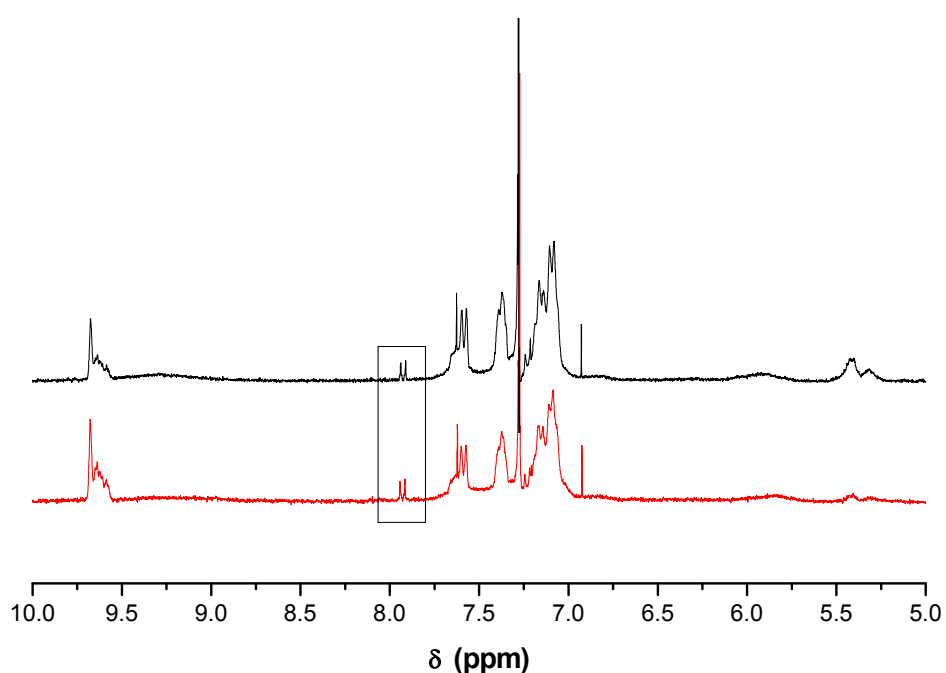


Figure 3.8 <sup>1</sup>H-NMR spectrum of PVP-X21 (CDCl<sub>3</sub>) after hydrolysis at 50 °C (top spectra) and 60 °C (bottom spectra) respectively.

### 3.7 Conclusion

Well-defined, narrowly distributed PVP was synthesized successfully *via* RAFT-mediated polymerization of NVP using two different CTAs. The end-functionalities synthesized with the CTAs include a fluorescent tag at the alpha chain-end and xanthate functionality at the omega chain-end (*via* X21) as well as two xanthate functionalities at alpha and omega chain-end respectively (X16). The two xanthate functionalities allow for post-polymerization modification reactions at their respective  $\alpha$ - and  $\omega$ -chain-ends. For the purpose of our work, it was necessary to synthesize well-defined xanthate end-functional homopolymer for post-polymerization modification. Chain end-functionality ratios confirm that this was done successfully for PVP-X21.

The end-groups were characterized *via*  $^1\text{H-NMR}$  spectroscopy and SEC.  $^1\text{H-NMR}$  spectroscopy confirmed the presence of the thiocarbonyl thio moiety along with the confirmation that side reactions due to the presence of this labile end-group were at a minimum. Chain-end functionality ratios confirm that this was done effectively for PVP-X21 with only a small percentage of the labile xanthate not present.

SEC indicated efficient control during polymerization as no bimodality was observed in the traces. The extent of side reactions was small and in general the dispersity indicated that good control was maintained throughout the polymerization ( $\mathcal{D} < 1.4$ ).

Optimized conditions were established for the conversion of the xanthate moiety into an  $\omega$ -aldehyde end-functionality. An increased acidic aqueous environment for the hydrolysis step seemed to effectively convert the xanthate moiety into a combination of hydroxyl and aldehyde end-groups. It was found that the hydrolysis reaction is effectively the determining factor in obtaining quantitative results where an increase in the reaction temperature favoured the formation of  $\omega$ -aldehyde PVP. It was concluded that at pH 1, a maximum conversion to the aldehyde functionality is obtained with minimal side reactions taking place.

### 3.8 References:

- (1) Yan, Y.; Zhang, W.; Qiu, Y.; Zhang, Z.; Zhu, J.; Cheng, Z.; Zhang, W.; Zhu, X. *J. Polym. Sci., Part A: Polym. Chem.*, **48**, 5206-5214.
- (2) Postma, A.; Davis, T. P.; Li, G.; Moad, G.; O'Shea, M. S. *Macromolecules* **2006**, *39*, 5307-5318.
- (3) Moad, G.; Rizzardo, E.; Thang, S. H. *Aust. J. Chem.* **2005**, *58*, 379-410.
- (4) Perrier, S.; Takolpuckdee, P. *J. Polym. Sci., Part A: Polym. Chem.* **2005**, *43*, 5347-5393.
- (5) Haaf, F.; Sanner, A.; Straub, F. *Polym. J. (Tokyo, Jpn.)* **1985**, *17*, 143-152.
- (6) Nicolas, J.; Mantovani, G.; Haddleton, D. M. *Macromol. Rapid Commun.* **2007**, *28*, 1083-1111.
- (7) Willcock, H.; O'Reilly, R. K. *Polymer Chemistry*, *1*, 149-157.
- (8) Qiu, X.-P.; Winnik, F. M. *Macromol. Rapid Commun.* **2006**, *27*, 1648-1653.
- (9) Zelikin, A. N.; Such, G. K.; Postma, A.; Caruso, F. *Biomacromolecules* **2007**, *8*, 2950-2953.
- (10) Pound, G.; McKenzie, J. M.; Lange, R. F. M.; Klumperman, B. *Chem. Commun. (Cambridge, U. K.)* **2008**, 3193-3195.
- (11) Marten, F. L. In *Encyclopedia of Polymer Science and Engineering*; John Wiley and Sons Inc.: 1989; Vol. 17, p 202.
- (12) Dutta, K.; Brar, A. S. *J. Polym. Sci., Part A: Polym. Chem.* **1999**, *37*, 3922-3928.
- (13) Pound, G.; Eksteen, Z.; Pfukwa, R.; McKenzie, J. M.; Lange, R. F. M.; Klumperman, B. *J. Polym. Sci., Part A: Polym. Chem.* **2008**, *46*, 6575-6593.
- (14) Smith, A. E.; Xu, X.; McCormick, C. L. *Prog. Polym. Sci.*, *35*, 45-93.



## Living N-carboxyanhydride (NCA) Ring Opening Polymerization of $\gamma$ -benzyl-L-glutamate *via* the Normal Amine Mechanism (NAM)

### 4.1 Introduction

The scope of the thesis includes the conjugation of a polypeptide, poly( $\gamma$ -benzyl-L-glutamate) (PBLG) with a synthetic polymer, poly(vinylpyrrolidone) (PVP). This is due to the increased interest in combinations of synthetic or natural polypeptides with other synthetic or natural polymer systems, leading to an array of interesting architectures. This in turn leads to advanced morphologies such as vesicles, micelles and organogels, which are formed *via* the synthesis of polypeptide conjugates and polypeptide block copolymers.<sup>1-5</sup> It is the progress made in recent years to synthesize these synthetic polypeptides *via* optimized N-carboxyanhydride ring-opening polymerization (NCA ROP) techniques, which allow for well-defined materials while still retaining the end-functionality for further modification.<sup>6-10</sup>

For the purpose of our work, it was crucial that the end-functionality of the synthetic polypeptide was retained, as some further modification of the polypeptide was done *via* a modular approach. Therefore, it was necessary to use a synthetic technique, which could minimize possible side-reactions either by end-group protection<sup>9,11</sup> or by using an optimized procedure that would provide the conditions for the necessary control.

As described in section 2.4.2 there are two main mechanisms for NCA ROP, namely the normal amine mechanism (NAM) and the activated monomer mechanism (AMM). Primary amines initiate the polymerization *via* the NAM and generally show better control. More basic initiators can abstract a proton from the NCA monomer and produce an anion, which subsequently initiates *via* the AMM, resulting in competing mechanisms. It is important to note that due to the nucleophilic/basic dual character of amines, the polymerization is never solely driven by only the NAM mechanism thus optimized conditions are necessary to sufficiently exclude the AMM.<sup>12</sup> Side-reactions are mainly due to solvent effects, end-group termination and competing mechanisms, which subsequently affect control of end-groups and molecular weight.<sup>13,14</sup>

Due to the potential use of the polypeptide in biological systems, it was decided to optimize the NAM conditions rather than adding regulating agents, which could

adversely affect the toxicity.<sup>9,11</sup> Previous reports have shown that the terminal  $\gamma$ -benzyl-L-glutamate unit on the chain can form a cyclic end-group, namely pyroglutamate resulting in the loss of the amine functionality.<sup>15</sup> Due to the necessity of retaining the  $\omega$ -amino group, it was decided to use some sort of protection that would not only inhibit the cyclization when in solution or the solid state but also allow for further conjugation.

As described in section 2.4.2, optimization of the ROP of NCAs effectively means lowering the temperature to increase the structural control as well as applying high vacuum where the result is two-fold. Removal of the CO<sub>2</sub> from the reaction mixture results in enhanced polymerization rates<sup>16</sup> (necessary when working at low temperatures) as well as suppression of possible side reactions between CO<sub>2</sub> and DMF.<sup>17</sup>

Earlier work on applying high vacuum with PBLG was done by Aliferis *et al.*,<sup>18</sup> who indicated that high molecular weight polypeptides with low dispersities were obtained. No study was reported, however, on the effect of these conditions on the structural composition of the polypeptide. Recently, Habraken *et al.*<sup>8</sup> have done comprehensive work on the optimization of the NAM conditions showing results for a wide range of NCAs from various  $\alpha$ -amino acids, which included  $\gamma$ -benzyl-L-glutamate NCA. They reported on the effects of temperature variation from 0 °C to 60 °C as well as the use of high vacuum,  $1 \times 10^{-5}$  bar. They showed that at 0 °C, no end-group termination takes place, but at 20 °C the formation of the pyroglutamate end-group was evident. This was said to be due to the higher conversion, which resulted in no more monomer being present in the system. Thus, it is necessary to keep track of conversion as cyclization is absent if monomer is still present. Alternatively, the polymerization needs to be carried out at 0 °C when the polymer is present in the reaction medium for an extended period of time. Furthermore, they have shown that high vacuum does not affect the composition and is indeed an effective way to increase the reaction kinetics when polymerizing at such low temperatures while still obtaining structural control.

The optimized NAM conditions as described by Habraken *et al.*<sup>8</sup> were applied in the present study to obtain the  $\omega$ -amino end-functional PBLG.

## 4.2 Experimental

### 4.2.1 Materials

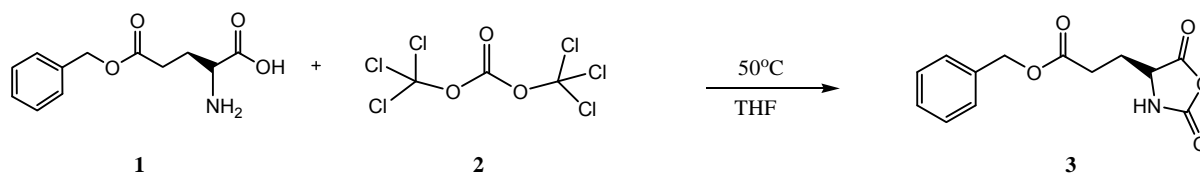
Benzylamine (99.5%, redistilled), L-glutamic acid (ReagentPlus), benzyl alcohol (anhydrous, 99.8%), bis(trichloromethyl) carbonate (triphosgene) (99%), phosphorous pentoxide (with MOI) were purchased from Sigma-Aldrich.

Tetrahydrofuran (THF) (dried Seccosolv™), diethyl ether (dried, Seccosolv™), 1,8-diazabicyclo[5.4.0]undec-7-ene (DBU, for synthesis) and *n*-pentane (for synthesis) were all purchased from Merck and used as is. Dichloromethane (DCM, KIMIX, CP-grade, 99.5%) and ethanol (KIMIX, CP-grade, 99.5%) were dried over molecular sieves (4 Å, 1.6 mm pellet). Ethyl acetate (anhydrous, 99.8%), *N,N*-dimethylformamide (DMF, Anhydrous, 99.8% Sigma), piperidine (ReagentPlus, 99%) and trifluoroacetic acid (TFA, ReagentPlus) were purchased from Sigma-Aldrich and used without further purification. DMF and ethyl acetate were used directly from the bottle and stored under an inert, dry atmosphere. Anisole (99%, Across Organics), *p*-toluenesulfonic acid (*p*-TSA, Across Organics) pyridine (99%, Across Organics) and hydrobromic acid (48%, Fluka) were used as is.

The pentafluorophenyl (Pfp) activated ester Fmoc-L-Cys(Acm)-OPfp, (912020, MilliGen, USA) and hydroxybenzotriazole (HOBT) were used as is. *N,N*-diisopropylethylamine (DiPEA) was used after purification by redistillation.

### 4.2.2 NCA of $\gamma$ -Benzyl-L-glutamate (BLG)

The NCA monomer was synthesized according to a literature procedure by Daly and Poché.<sup>19,20</sup> The amino acid (**1**) was reacted with triphosgene in a reaction flask fitted with a condenser and vented into concentrated sodium hydroxide to trap HCl or phosgene gas. Generally, modern techniques will include an HCl scavenger such as  $\alpha$ -pinene<sup>21</sup> or TEA<sup>22</sup> when synthesizing various NCA monomers, but this can potentially lead to lower product yields as the salt produced in the reaction with phosgene needs to be removed. Purification of the monomer was done by repeated recrystallization from THF/*n*-hexane. <sup>1</sup>H-NMR showed a clean spectrum of the NCA after only two recrystallizations and thus allowed for yields *via* this route to be above 80%.

Scheme 4.1 Synthesis of NCA of  $\gamma$ -benzyl-L-glutamate (BLG)

#### 4.2.2.1 Synthesis of BLG (1)

The general procedure used for the synthesis of  $\gamma$ -benzyl-L-glutamate was adapted from the method used by Blout *et al.*<sup>23</sup> L-glutamic acid (100 g, 0.680 mol) and 182 mL of 48% hydrobromic acid were added to 670 mL of benzyl alcohol under stirring. The mixture was immersed into a preheated oil bath of 65 °C and kept under continuous stirring until all the glutamic acid was in solution (ca. 30 min). Once the solution had turned clear, it was rapidly cooled to ca. 30 – 40 °C. A solution of 200 mL pyridine in 1350 mL of 95% ethanol was added to the clear solution after which precipitation occurred upon further cooling. The reaction mixture was kept at 0 – 4 °C for a further 12 hours to ensure complete precipitation of the product. The precipitate was filtered off and washed with ethanol and diethyl ether and dried under high vacuum at room temperature.

The product was recrystallized from 5% aqueous ethanol (keeping the temperature at 65 °C to prevent thermal decomposition) with a sufficient amount of sodium bicarbonate to keep the pH of the mixture at 7. The solution was kept at high temperature for a minimum amount of time to prevent decomposition into benzyl alcohol and glutamic acid. The solution was rapidly cooled and kept at 0-4 °C for a further 12 hours to ensure complete precipitation. The product was isolated *via* filtration and subsequently washed with water (pH adjusted to 7 with sodium bicarbonate), distilled water and then dispersed in ethanol. The product was isolated *via* filtration, washed with diethyl ether and dried under high vacuum at room temperature. The product was stored under refrigeration. Yield: 36.7 g, 155 mmol, 23%.

<sup>1</sup>H NMR (300 MHz, TFA,  $\delta$ , ppm) 11.63 (s, 1H, OH), 7.47 – 7.32 (m,  $J = 9.3$  Hz, 5H, ArH), 5.31 (s, 2H, -OCH<sub>2</sub>), 4.56 (t,  $J = 6.1$  Hz, 1H, -(CO)CH(NH<sub>2</sub>)), 2.98 (t,  $J = 6.6$  Hz, 2H, -COCH<sub>2</sub>), 2.73 – 2.46 (m, 2H, CH<sub>2</sub>). <sup>13</sup>C NMR (400 MHz, TFA,  $\delta$ , ppm) 176.12 (CHCO<sub>2</sub>H), 172.46 (CH<sub>2</sub>CO<sub>2</sub>), 133.67 (Ar), 128.63 (Ar), 128.30 (Ar), 127.82 (Ar), 68.83 (CH<sub>2</sub>O), 53.38 (CH), 30.11 (CH<sub>2</sub>CO), 24.27 (CH<sub>2</sub>CH).

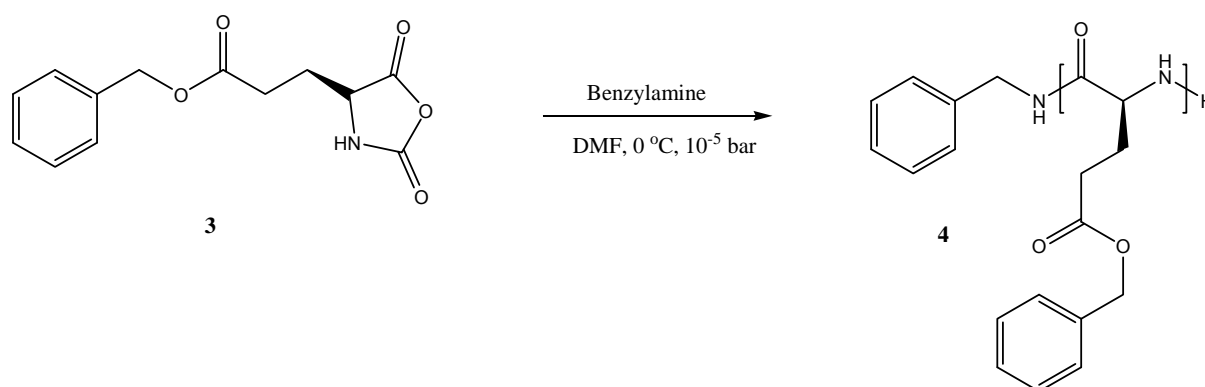
### 4.2.2.2 Synthesis of NCA of BLG (3)

$\gamma$ -Benzyl-L-glutamate (10 g, 0.042 mol) was dissolved in 100 mL of anhydrous THF and the mixture warmed to 50 °C under stirring. One third of an equivalent triphosgene (4.98 g, 0.0168 mol) was added in a single aliquot after which the reaction mixture was left under reflux while venting into a 1 M NaOH trap. The solution became homogenous after 1 hour, but was left for three hours after which the reaction mixture was poured into 300 mL of hexane. Crystals formed immediately, but the suspension was left overnight at -10 °C to ensure complete precipitation. The NCA was recrystallized from THF/*n*-pentane (1:3 *v/v*) and subsequently stored in the refrigerator under P<sub>2</sub>O<sub>5</sub>. Yield: 8.4 g, 31.9 mmol, 76%

<sup>1</sup>H NMR (400 MHz, CDCl<sub>3</sub>,  $\delta$ , ppm): 7.36 (m, 5H, ArH ), 6.51 (s, 1H, (NH)), 5.14 (s, 2H, OCH<sub>2</sub>), 4.37 (t, *J* = 6.1 Hz, 1H, CH), 2.60 (t, *J* = 6.8 Hz, 2H, COCH<sub>2</sub>), 2.36 – 2.03 (m, 2H, CH<sub>2</sub>). <sup>13</sup>C NMR (400 MHz, CDCl<sub>3</sub>,  $\delta$ , ppm) 171.42 (CHCO<sub>2</sub>), 168.39 (CH<sub>2</sub>CO<sub>2</sub>), 150.89 (NHCO<sub>2</sub>), 134.24 (Ar), 127.77 (Ar), 127.64 (Ar), 127.43 (Ar), 66.16 (CH<sub>2</sub>O), 55.97 (CH), 28.88 (CH<sub>2</sub>CO), 25.95 (CH<sub>2</sub>CH).

### 4.2.3 Polymerization system

The general polymerization procedure for the ROP of the  $\gamma$ -benzyl-L-glutamate NCA was adjusted from the procedure used by Habraken *et al.*<sup>8</sup> The reaction flask was immersed in a water bath cooled to 0 °C while intermittently applying a vacuum of 10  $\mu$ bar throughout the polymerization period to increase the reaction rate.



Scheme 4. 2 ROP of NCA of  $\gamma$ -benzyl-L-glutamate.

Benzylamine was used to initiate the polymerization which would allow the living NCA ROP to propagate mainly through the normal amine mechanism. The

theoretical number average molecular weight,  $M_n$ , could be calculated using the initial monomer to initiator concentration ratio,  $[M]_0/[I]_0$ , while taking into account that  $\text{CO}_2$  splits off from the monomer when calculating the molecular weight from the degree of polymerization.

The NCA monomer solution was placed in a Schlenk flask and degassed *via* three freeze-pump-thaw cycles after which argon was introduced into the flask. The benzylamine initiator solution was degassed by bubbling argon through the solution for 20 minutes and the polymerization was started by the introduction of the initiator solution into the Schlenk flask through a septum. The polymerization then proceeded at 0 °C with intermittent applications of high vacuum (10  $\mu\text{bar}$ ).

Emphasis must be placed on the importance of retaining the primary amine end-functionality (**4**) as the possibility remains that the end-group can undergo cyclization (**5**) which will subsequently result in dead chains. Hence, polymerizing at 0 °C while stopping the polymerization before 100% conversion would minimize the possibility of any cyclization reactions (Figure 4.1).<sup>8,15</sup>

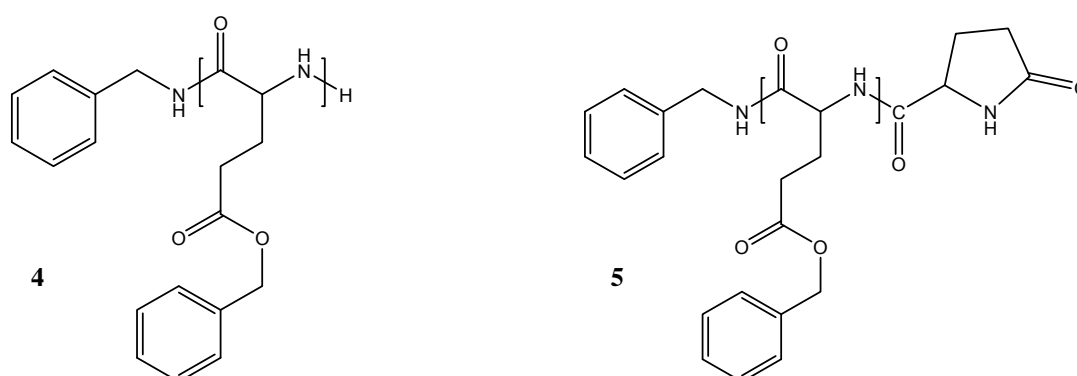


Figure 4.1 Possible end-group configurations found in the NCA ROP of PBLG. Structure 5 is due to cyclization of the the terminal  $\gamma$ -benzyl-L-glutamate unit on the chain.

#### 4.2.3.1 Experimental procedure for ROP of BLG NCA

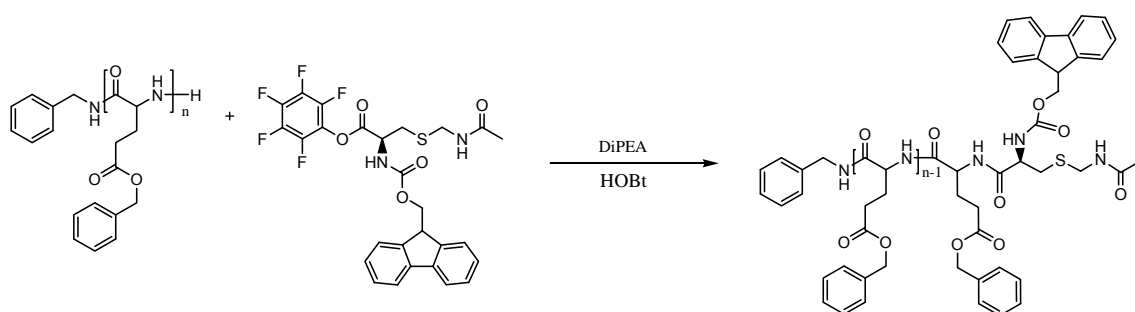
In a typical experiment, the NCA monomer of  $\gamma$ -benzyl-L-glutamate (2.06 g, 7.60 mmol) was dissolved in 14.5 mL of DMF in a pear-shaped Schlenk flask. A solution of benzylamine (0.181 g, 1.69 mmol) in 5 mL of DMF was degassed by bubbling with nitrogen for 20 minutes. 0.5 mL of the benzylamine solution was added to the dissolved monomer mixture and subsequently degassed with a minimum of three

freeze-pump-thaw cycles followed by the introduction of ultra-high purity argon. The reaction was left to stir in a cold water bath of 0 °C for 4 days while intermittently applying 30 minutes of high vacuum to the reaction mixture. The polypeptide solution was precipitated in diethyl ether, washed with diethyl ether, filtered and dried *in vacuo* at room temperature.

#### 4.2.4 Peptide coupling reaction

For the purpose of our study, it was necessary to synthesize a polypeptide with a cysteine end-functionality. This was done *via* a peptide coupling reaction with an activated ester. The coupling reaction serves two purposes, *i.e.* the introduction of the cysteine functionality as well as the protection of the primary amine at the  $\omega$ -chain end.

The coupling reaction was done using a pentafluorophenyl (Pfp) activated ester (scheme 4.3) with a protected cysteine moiety, Fmoc-L-Cys(Acm)-OPfp. The primary amine was protected with a fluorenylmethyloxycarbonyl (Fmoc) group and the thiol functionality was protected with an acetamidomethyl (Acm) group.



**Scheme 4.3** Coupling reaction resulting in a PBLG polypeptide with the protected, terminal cysteine functionality.

For the eventual conjugation reaction between the aldehyde end-functional PVP and the cysteine group at the PBLG  $\omega$ -chain-end, the deprotection steps required optimization. This is because the deprotection of the Acm group is done under harsh conditions, which can easily hydrolyze the benzyl ester bonds of the PBLG or form possible toxic side products. To prevent the hydrolysis of the benzyl ester bonds, a procedure was adapted from Guo *et al.*<sup>24</sup> whereby they report a facile method for the synthesis of functional PBLG by ester exchange reactions using functional alcohols. They showed that the inclusion of benzyl alcohol (2.5 molar equivalents to the repeat



units of PBLG) allowed for the successful suppression of the PBLG hydrolysis under acidic conditions.

#### 4.2.4.1 Synthesis of Fmoc-cys(Acm) end-functional PBLG

Fmoc-L-Cys(Acm)-OPfP (51 mg,  $8.70 \times 10^{-5}$  mol) was dissolved in 1 mL of distilled DMF and degassed with argon in a 50 mL three neck flask while the  $\omega$ -amino end-functional PBLG (200 mg,  $4.35 \times 10^{-5}$  mol) and HOBt (12.6 mg,  $8.70 \times 10^{-5}$  mol) were dried under vacuum at room temperature in the presence of  $P_2O_5$  for 2 hours. The PBLG and HOBt were then dissolved in 1 mL of distilled DMF after which Dipea (15  $\mu$ L,  $8.70 \times 10^{-5}$  mol) was added to the reaction mixture. The latter was then added to the activated ester solution and left to stir under an inert atmosphere for 2 hours in a preheated oil bath of 35 °C. The solution was precipitated in diethyl ether and washed with water. The product was dried under vacuum and subjected to the Kaiser test<sup>25</sup>, which did not turn blue, indicating efficient coupling. Yield: 0.188 g,  $3.63 \times 10^{-5}$  mol, 83%.

#### 4.2.4.2 Deprotection of primary amine - Fmoc group removal

PBLG-Fmoc-L-Cys(Acm) (509 mg,  $4.07 \times 10^{-5}$  mol) was dissolved in 8 mL of DMF after which 2 mL of piperidine was added and a catalytic amount of 1,8-diazobicyclo[5.4.0]undec-7-ene (DBU). The reaction mixture was left to stir for 2 hours at room temperature. The reaction mixture was then concentrated under vacuum after which it was precipitated in diethyl ether twice and dried under vacuum. The product was subjected to the Kaiser test, which turned blue, indicating the presence of primary amines. Yield: 413 mg,  $3.30 \times 10^{-5}$  mol, 81%.

#### 4.2.4.3 Simultaneous thiol deprotection and oxidation - Acm group removal

The literature procedure used was adjusted from a patent submitted by Cuthbertson *et al.*<sup>26</sup> and optimized to avoid possible hydrolysis of the benzyl ester linkages. PBLG- L-Cys(Acm) (200 mg,  $1.8 \times 10^{-5}$  mol), benzyl alcohol (0.219 g, 2.03 mmol) and 100 mg of *p*-TSA (0.5/1, (g/g, cat./PBLG)) were dissolved in 2 mL of TFA. The solution was added to a mixture of anisole (200  $\mu$ L, 1.84 mmol), DMSO (2 mL) and TFA (30 mL) preheated to 50 °C. After the reaction proceeded for 5 hours at this temperature, the reaction mixture was concentrated under high vacuum and precipitated in diethyl ether. Verification of the deprotection step was done *via* SEC,



where the formation of the disulfide bonds could be seen in the doubling of the molecular weight.

### 4.3 Analysis

#### 4.3.1 NMR Spectroscopy

$^1\text{H}$  NMR and  $^{13}\text{C}$  NMR spectra were acquired with a Varian VXR-Unity (400 MHz) spectrometer in  $\text{CDCl}_3$  and  $\text{DMSO-d}_6$ . All chemical shifts are reported in parts per million (ppm) with tetramethylsilane (TMS) as the internal reference.

#### 4.3.2 SEC

SEC analysis was carried out on a DMAc solvent system using a flow rate of 1.0 mL/min. The instrument setup consisted of a Shimadzu, LC-10AD pump, a column system fitted with a 50x8 mm guard column in series with three 300x8 mm, 10  $\mu\text{m}$  particle size GRAM columns (2 x 3000Å and 100Å) obtained from PSS, a Waters 2487 dual wavelength UV detector and a Waters 2414 differential refractive index (DRI) detector all in series. 100  $\mu\text{L}$  injection volumes are sampled individually with the oven temperature of the column and DRI detector kept at 40 °C. The solvent was stabilized with 0.05% BHT (w/v) and 0.03% LiCl (w/v), and samples were filtered through a 0.45  $\mu\text{m}$  GHP filter to prevent any impurities entering the system. Calibration was done using PMMA standard sets (Polymer Laboratories) ranging from 690 to  $1.2 \times 10^6$  g/mol. Data acquisition was done using Millennium<sup>32</sup> software, version 4.

#### 4.3.3 MALDI-ToF-MS

MALDI-ToF-MS analysis was carried out on a Voyager-DE STR from Applied Biosystems. The laser frequency was 20 Hz, wavelength of 337 nm and a voltage of 25 kV. The matrix used was trans-2-[3-(4-tert-butylphenyl)-2-methyl-2-propenylidene]malononitrile (DCTB) (40 mg/mL). Potassium trifluoroacetic acid (KTFA) was added as cationic ionization agent (5 mg/mL). The sample was dissolved in HFIP (1 mg/mL). The matrix, cationization agent and sample solutions were mixed (5:1:5), handspotted on the target plate and left to dry.

## 4.4 Results and discussion

### 4.4.1 ROP of BLG NCA

#### 4.4.1.1 $^1\text{H-NMR}$ analysis

The structural assignment of the PBLG polypeptide was done *via*  $^1\text{H-NMR}$  spectroscopy (Figure 4.2). Although not used in the determination of the molecular weight, it was still possible to obtain qualitative data regarding the protection and deprotection of certain functional groups.

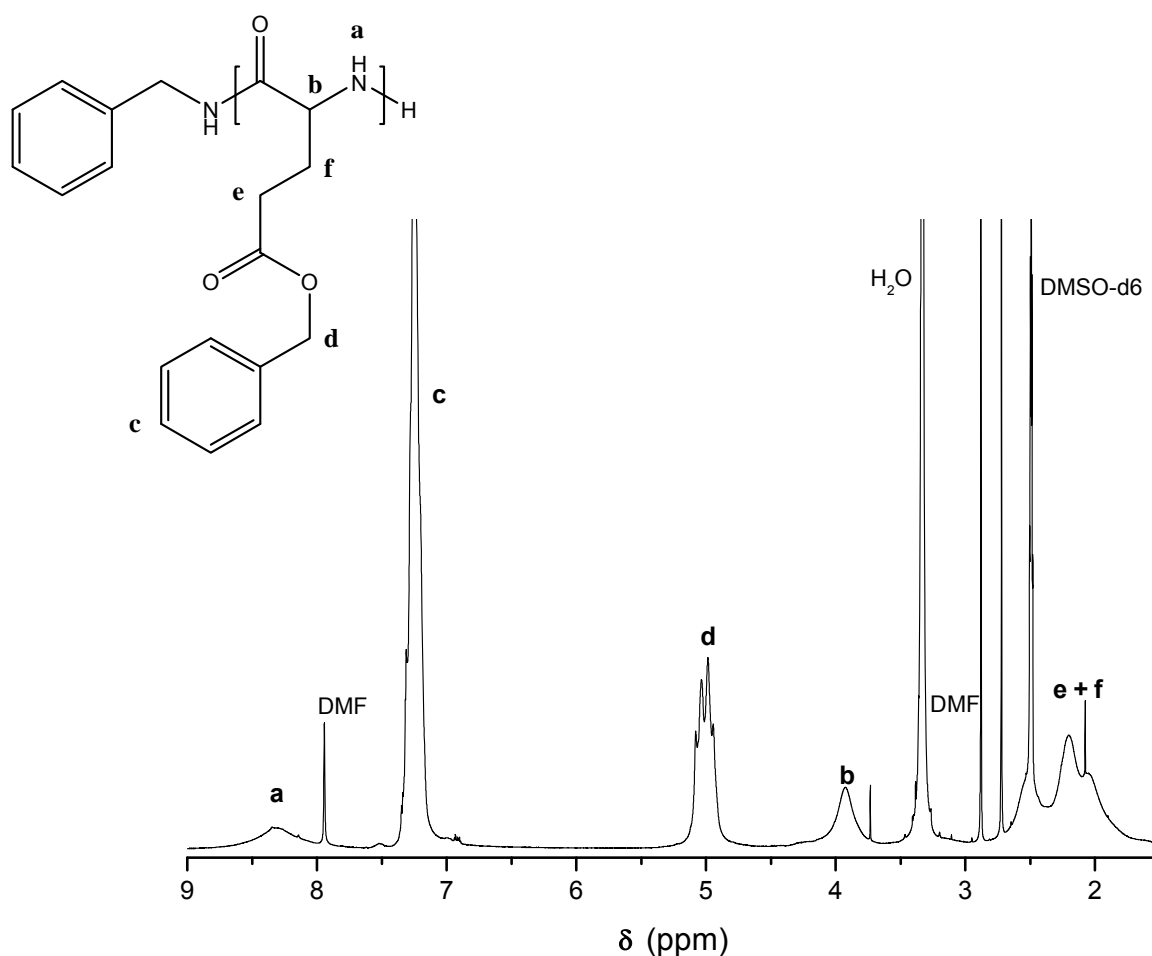


Figure 4.2  $^1\text{H-NMR}$  spectrum of PBLG synthesized via the ROP of BLG NCA.

The characteristic resonance peaks associated with the polypeptide are easily assigned to their corresponding repeat unit protons, while the assignment of end-group protons is more difficult. This is due to the overlap of the initiating amine's aromatic protons and the aromatic protons found on the repeat unit. Hence, the

determination of the molecular weight was done *via* SEC. A summary of the SEC results for the ROP of the PBLG NCA is given in table 4.1.

**Table 4.1** SEC results for the NCA polymerization of PBLG.

System	Conditions	Time (days)	Target		$M_{n, SEC}$ (g/mol)	$DP_{exp}^b$	$\mathcal{D}^c$
			MW	$DP_{100\% conv}^a$			
A	0 °C,	5	10 000	45	5 300	24	1.12
B	0 °C, Ar	5	15 000	68	9 400	42	1.11
C	0 °C, HV	3	15 000	68	11 900	54	1.13
C	0 °C, HV	5	30 000	136	22 000	100	1.15

<sup>a</sup>Degree of polymerization (DP) at 100% conversion

<sup>b</sup>Degree of polymerization as determined *via* SEC

<sup>c</sup> $\mathcal{D}$  calculated from SEC results as  $M_w/M_n$

For the initial polymerization of the PBLG NCA, various reaction conditions were investigated to obtain high molecular weight polypeptides of low dispersity,  $\mathcal{D}$ . All the reactions were run at 0 °C and degassed *via* successive freeze-pump-thaw cycles. Variations were made once the polymerization was running. The variations included running the polymerization in A) a closed system under an inert atmosphere, B) an open system with argon flushing for the entire reaction period and lastly, C) under high vacuum. The conditions under system C gave the best results as very little end-group cyclization was found. Although not 100% conversion was obtained, the target molecular weight for system C could effectively be reached within 3 days for the lower molar mass polypeptide while system B would require at least five days. In contrast, system A did not reach any target molecular weights above 10 000 g/mol in a five-day period. It should be mentioned that 100% conversion was not reached for any of the systems, which was a favourable result for our purpose as the excess NCA monomer could minimize any possible end-group cyclization from occurring.<sup>8,15</sup>

#### 4.4.1.2 MALDI-ToF-MS

End-group characterization was done *via* MALDI-ToF-MS to confirm whether the  $\omega$ -amino group was retained in the polypeptide.

MALDI-ToF-MS separates molecules according to different mass to charge ratios. This is done by ionizing molecules under high vacuum and exposing the resulting ionized molecules to an electric field. These ionized molecules are accelerated, inversely proportional to their mass, and travel through high vacuum over a fixed distance to a detector. The ions are detected as  $\{X-[M]_n-Y\}^+C^+$  with X and Y being the polymer/polypeptide end-groups, M the repeat unit, n the degree of polymerization and  $C^+$  representing the cationizing ion.

The peaks in the main distribution, Figure 4.3 are separated at intervals of 219.2 mass units and represent the repeat unit of the PBLG polypeptide. Potassium trifluoroacetate was added as the cationizing agent.

The main distribution (peak **A**) corresponds to structure **4** (Figure 4.1), confirming the presence of the free primary amine end-group. The  $m/z$  region 7550 – 7850 g/mol is shown to indicate the interval between successive peaks in the main distribution. This shows the presence of an underlying secondary distribution (peak **B**) corresponding to structure **5** (Figure 4.1), which represents a PBLG chain with a cyclized end-group. However, the possibility of the cyclization reaction taking place during the MALDI experiment should also be taken into consideration.

Experimentally, the low MW polymer in the distribution agreed well with the calculated values. Due to calibration inaccuracies, the high MW polypeptides constantly deviated from the isotopic distribution calculations by roughly 4  $m/z$  units.

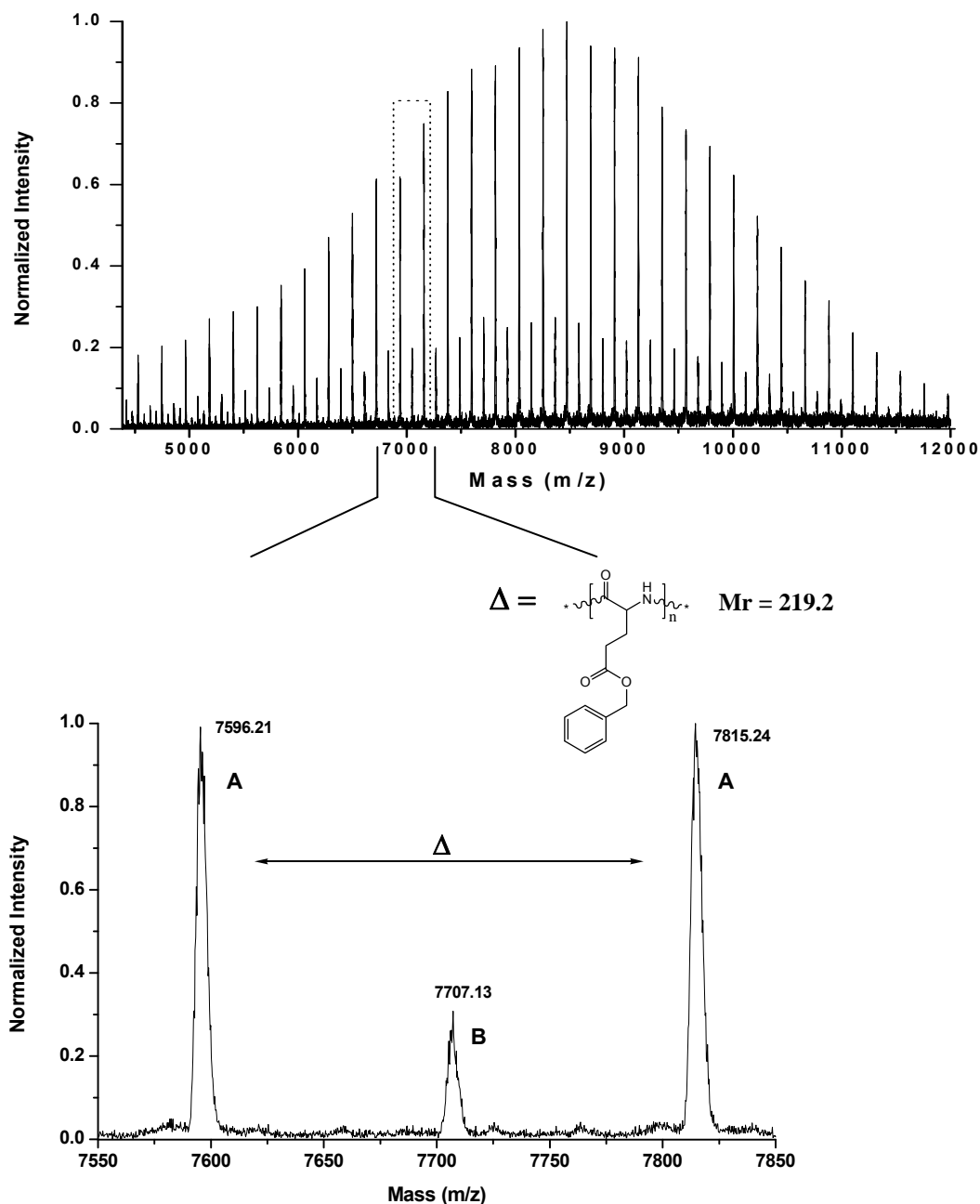


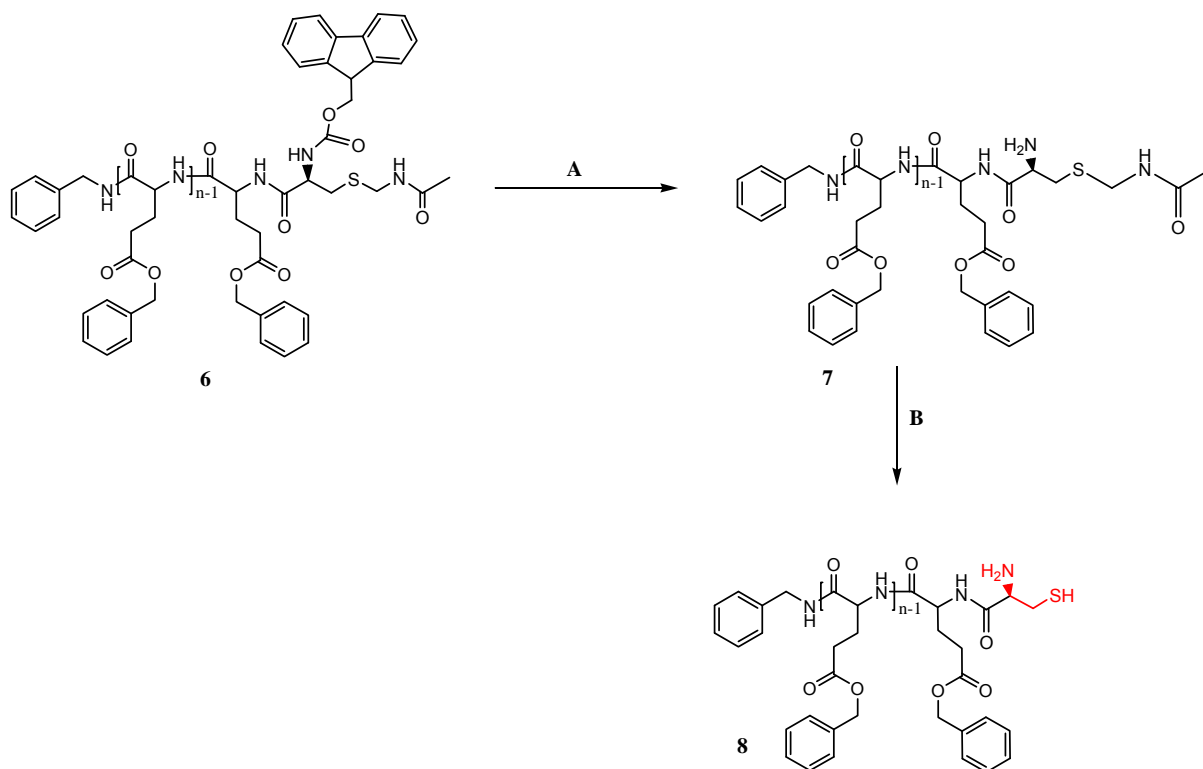
Figure 4.3 MALDI-ToF-MS of PBLG prepared by the ROP of PBLG NCA at 0 °C for 3 days under high vacuum.

#### 4.4.2 Peptide coupling reaction

The typical peptide coupling reaction involves activation of a carboxylic acid functionality by an appropriate coupling agent, followed by reaction with an amine present on the polypeptide, *i.e.* in this case PBLG. As a qualitative way of following the reaction, we used the Kaiser test<sup>25</sup>, which gives either a positive or negative result for the presence of any free primary amines. This was applied for the coupling

reaction as well as the subsequent deprotection steps. No colour change indicates that no free amines are present, while a dark blue colour confirms the presence of free primary amines.

Scheme 4.4 indicates the deprotection sequence of the Fmoc-cys(Acm) end-functional PBLG resulting in the terminal cysteine moiety.



**Scheme 4.4** Deprotection steps of the Fmoc-cys(Acm) end-functional PBLG resulting in the terminal cysteine moiety.

The initial deprotection step (**A**) entails the removal of the Fmoc group resulting in free primary amine and the protected cysteine. The subsequent step (**B**) cleaves the Acm group to produce the free thiol and subsequently the terminal cysteine.

#### 4.4.2.1 Synthesis of PBLG-Fmoc-Cys(Acm) (7)

After the peptide coupling and initial deprotection step as well as the subsequent purification of the product, end-group analysis was done using  $^1\text{H-NMR}$  spectroscopy (with DMSO- $d_6$  as solvent) and MALDI-ToF-MS. These two techniques could clearly show that aside from the presence of a small fraction of pyroglutamate end-group structures, the PBLG polypeptide did contain the protected terminal cysteine functionality (Figure 4.4).

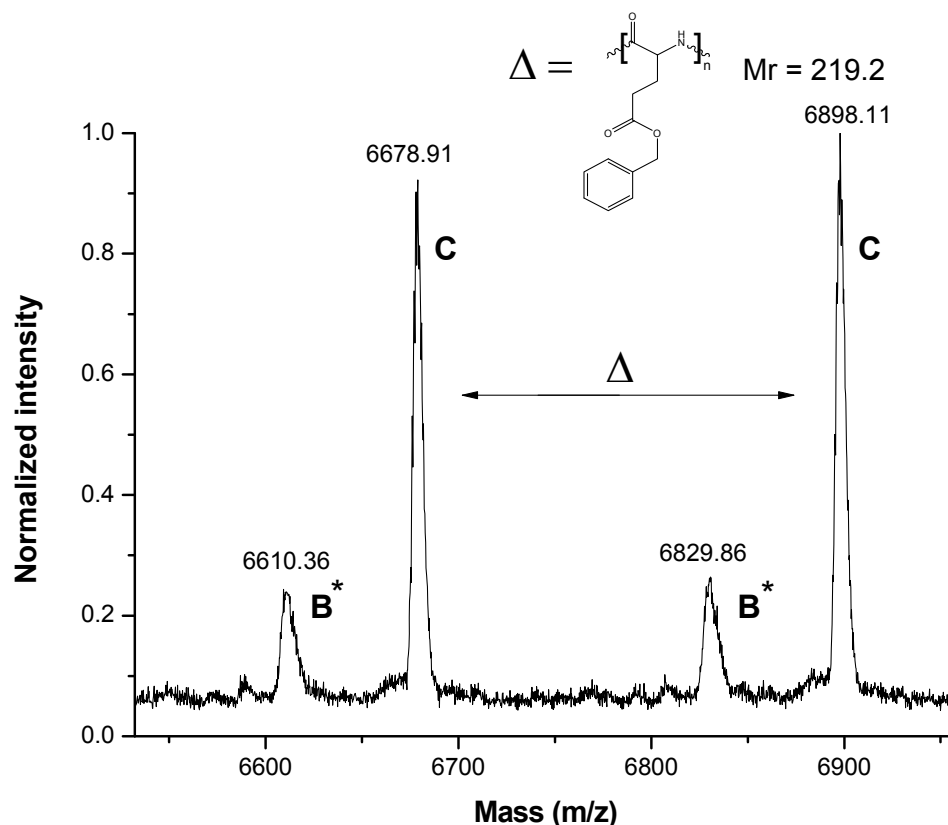


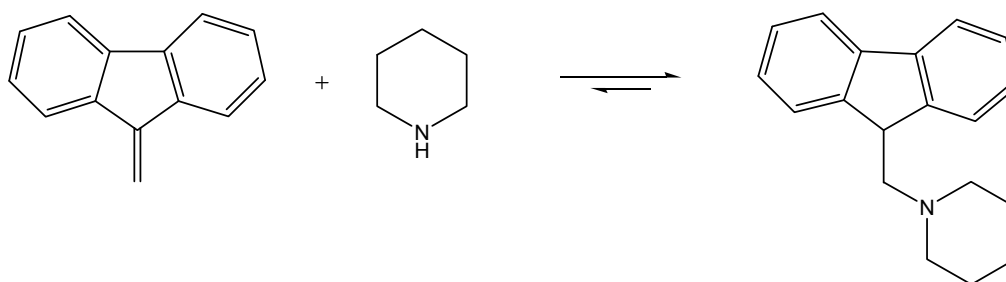
Figure 4.4 MALDI-ToF-MS of PBLG after the coupling reaction with Fmoc-Cys(Acm) group.

The main distribution, peak **C**, represents PBLG with the protected cysteine end-groups (**7**) (DP = 28). In addition, there is a secondary distribution (peak **B**) due to intramolecular ring-closure resulting in the terminal pyroglutamate chain-end.

Also, the Kaiser test was performed for the coupling reaction of the Fmoc-L-Cys(Acm) group with the primary amine functionality on PBLG. The test indicated that no free amines were present and that coupling has thus taken place.

The general deprotection of the amine-functionality by removal of the Fmoc group *via* a piperidine solution, results in an equilibrium between dibenzofulvene (DBF) and piperidine (Scheme 4.5).<sup>27</sup> Thus, the deprotection of the terminal cysteine was done in two independent steps. It was necessary to deprotect the amine before the thiol due to the possibility of a thiol-ene reaction taking place between the free thiol and any DBF present. This would eliminate the possibility to form the thiazolidine linkage when doing the conjugation reaction at a later stage.

## Chapter 4: PBLG Synthesis and Modification reactions



Scheme 4.5 Equilibrium of DBF and piperidine after Fmoc deprotection.<sup>27</sup>

The deprotection of the Fmoc group was done using a 20% piperidine solution in DMF with a catalytic amount of DBU. In addition to the Kaiser test and MALDI-ToF-MS, the deprotection was verified *via* <sup>1</sup>H-NMR spectroscopy. Figure 4.5 shows the absence of the aromatic proton signals (7.44 – 7.81 ppm) previously due to the Fmoc group.

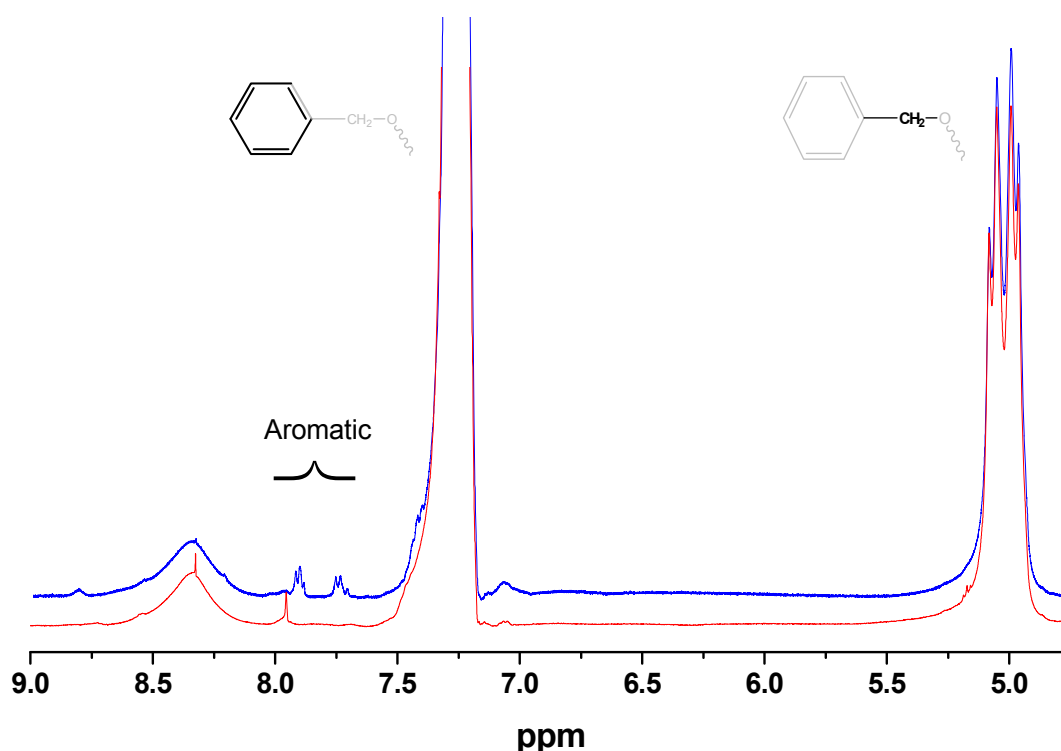


Figure 4.5 <sup>1</sup>H-NMR spectra showing PBLG before deprotection (top) and after deprotection (bottom) of the amine (*via* the removal of the Fmoc group).

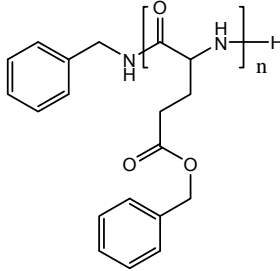
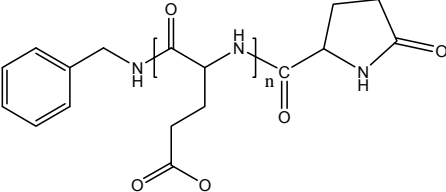

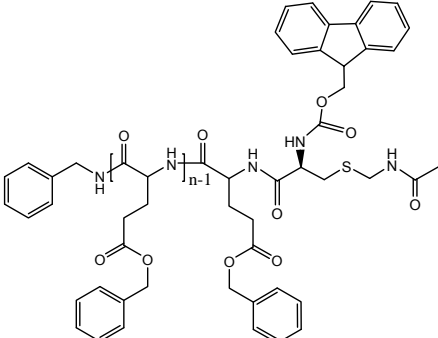
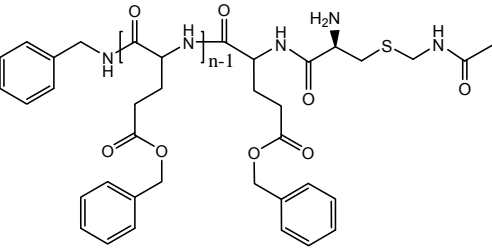
Table 4.2 shows all the structural assignments for the MALDI-ToF-MS data obtained in the synthesis of PBLG as well as the protection/deprotection steps. The products obtained after the deprotection of the amine functionality (removal of the Fmoc group) have been identified (spectrum not shown). The main distribution is labelled in



## Chapter 4: PBLG Synthesis and Modification reactions

Table 4.2 as peak **D**, while a secondary distribution of peaks was identified as PBLG with the pyroglutamate end-group structure, **B**.

Table 4.2 Structural assignments for the MALDI-ToF-MS spectra in figures 5.3 and 5.4.

Peak	Monoisotopic mass (+K <sup>+</sup> )		Structure	°n
	<sup>a</sup> Expt.	<sup>b</sup> Theo.		
A	7596.21	7600.08		34
B	7707.13	7711.18		34
B*	6610.36	6613.97		29
C	6678.91	6681.09		28
D	4703.03	4704.87		20

<sup>a</sup> Experimentally determined number average molar mass, <sup>b</sup> theoretical molar mass, <sup>c</sup> degree of polymerization

\*Chains of a different degree of polymerization with identical end-groups.

#### 4.4.2.3 Synthesis of PBLG-Cys (8)

The deprotection of the thiol functionality (removal of the AcM group) is the most challenging part in obtaining the cysteine end-functionality. Traditional methods for its removal employed harsh conditions and resulted in a toxic, albeit deprotected peptide when heavy metal ions such as mercury (II) acetate or silver (I) salts were used. This was due to the affinity of the salts for the thiol.<sup>28</sup> Due to the possible toxicity effects, the only traditional method left for the AcM group removal was *via* a simultaneous iodation and oxidation reaction resulting in the formation of disulfide bonds.<sup>29</sup> Harris *et al.*<sup>30</sup> have however reported that a gentler cleavage cocktail of 2,2-dithiobis(5-nitropyridine) (DTNP) with thioanisole and TFA was effective in certain cases.

The I<sub>2</sub>-mediated deprotection and oxidation only resulted in partial removal of the AcM group even under harsh conditions for an extended period of time (6 hours at 55 °C).

It was thus necessary to find another method, which would allow full deprotection. A patent by Cuthbertson<sup>26</sup> concluded that it is possible to remove protecting groups like AcM, 4-methylbenzyl (MBzl) and t-butyl (tBu) by subjecting them to acids under oxidizing conditions at an elevated temperature. However, when using these conditions, it was necessary to consider the lability of the benzyl ester bonds and thus their potential hydrolysis which would reduce the hydrophobicity of the polypeptide.

This was the case for the initial deprotection run as complete deprotection was achieved in 5 hours at 50 °C. Hydrolysis was evident in the <sup>1</sup>H-NMR spectra due to the near complete disappearance of the aromatic benzyl protons. Hydrolysis could also be confirmed with ATR FT-IR by the reduction of the ester carbonyl stretches at 1737 cm<sup>-1</sup> and 1171 cm<sup>-1</sup>.

In a recent article by Guo *et al.*<sup>24</sup> it was reported that the inclusion of an alcohol, which would result in an ester exchange reaction, could inhibit hydrolysis as these are competitive reactions. They showed that the inclusion of 2.5 molar equivalents of benzyl alcohol (to the repeat units of PBLG) could completely suppress hydrolysis by taking part in the ester exchange reaction while maintaining the backbone structure of PBLG.

Thus, it was attempted to modify the Acm deprotection reaction by including the benzyl alcohol and thereby avoiding the hydrolysis of the ester bonds. In this way, it was possible to obtain the deprotected PBLG chains without forming the glutamic acid residues. The removal of the Acm group could be confirmed by SEC as the subsequent oxidation of the thiol linkages led to a doubling of the molecular weight.

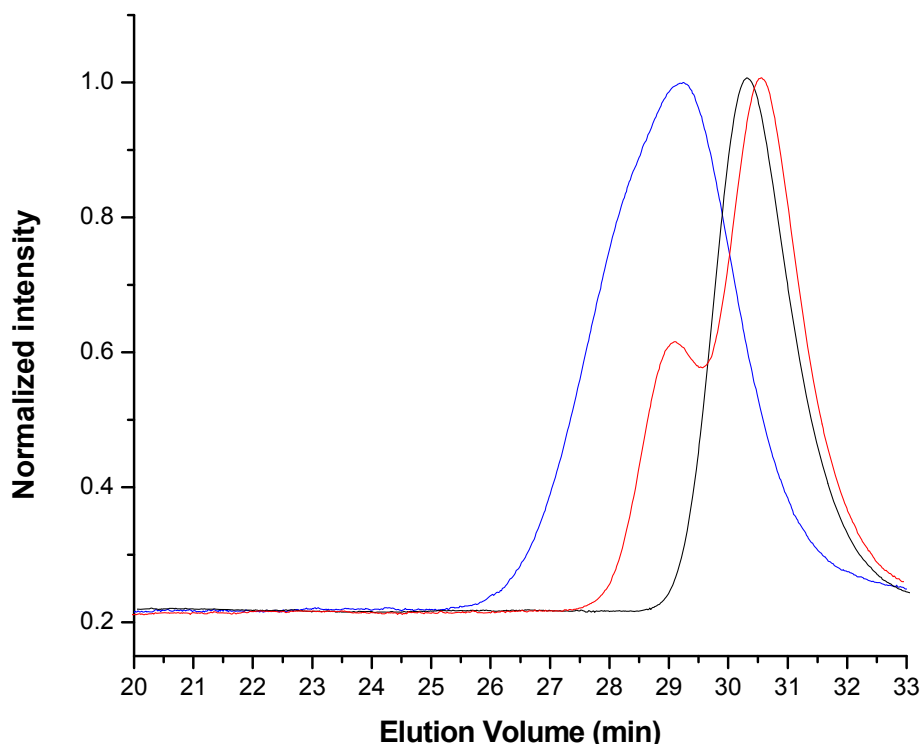


Figure 4.6 SEC traces indicating the extent of Acm deprotection and subsequent oxidation of PBLG. The black trace is fully protected, the red trace partially deprotected ( $I_2/[Ox]$ ) and the blue trace fully deprotected (TFA).

Figure 4.6 indicates the elution of the polypeptides before and after the application of the deprotection steps as well as the incomplete deprotection that was achieved using the iodation method. The black trace represents the original protected PBLG ( $M_n$  13 200 g/mol,  $\mathcal{D}$  = 1.13). The blue trace is the result of successful deprotection and subsequent oxidation of the thiol functionality using the modified TFA/p-TSA/benzyl alcohol method. This leads to the doubling of the molecular weight as well as a slight increase in the dispersity ( $M_n$  26 100 g/mol,  $\mathcal{D}$  = 1.21).

## 4.5 Conclusions

Low dispersity, well-defined PBLG was synthesized under conditions that promote the NAM mechanism. These conditions allowed for the polymerization of the NCA monomer with mainly  $\omega$ -amino chain-ends. MALDI-ToF-MS analysis did however show a secondary distribution which could be assigned to cyclized end-groups, this was most probably due to high monomer conversion and inadequate temperature regulation.<sup>8</sup>

The primary amine end-functionalized PBLG was protected with a Pfp-activated ester, namely a protected cysteine moiety, Fmoc-L-Cys(Acm)-OPfp. Further deprotection steps allowed for the synthesis of thiol-functional PBLG, which upon oxidation formed disulfide linkages. The deprotection problems of the Acm group when using traditional deprotection methods were overcome with a modified procedure. A modified procedure using excess TFA under oxidizing conditions allowed for the efficient removal of the Acm group. This was incorporated with work done by Guo *et al.*<sup>31</sup> where the inclusion of the catalyst p-TSA and benzyl alcohol created an equilibrium between ester exchange and hydrolysis. Sufficient excess of the benzyl alcohol forced the equilibrium towards the ester exchange reactions thereby effectively suppressing the hydrolysis of the benzyl ester group. This resulted in two PBLG chains with free primary amines being linked *via* the subsequently oxidatively coupled thiols.

#### 4.6 References

- (1) Holowka, E. P.; Pochan, D. J.; Deming, T. J. *J. Am. Chem. Soc.* **2005**, *127*, 12423-12428.
- (2) Iatrou, H.; Frielinghaus, H.; Hanski, S.; Ferderigos, N.; Ruokolainen, J.; Ikkala, O.; Richter, D.; Mays, J.; Hadjichristidis, N. *Biomacromolecules* **2007**, *8*, 2173-2181.
- (3) Sun, J.; Chen, X.; Deng, C.; Yu, H.; Xie, Z.; Jing, X. *Langmuir* **2007**, *23*, 8308-8315.
- (4) Osada, K.; Christie, R. J.; Kataoka, K. *Journal of The Royal Society Interface* **2009**, *6*, S325-S339.
- (5) Heffernan, M.; Murthy, N. *Annals of Biomedical Engineering* **2009**, *37*, 1993-2002.
- (6) Gibson, M. I.; Cameron, N. R. *J. Polym. Sci., Part A: Polym. Chem.* **2009**, *47*, 2882-2891.
- (7) Habraken, G. J. M.; Peeters, M.; Dietz, C. H. J. T.; Koning, C. E.; Heise, A. *Polymer Chemistry* **2010**, *1*, 514-524.
- (8) Habraken, G. J. M.; Wilsens, K. H. R. M.; Koning, C. E.; Heise, A. *Polymer Chemistry*, *2*, 1322-1330.
- (9) Lu, H.; Cheng, J. *J. Am. Chem. Soc.* **2008**, *130*, 12562-12563.
- (10) Vayaboury, W.; Giani, O.; Cottet, H.; Deratani, A.; Schué, F. *Macromol. Rapid Commun.* **2004**, *25*, 1221-1224.
- (11) Deming, T. J. *Nature* **1997**, *390*, 386.
- (12) Deming, T. J. *J. Polym. Sci., Part A: Polym. Chem.* **2000**, *38*, 3011-3018.
- (13) Kricheldorf, H. R.; von Lossow, C.; Schwarz, G. *Macromolecules* **2005**, *38*, 5513-5518.
- (14) Kricheldorf, H. R. *Angew. Chem., Int. Ed.* **2006**, *45*, 5752-5784.
- (15) Mitchell, J. C.; Woodward, A. E.; Doty, P. *J. Am. Chem. Soc.* **1957**, *79*, 3955-3960.

- (16) Hadjichristidis, N.; Iatrou, H.; Pitsikalis, M.; Sakellariou, G. *Chem. Rev. (Washington, DC, U. S.)* **2009**, *109*, 5528-5578.
- (17) Muzart, J. *Tetrahedron* **2009**, *65*, 8313-8323.
- (18) Aliferis, T.; Iatrou, H.; Hadjichristidis, N. *Biomacromolecules* **2004**, *5*, 1653-1656.
- (19) Daly, W. H.; Poché, D. *Tetrahedron Lett.* **1988**, *29*, 5859-5862.
- (20) Poche, D. S.; Daly, W. H.; Russo, P. S. *Macromolecules* **1995**, *28*, 6745-6753.
- (21) Habraken, G. J. M.; Koning, C. E.; Heuts, J. P. A.; Heise, A. *Chem. Commun. (Cambridge, U. K.)* **2009**, 3612-3614.
- (22) Hernández, J. R.; Klok, H.-A. *J. Polym. Sci., Part A: Polym. Chem.* **2003**, *41*, 1167-1187.
- (23) Blout, E. R.; Karlson, R. H. *J. Am. Chem. Soc.* **1956**, *78*, 941-946.
- (24) Guo, J.; Huang, Y.; Jing, X.; Chen, X. *Polymer* **2009**, *50*, 2847-2855.
- (25) Kaiser, E.; Colescott, R. L.; Bossinger, C. D.; Cook, P. I. *Anal. Biochem.* **1970**, *34*, 595-598.
- (26) Cuthbertson, A.; Amersham Health AS (Oslo, NO): United States, 2005; Vol. 6906171.
- (27) Carpino, L. A. *Acc. Chem. Res.* **1987**, *20*, 401-407.
- (28) Moyle, P. M.; Olive, C.; Good, M. F.; Toth, I. *J. Pept. Sci.* **2006**, *12*, 800-807.
- (29) Kamber, B.; Hartmann, A.; Eisler, K.; Riniker, B.; Rink, H.; Sieber, P.; Rittel, W. *Helv. Chim. Acta* **1980**, *63*, 899-915.
- (30) Harris, K. M.; Flemer, S.; Hondal, R. J. *J. Pept. Sci.* **2007**, *13*, 81-93.
- (31) Guo, J.; Huang, Y.; Jing, X.; Chen, X. *Polymer* **2009**, *50*, 2847-2855.

## **Biohybrid poly(N-vinylpyrrolidone)-*b*-poly( $\gamma$ -benzyl-L-glutamate) copolymers *via* thiazolidine chemistry**

### **5.1 Introduction**

In the last couple of decades, the conjugation of synthetic and natural macromolecules has enjoyed increased interest. This is due to the advancement in controlled radical polymerization (CRP) systems which allowed for tailor made synthesis of polymer-based pharmaceuticals using various facile processes. The term “polymer therapeutics” has been coined to describe a diverse range of polymeric nanovehicles which incorporate water-soluble polymers as components in drug delivery systems (DDS), either by being bioactive itself or as an inert, yet integral part of the drug delivery process.<sup>1,2</sup>

These nanovehicles include polymer-drug conjugates,<sup>3</sup> polymer-protein bioconjugates<sup>4,5</sup> and amphiphilic block copolymers which transport hydrophobic drugs either *via* physical or chemical encapsulation.<sup>6</sup> The main purpose of this combinatorial science is to improve the polymer therapeutics by increasing the residence time of the drug delivery vehicle in the desired environment. This could result in better targeting as well as an improvement in the solubilization of the drug *via* complexation or encapsulation.

#### **5.1.1 Biohybrid amphiphilic block copolymers**

Traditionally, poly(ethylene glycol) (PEG) has been used as the hydrophilic segment in amphiphilic block copolymers due to its inherent biocompatibility. The term PEGylation is used when PEG is conjugated to another molecule, normally a drug or bioactive polypeptide.<sup>4,7</sup>

Furthermore, the interest in biohybrid materials *i.e.* the combination of natural and synthetic polymers has largely increased in recent years. Living polymerization techniques that are combined with *N*-carboxyanhydride ring-opening polymerization (NCA ROP) need specific functionalities to either facilitate polymerization or form covalent linkages. This is achieved using an amine end-functional macroinitiator or by end-group modification of the synthetic polymer.<sup>8-11</sup>

In the present study, poly(*N*-vinylpyrrolidone) (PVP) is covalently linked to poly( $\gamma$ -benzyl-L-glutamate) (PBLG) using a modular approach. Post-polymerization

## Chapter 5: PVP and PBLG hybrid block copolymers

modification on both the PVP (Chapter 3) and PBLG (Chapter 4) chain-ends allows for conjugation *via* a thiazolidine linkage (Figure 5.1).

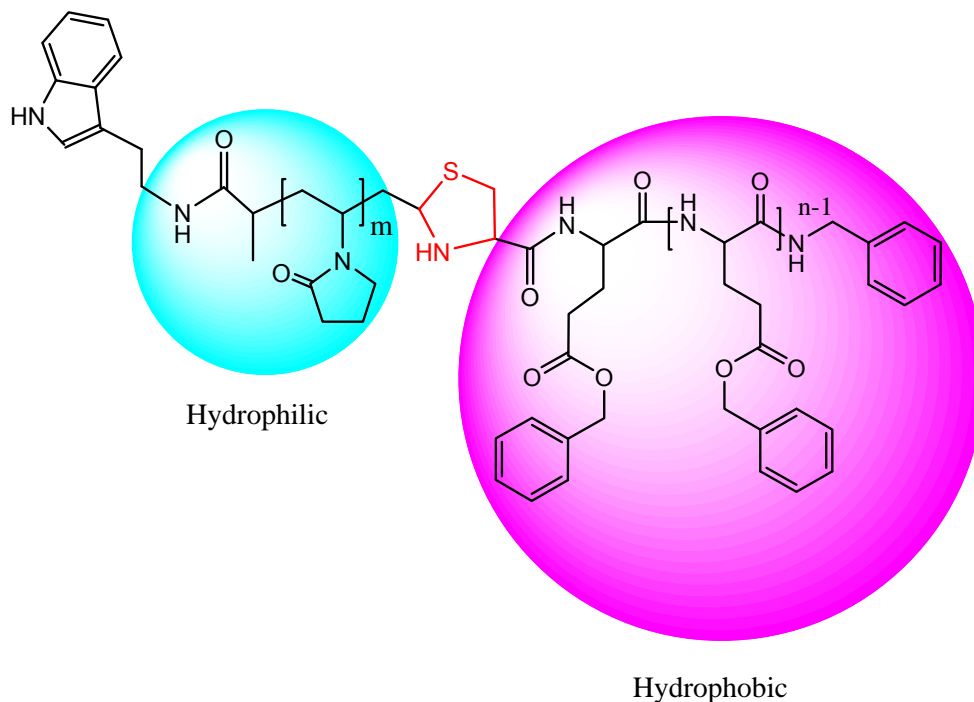


Figure 5.1 Graphical representation of the hydrophilic PVP block conjugated to the hydrophobic PBLG block *via* a thiazolidine linkage.

Furthermore, well-defined cysteine containing PBLG was obtained from the group of Habraken *et al.* (Figure 5.2, **2**). The copolypeptide, P(BLG<sub>40</sub>-*b*-tBMLC<sub>3</sub>) was synthesized using a protected cysteine with the potential of applying secondary modification reactions.<sup>12</sup> In the present study, the conjugation efficiency of end-functionalized PBLG (terminal cysteine, **1**) and a copolypeptide with several cysteine repeat units (PBLG-*b*-Cys, **2**) was investigated.

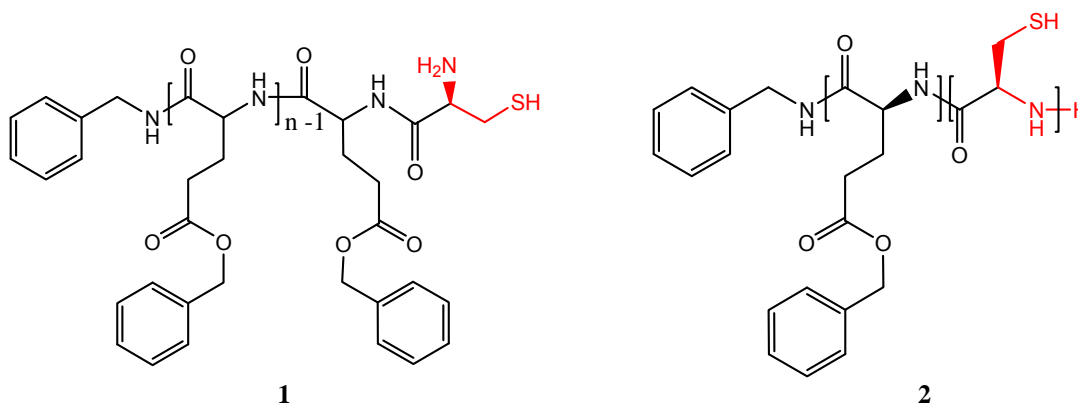


Figure 5.2 The two different cysteine end-functional PBLG chains incorporated in the study *i.e.* PBLG-Cys (**1**) and PBLG-*b*-Cys (**2**).

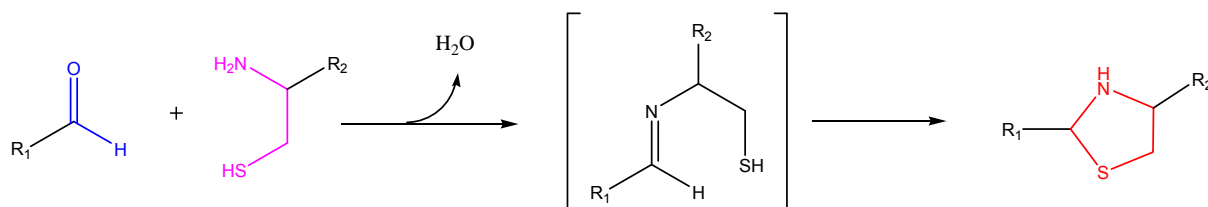


## Chapter 5: PVP and PBLG hybrid block copolymers

This synthesis of cysteine-terminal PBLG using the procedure of Habraken *et al.*<sup>12</sup> is a more routine method for preparing this end-functionality as no real knowledge of peptide chemistry is necessary beforehand. However, it is not possible to limit the cysteine containing polypeptide to one unit which results in an average of two – three free thiols per chain after deprotection. The effect of these free thiols regarding the conjugation reaction with PVP is unknown was investigated.

With the purpose of conjugating the PVP homopolymer to the polypeptide PBLG, a model study was done to investigate the conditions for the synthesis of a covalent thiazolidine linkage.

The thiazolidine linkage was chosen because its formation proceeds *via* a facile reaction without the need for an external stimulus or catalyst and the linkage is biocompatible.<sup>13</sup> This reaction typically takes place *via* a cysteine residue (1,2-aminothiols) and an aldehyde (Scheme 5.1). Tam *et al.*<sup>14</sup> reported the synthesis of peptide dendrimers *via* oxime, hydrazone and thiazolidine linkages. They concluded that the thiazolidine linkage had the fastest ligation rate of the three linkages, and they optimized the conditions which included running the reaction in a water-miscible solvent like *N,N*-dimethylformamide (DMF) at 37 °C at an optimal pH of 4.5.



**Scheme 5.1** The mechanism for thiazolidine formation is depicted. This proceeds *via* the reaction of a 1,2-aminothiol and an aldehyde.

The Grinstaff group focussed on the thiazolidine linkage to fabricate materials that could eventually be used in cataract surgery. Recent work in dynamic combinatorial chemistry (DCC) has shown the versatility of the linkage. However, they did mention that the formation of the linkage is synthetically challenging and thus limited in its applicability.<sup>15,16</sup>

A model study was carried out with cysteamine and aldehyde end-functional PVP to investigate optimal conditions for the conjugation reaction.

## 5.2 Experimental details

### 5.2.1 Materials

*N,N*-dimethylformamide (DMF, molecular biology, > 99%), DL-Dithiothreitol (DTT, > 98%) Nile red (bioreagent, > 98%) and Tris(2-carboxyethyl)phosphine hydrochloride (TCEP, > 98%) were purchased from Sigma-Aldrich and used without further purification. DMF was used as received and stored under an inert, dry atmosphere. 5,5'-Dithiobis(2-nitrobenzoic acid) (Ellman's reagent, Fluka,  $\geq 97.5\%$ ) and cysteamine (Fluka, > 98%) were used as received. Phosphate buffered saline tablets (Merck) were used to make a PBS solution.

### 5.2.2 General reaction procedure for thiazolidine formation

The general experimental procedure for the ligation reactions was as follows, with variations in the solvent choice as well as in the reducing agent.

PVP-CHO (0.2 g, 0.033 mmol), a 15-fold molar excess of cysteamine (0.039 g, 0.5 mmol) and DTT (0.5 mg, 0.033 mmol) were placed in a 50 mL Schlenk flask and dissolved in 5 mL of an 80/20 v/v mixture of DMF and PBS buffer (0.5 M, pH 4.5). The reaction mixture was degassed *via* three freeze-pump-thaw cycles followed by the introduction of argon into the flask. The reaction was left to stir for three hours at room temperature. The solution was purified by dialysis against deionized water using SnakeSkin® pleated dialysis tubing (Pierce, molecular weight cut-off = 3500 g·mol<sup>-1</sup> dextran equivalents) for 24 h at room temperature. The solution was initially replaced three times every two hours and then every nine hours. The concentrated product was subsequently isolated *via* freeze-drying.

#### 5.2.2.1 Synthesis of cysteine containing PBLG (1)

The deprotection of the terminal cysteine unit in PBLG (1) is described in section 4.4.2

#### 5.2.2.2 Synthesis of cysteine containing PBLG (2)

The polypeptide obtained from Habraken *et al.*<sup>12</sup> has a cysteine protected with a tertiary butyl group, S-tert-butylmercapto-L-cysteine (tBMLC). The polymer P(BLG<sub>40</sub>-*b*-tBMLC<sub>3</sub>) (M<sub>n</sub> = 11 000 g/mol) was deprotected using the method described by Habraken *et al.*<sup>17</sup> The polymer P(BLG<sub>40</sub>-*b*-tBMLC<sub>3</sub>) (0.392 g, 0.0356 mmol) and DTT

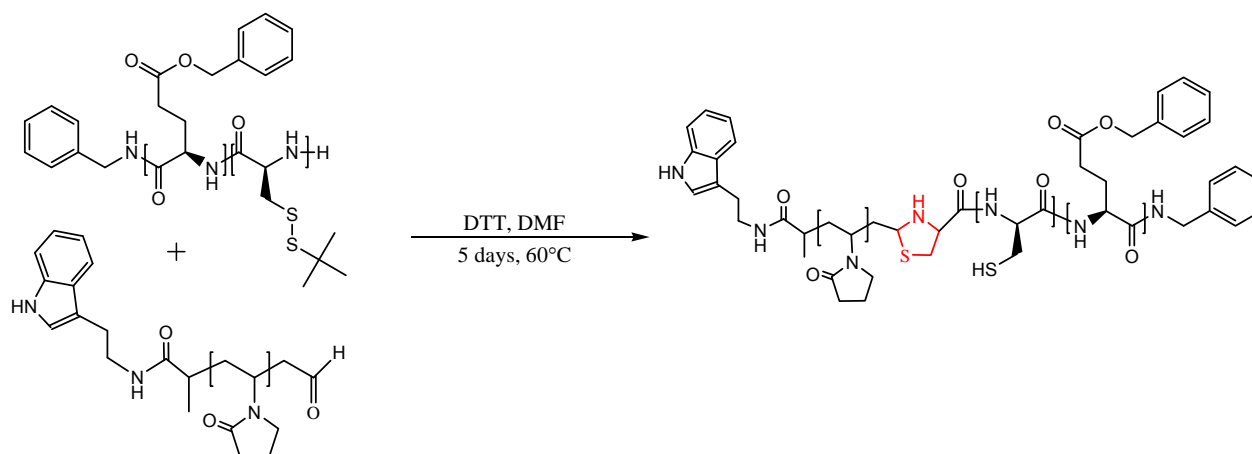
## Chapter 5: PVP and PBLG hybrid block copolymers

(0.118 g, 0.76 mmol) were dissolved in 8 mL of DMF. The reaction mixture was degassed *via* four freeze-pump-thaw cycles followed by the introduction of argon into the flask. The reaction was maintained for 5 days at 60 °C after which the reaction mixture was concentrated and precipitated in diethyl ether. The final product was dried under vacuum at 20 °C. The yield was 0.097 g (83%).

### 5.2.2.3 Synthesis of PVP-*b*-PBLG amphiphilic block copolymers

The conjugation reaction between the  $\omega$ -aldehyde PVP and the cysteine end-functional PBLG has been achieved *via* a similar pathway for both **1** and **2**. DMF has been shown to be an effective solvent for the conjugation reaction and also the inclusion of a reducing agent like DTT has no significant effect on the thiazolidine formation (section 5.4.1). The presence of DTT inhibits disulfide formation. The aldehyde end-functionality was varied from an equivalent molar ratio to a four-fold excess compared to the cysteine moiety on the PBLG. This was done for the conjugation reactions of both **1** and **2**. There was an additional variation in the experimental procedure for **2** in which simultaneous deprotection and conjugation of the polypeptide was attempted *in situ*.

The general procedure for the *in situ* simultaneous deprotection and conjugation reaction proceeded as follows (Scheme 5.2).



**Scheme 5.2** One-pot deprotection of P(BLG<sub>40</sub>-*b*-tBMLC<sub>3</sub>) and conjugation with  $\omega$ -aldehyde PVP.

P(BLG<sub>40</sub>-*b*-tBMLC<sub>3</sub>) (0.4 g, 0.036 mmol), dithiothreitol (DTT) (0.138 g, 0.89 mmol) and PVP-CHO in four-fold excess to the cysteine group (0.81 g, 0.15 mmol) were dissolved in 15 mL DMF. The reaction mixture was degassed *via* three freeze-pump-

## Chapter 5: PVP and PBLG hybrid block copolymers

thaw cycles followed by the introduction of argon into the flask. The reaction was left for five days under magnetic stirring at 60 °C. The reaction mixture was purified by dialyzing against distilled water using SnakeSkin® pleated dialysis tubing (Pierce, molecular weight cut-off = 7000 g/mol dextran equivalents) for 24 h at room temperature. The solution was initially replaced three times every two hours and then every nine hours. The concentrated product was subsequently isolated *via* freeze-drying.

The general procedure for the conjugation reaction of **1** and **2** was as follow.

PBLG-Cys (**1**) (0.1g,  $7.69 \times 10^{-6}$  mol) and a 1.5 molar excess of aldehyde end-functional PVP (0.115 g,  $1.15 \times 10^{-5}$  mol) were dissolved in 5 mL of DMF in a Schlenk flask. An excess of DTT was added to the reaction mixture and subsequently degassed *via* three freeze-pump-thaw cycles followed by the introduction of argon into the flask. The reaction was left under magnetic stir for 24 hours at 37 °C. Purification was done by dialyzing against distilled water using SnakeSkin® pleated dialysis tubing (Pierce, molecular weight cut-off = 7000 g/mol dextran equivalents) for 24 h at room temperature. The solution was initially replaced three times every two hours and then every nine hours. The concentrated product was subsequently isolated *via* freeze-drying.

Characterization of the amphiphilic block copolymers was done *via*  $^1\text{H-NMR}$  spectroscopy and SEC.

### 5.2.3 Preparation of polymeric micelles

The PVP-*b*-PBLG diblock copolymers (10 mg) were dissolved in DMF (1 mL) after which 10 mL of a PBS buffer solution (0.5 M, pH 7.4) was added dropwise (1 drop every 2 – 4 seconds). Purification was done by dialyzing against distilled water using SnakeSkin® pleated dialysis tubing (Pierce, MWCO 7000 g/mol dextran equivalents) for 24 h. The polymeric micelles obtained were then isolated *via* freeze-drying.

### 5.2.4 Determination of the critical micelle concentration

The critical micelle concentration (CMC) was determined using Nile red (NR) as a fluorescence probe. Different dilutions were prepared from a 2 mg/mL stock solution of micelles with concentrations ranging from  $10^{-5}$  to 0.5 mg/mL. The total volume of the final micelle solution was 2 mL. NR dissolved in acetone was added to the vials

## Chapter 5: PVP and PBLG hybrid block copolymers

containing the polymer solution (30  $\mu\text{L}$  aliquots,  $1 \times 10^{-4}$  M) to obtain a final NR concentration of  $6 \times 10^{-7}$  M. The polymer solutions with NR were incubated for 24 hours at room temperature in the dark to allow evaporation of acetone. The fluorescence emission spectra were recorded from 500 to 720 nm using 550 nm as the excitation wavelength. The CMC was determined as the inflection point on the plots representing the maximum emission wavelength as a function of the negative Log copolymer concentration. Spectra were obtained on a Perkin-Elmer LS 50B fluorescence spectrometer at room temperature.

### 5.2.5 Preparation of pyrene-loaded micelles

Pyrene (at different pyrene/polymer ratio) was dissolved in DMSO (1 mL) and stirred overnight. Then 20 mg of PVP-*b*-PBLG in 1 mL DMSO was added to the pyrene solution. To this solution pH 7.4 phosphate buffer (10 mL, 20 mM) was added dropwise (1 drop per 1–2 s) under vigorous stirring. The resulting solution was continuously stirred for another 4–6 h, and then dialyzed against 2 L of water for 24 h using SnakeSkin® pleated dialysis tubing (Pierce, MWCO 3500 g/mol dextran equivalents). The solution was initially replaced three times every two hours and then every nine hours. The solution was filtered through a 0.45- $\mu\text{m}$  GHP (Millipore) filter and freeze-dried. The incorporation of pyrene was confirmed by measuring the UV absorbance at 338 nm of the polymeric micelles dissolved in DMSO.

### 5.2.6 Cell viability study

Rat heart myoblast (H9c-2) cells were grown at the Cell Death Group of the Physiology Department at University of Stellenbosch. The H9c-2 cells were seeded at a density of  $10^5$  cells/well into petri dishes, and grown to a confluency of 70–80 %. Hoechst (Hoechst 33342, Sigma) and propidium iodide (PI) (Sigma, P4170), in a 1:200 dilution in PBS, were directly added onto the cells, using a final concentration of 50  $\mu\text{g}/\text{mL}$  and 1  $\mu\text{g}/\text{mL}$ , respectively. Incubation took 10 min and images were acquired immediately thereafter. Samples were observed on an Olympus Cell<sup>R</sup> system attached to an IX-81 inverted fluorescence microscope equipped with an F-view-II cooled CCD camera (Soft Imaging Systems). Using a Xenon-Arc burner (Olympus Biosystems GMBH) as light source, images were excited with the 360 nm or 572 nm excitation filter. Emission data was collected using a UBG triple-bandpass emission filter cube. Images were processed and background-subtracted using the Cell<sup>R</sup> software.

### 5.3 Analysis

#### 5.3.1 NMR spectroscopy

$^1\text{H}$  NMR and  $^{13}\text{C}$  NMR spectra were acquired with a Varian VXR-Unity (300 MHz) spectrometer in  $\text{CDCl}_3$  (unless specified otherwise). All chemical shifts are reported in parts per million (ppm) with tetramethylsilane (TMS) as an internal reference.

#### 5.3.2 SEC

SEC analysis was carried out on a DMAc solvent system using a flow rate of 1.0 mL/min. The instrument setup consisted of a Shimadzu LC-10AD pump, a column system fitted with a 50x8 mm guard column in series with three 300x8 mm, 10  $\mu\text{m}$  particle size GRAM columns (2 x 3000Å and 100Å) obtained from PSS, a Waters 2487 dual wavelength UV detector and a Waters 2414 differential refractive index (DRI) detector all in series. 100  $\mu\text{L}$  injection volumes are sampled individually with the oven temperature of the column and DRI detector kept at 40 °C. The solvent was stabilized with 0.05% BHT (*w/v*) and 0.03% LiCl (*w/v*), and samples were filtered through a 0.45  $\mu\text{m}$  GHP filter to prevent any impurities entering the system. Calibration was done using PMMA standards (Polymer Laboratories) ranging from 690 to  $1.2 \times 10^6$  g/mol. Data acquisition was done using Millennium<sup>32</sup> software, version 4.

#### 5.3.3 ATR-FTIR spectroscopy

IR spectra were recorded using a Thermo-Nicolette iS10 FTIR spectrometer with a ZnSe ATR attachment and a LC-transform attachment. This allowed the examination of samples in solid or liquid state without prior sample preparation. Spectra were recorded in the range of 500-4000  $\text{cm}^{-1}$ . The resolution was set to 8  $\text{cm}^{-1}$  and 32 scans were collected per sample. Omnic spectra software (version 8.1) was used for all data acquisition and processing.

#### 5.3.4 Fluorescence spectroscopy

Fluorescence spectroscopy was measured on a Perkin-Elmer LS-50B luminescence spectrometer. FL Winlab V4 was used for data acquisition and processing.

### 5.3.5 UV-Vis spectroscopy

UV-Vis spectra were measured using a Perkin Elmer double-beam spectrometer. The model of the spectrometer was a Lambda 20 which comprised a holographic monochromator, pre-aligned deuterium and halogen lamps and a photodiode array detector. Samples were measured in a cuvette with a 10 mm light path at 25 °C. UV Winlab (version 2.0) software was used for data acquisition and processing.

### 5.3.6 Transmission electron microscopy

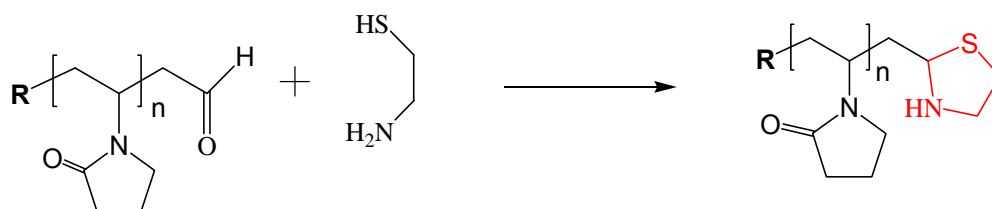
The transmission electron microscopy (TEM) images were recorded with an FEI Tecnai TF20 field emission gun transmission electron microscope (FEG-TEM) operated at 200 keV. Prior to imaging, the samples were stained with uranyl acetate to induce contrast in the sample during imaging. The uranyl acetate stain consisted of 2 wt% uranyl acetate dissolved in deionised water. During staining, one drop of sample was placed on a carbon coated copper grid and left for 60 seconds. The carbon coated copper grids were glow-discharged beforehand to induce hydrophilicity in the carbon layer of the copper grid, which assists in the dispersion of the sample prior to staining. After 60 seconds the excess sample was blotted using filter paper and the stain applied by dipping the sample containing copper grid in the stain solution. The excess stain was then blotted and the sample placed under xenon light to dry.

### 5.3.7 Dynamic Light Scattering

The average hydrodynamic diameter of the micelles was determined *via* dynamic light scattering (DLS). This was achieved with a Zetasizer nano ZS90 instrument. Particle sizes are detected at a 90° scattering angle with a 4 mW He-Ne laser and a 633 nm incident beam (Malvern instruments, UK). The final particle size and particle size distribution were obtained from three measurements, each comprising 10–15 sub-runs. The particle size and particle size distribution were calculated using CONTIN analysis. Results are presented as the Z-average droplet size.

## 5.4 Reaction of $\omega$ -aldehyde end functional PVP with cysteamine

The reaction between the aldehyde end-functional PVP and cysteamine was investigated to identify the optimum conditions for the formation of the thiazolidine linkage (Scheme 5.3).



Scheme 5.3 General reaction of cysteamine and the  $\omega$ -aldehyde end-functional PVP for the formation of the thiazolidine linkage.

Optimum parameters were investigated to identify whether certain conditions could possibly impede the cyclization reaction or inhibit it completely. This was necessary to determine successful conditions for bioconjugation, the most prominent variations included the type of reaction medium as well as the presence of a reducing agent.

The mechanism is based on the elimination of a molecule of water after the nucleophilic addition step. Tam *et al.*<sup>14</sup> have previously reported conditions for the ligation reactions where they use DMF in a cosolvent system (50% buffer solution at a pH of 4.5) at 37 °C. They concluded that the ligation rate is fastest at a pH of 4.5.

## 5.4 Results and discussion

### 5.4.1 Chain-end analysis

The characterization of the thiazolidine moiety itself is difficult as individual techniques tend to be inconclusive as to whether the ligation is due to the formation of a Schiff base or whether cyclization has indeed occurred to form the thiazolidine linkage. Bi *et al.*<sup>18</sup> reported the confirmation of the linkage *via* ATR-FTIR spectroscopy as a broad peak at 1128  $\text{cm}^{-1}$ , this was assigned to the C-N group in the thiazolidine ring.<sup>13</sup> The difficulty lies in distinguishing between the ring-opened and ring-closed structure. In the present study, a combination of characterization techniques were utilized which included  $^1\text{H-NMR}$  spectroscopy, MALDI-ToF-MS and Ellman's test for the detection of free thiols.<sup>19</sup>



## Chapter 5: PVP and PBLG hybrid block copolymers

The ligation reaction of the  $\omega$ -aldehyde PVP and cysteamine was not run to full conversion of the thiazolidine structure. The incomplete reaction allowed for comparative studies using the quantitative analysis of the reduction in the aldehyde peak using  $^1\text{H-NMR}$  spectroscopy (this reduction was attributed to thiazolidine formation. No clear formation of the thiazolidine linkage itself was evident from  $^1\text{H-NMR}$  spectroscopy, possibly due to masking by the broad polymeric signals.

The formation of the thiazolidine linkage was investigated and quantified under different conditions. The eventual conjugation reaction with the hydrophobic PBLG needed to be efficient in an organic solvent, in the presence of a reducing agent. An aqueous cosolvent system (required to reduce the pH) could potentially affect the conjugation efficiency due to precipitation of the hydrophobic block.

Variations in reaction conditions included the solvent system, the amount of reducing agent as well as the type of reducing agent. The conversion of the thiazolidine formation was correlated with the reduction of the aldehyde signal (9.66 ppm).

Comparisons are drawn between the effectiveness of two different reducing agents, namely dithiothreitol (DTT) and tris(2-carboxyethyl)phosphine (TCEP). It has been reported that DTT adducts can form, *i.e.* the two sulfur atoms of DTT may form disulfide bonds to different sulfur atoms and not cyclize.<sup>20</sup> It was investigated whether DTT could influence ligation due to thiol competition during the cyclization process in which the Schiff base intermediate ring closes to form the thiazolidine structure.

The reagents were dissolved in an 80/20 *v/v* mixture of DMF and PBS buffer of which the pH was lowered with acetic acid (0.2 M, pH 4.5). The 80/20 *v/v* ratio was determined as the limit where PBLG was still fully soluble.

Cysteamine was added in sufficient excess to ensure that only the solvent system could influence the thiazolidine formation. The conditions are summarized in table 5.1.

## Chapter 5: PVP and PBLG hybrid block copolymers

Table 5.1 Summary of the varying conditions tested for the thiazolidine formation.

Experiment	Solvent system	Reducing agent	Time (min)	Temperature (°C)	$\int_{\text{PVP-CHO}}$ (9.66 ppm)	
					before modification	after modification
<b>A</b>	<sup>a</sup> DMF/PBS	DTT	240	25	0.94	0.59
<b>B</b>	<sup>a</sup> DMF/PBS	TCEP	240	25	0.94	0.59
<b>C</b>	DMF	n/a	240	25	0.94	0.53
<b>D</b>	<sup>b</sup> PBS (0.2 M, 4.5)	n/a	240	25	0.94	0.51
<b>E</b>	<sup>a</sup> DMF/PBS	DTT	240	37	0.94	0.11
<b>F</b>	<sup>a</sup> DMF/PBS	n/a	240	37	0.94	0.13

<sup>a</sup>The pH of a solution of PBS (0.2 M, 7.4) was lowered to 4.5 via the addition of acetic acid and mixed with DMF in a 80/20 (DMF/PBS, V/V) ratio.

<sup>b</sup>The pH of a solution of PBS (0.2 M, 7.4) was lowered to 4.5 via the addition of acetic acid.

Experiments **A** and **B** indicated a negligible difference when comparing the extent of the thiazolidine formation in the presence of DTT or TCEP, respectively. This implies that the ligation of the aldehyde and cysteamine is independent of the type of reducing agent.

When PVP is dissolved in water the pH decreases to pH 4.5. Therefore, the formation of the thiazolidine structure in two different solvent systems was investigated, *i.e.* in DMF and in an aqueous system with pH 4.5. Experiments **C** and **D** do not show a significant difference either. The integrated aldehyde peaks indicated that the extent of the conversion to the thiazolidine end-group is similar for both experiments. This result supports the use of DMF for the conjugation reactions as it is an excellent solvent for both PVP and PBLG.

Lastly, experiments **E** and **F** showed the effect of temperature on the efficiency of the thiazolidine formation. The PVP aldehyde integral decreased when compared to experiments **A** to **D**, which were run at room temperature. Furthermore, no significant differences were noticed between experiments in absence and presence of DTT, respectively.

Unexpected side reactions are inevitable with the RAFT-mediated polymerization of NVP in the presence of functional xanthates. In addition, Pound *et al.*<sup>21</sup> have reported that the xanthate adjacent to an NVP unit was found to undergo elimination at moderate temperatures which resulted in unsaturated species. The conversion of the O-ethyl xanthate to the aldehyde end-group is quantitative, but a small fraction of unsaturated end-groups were still expected to be present due to initial synthesis conditions. It should however be mentioned that these side reactions can also happen during analysis. The side products were confirmed with MALDI-ToF-MS, which indicated a third type of end-group, structure (C) along with the expected aldehyde (B) and thiazolidine (A) moieties (Figure 5.3). Peak C was attributed to the elimination of the xanthate moiety which results in the formation of unsaturated chain ends. The peaks labeled with the asterisk are due to identical chain end-group structures, but the following repeat unit. Due to the lability of the xanthate moiety, the occurrence of unsaturated PVP chain-ends is common. This is most probably due to the polymerization conditions itself (even though the polymerizations were carried out in bulk at 60 °C).

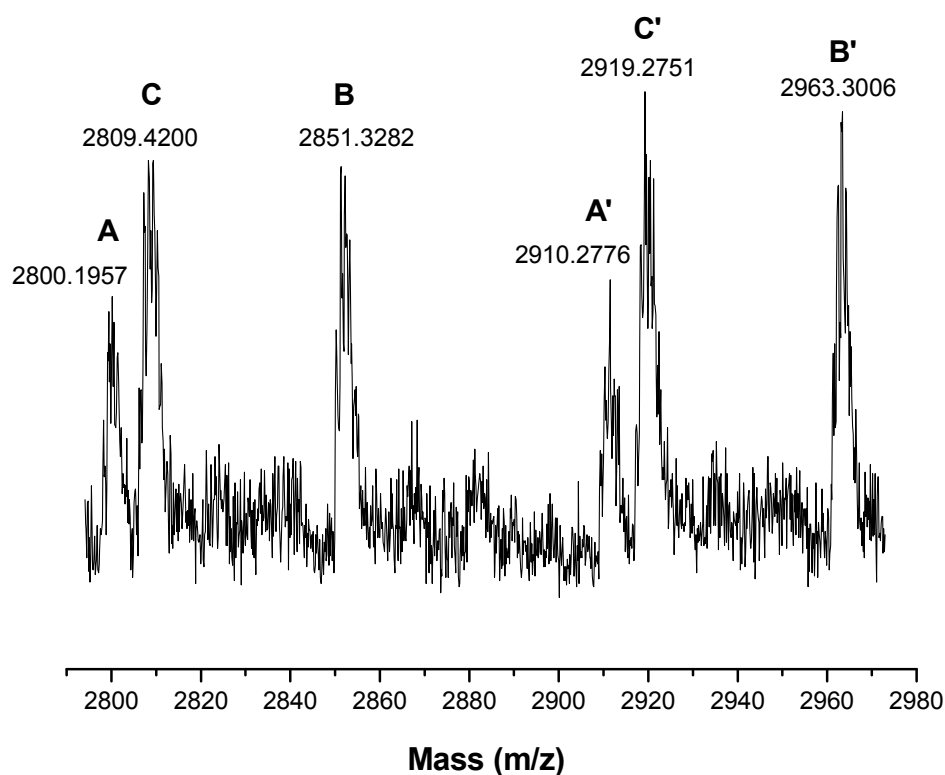


Figure 5.3 MALDI-ToF-MS spectrum of  $\omega$ -thiazolidine PVP prepared *via* the reaction of cysteamine with  $\omega$ -aldehyde PVP.

## Chapter 5: PVP and PBLG hybrid block copolymers

Peaks **A** and **B** were attributed to the thiazolidine and aldehyde end-functional PVP respectively. Both peaks were expected as the reaction to the thiazolidine end-group was not run to completion. The different end-group structures are shown in table 5.2. The mass for the most abundant peak is reported.

**Table 5.2** Structural assignments for the MALDI-ToF-MS spectrum of the thiazolidine end-functional chains in Figure 5.5.

Peak	Monoisotopic mass (+K <sup>+</sup> )		Structure	<sup>c</sup> n
	<sup>a</sup> Expt.	<sup>b</sup> Theo.		
A	2800.1957	2800.6277		22
B	2851.3282	2852.6768		23
C	2809.4200	2808.6505		22

a. Experimentally determined *m/z* ratio <sup>b</sup>. Theoretical *m/z* ratio, <sup>c</sup>. Degree of polymerization

The polymers were further characterized *via* SEC and *via* Ellman's test for the detection of free thiols to further verify that the ligation was achieved with thiazolidine chemistry. SEC showed no doubling of the product's molecular weight which would have indicated that disulfide formation had occurred. The presence of free thiol would have indicated that the thiazolidine structure did not form but rather the ring-opened structure.

Ellman's reagent<sup>19</sup> (5,5'-dithiobis (2-nitrobenzoic acid)) reacts with free thiols to produce a colored product which absorbs light of 412 nm thereby allowing for quantification using UV-Vis spectroscopy. The colour change is distinct, thereby producing a qualitative result almost instantaneously. No free thiols could be detected which along with the combined results of <sup>1</sup>H-NMR spectroscopy, MALDI-ToF-MS and SEC confirmed that the ligation was due to thiazolidine chemistry.

## **5.5 PVP-*b*-PBLG copolymer synthesis and characterization.**

### **5.5.1 Conjugation of $\omega$ -aldehyde PVP and PBLG cysteine.**

Conjugation reactions were primarily characterized with SEC to establish whether an increase in molar mass was evident. Furthermore, the presence of any starting compound and any broadening/bimodality could indicate the occurrence of side reactions.

### **5.5.2 Conjugation of $\omega$ -aldehyde PVP and P(BLG<sub>40</sub>-*b*-tBMLC<sub>3</sub>)**

#### **5.5.2.1 *In situ* deprotection and conjugation.**

The one-pot deprotection and conjugation reaction was attempted using the  $\omega$ -aldehyde PVP in molar ratios of 1:1, 2:1 and 4:1. It was found that even when using an excess of four aldehyde moieties to one cysteine residue, no quantitative conversion to the amphiphilic block copolymer was obtained (Figure 5.4). The PBLG block length was kept constant at 11 000 g/mol while the PVP block length was varied from 3000 to 7000 and 25 000 g/mol.

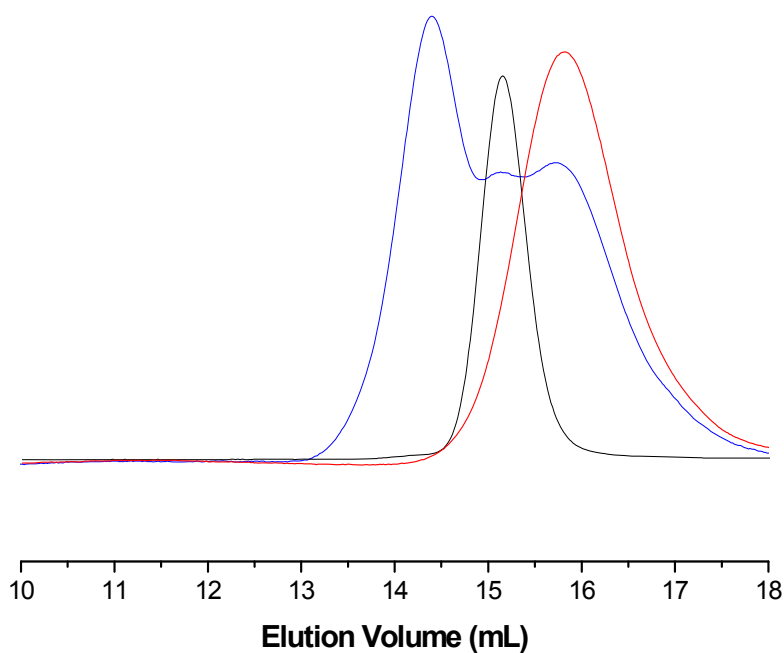


Figure 5.4 Comparison of SEC traces which include the PVP-*b*-PBG copolymer (blue) and the starting materials which include PBLG (black) and  $\omega$ -aldehyde PVP (red).

Purification of the copolymer was attempted *via* isolation of the PBLG starting material from the block copolymer using dialysis. It was expected that the PBLG would precipitate out of solution and could then subsequently be removed. Upon isolation of the dialyzed sample, analysis *via* SEC however showed an increase in the molar mass of the conjugate (Figure 5.5).

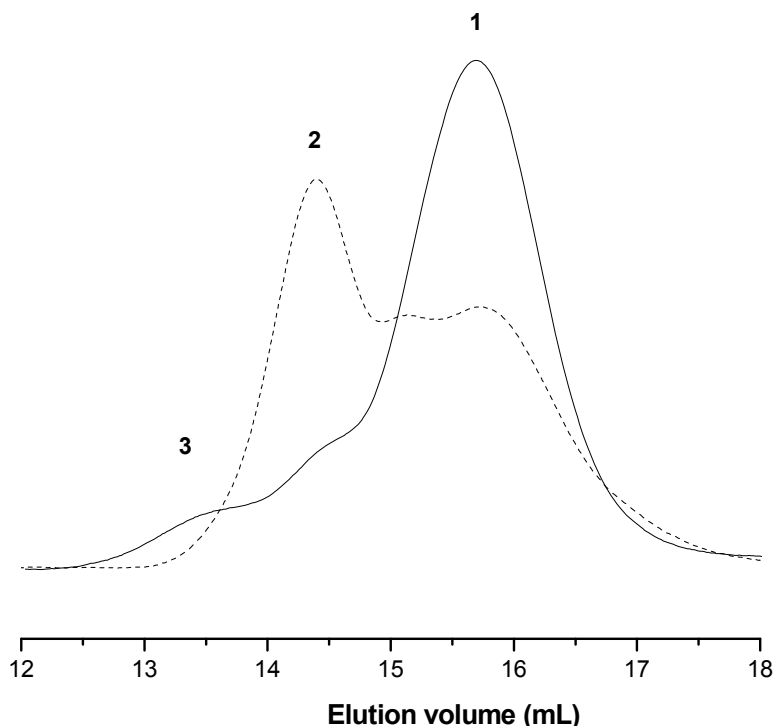


Figure 5.5 SEC trace of (PVP-*b*-Cys-*b*-PBLG) before (dashed line) and after dialysis (solid line). The structural assignments of the peaks are presented in Table 5.3.

The presence of the higher molar mass peaks present in the SEC traces after dialysis was expected to be due to disulfide formation. The free thiols present on the PBLG could undergo disulfide formation after dialysis as the low molar mass reducing agent, DTT, would be dialyzed out. Table 5.3 confirms that the increase in the molar mass of the conjugate correlates with coupling of the PBLG starting material.

Table 5.3 Identification of possible structures with SEC after dialysis of the *in situ* deprotection of PBLG-*b*-Cys and conjugation with  $\omega$ -aldehyde functional PVP.

	Dialysis:	$M_p$	Possible structure
Peak 1	Before	7000	PVP-CHO
	After	7200	PVP-CHO
Peak 2		17500	PVP- <i>b</i> -PBG
Peak 3		32200	PVP- <i>b</i> -(PBLG) <sub>2</sub>

Upon the addition of DTT the disulfide linkages were reduced and the diblock copolymer was formed. A procedure by Villain *et al.*<sup>22</sup> allowed for the cleavage of the

thiazolidine moiety with a hydroxylamine derivative. SEC confirmed that the addition of methoxylamine successfully cleaved the linkage to provide the individual blocks back (results not shown).

### 5.5.2.2 Conjugation reactions with deprotected P(BLG<sub>40</sub>-*b*-tBMLC<sub>3</sub>) (using the two-step approach)

The selective deprotection of P(BLG<sub>40</sub>-*b*-tBMLC<sub>3</sub>) was confirmed by <sup>1</sup>H-NMR spectroscopy. The disappearance of the *tert*-butylmercapto signal at 1.48 ppm indicated that the protecting group was effectively removed (> 95%).

P(BLG<sub>40</sub>-*b*-Cys) (**2**) was initially run on a 1:1 molar ratio with the  $\omega$ -aldehyde PVP in DMF (as solvent). DTT was added due to the presence of the free thiol functionalities on the repeat units and thus necessary to prevent disulfide formation.

The bimodality in Figure 5.6 below indicates that even after a 24 hour period it was not possible to quantitatively form the thiazolidine linkage. Peak **A** represents the PVP-CHO starting material ( $M_p$  10 600 g/mol) while the shoulder, **B**, represents the PVP-*b*-PBLG copolymer ( $M_p$  21 200 g/mol). The copolymer was analyzed with SEC after dialysis in the presence of TCEP to remove any low molar mass impurities and to isolate unreacted PBLG starting material by precipitation. The water-soluble TCEP inhibits any unreacted PBGL to form disulfide linkages with free thiols on the PBLG block of the copolymer.



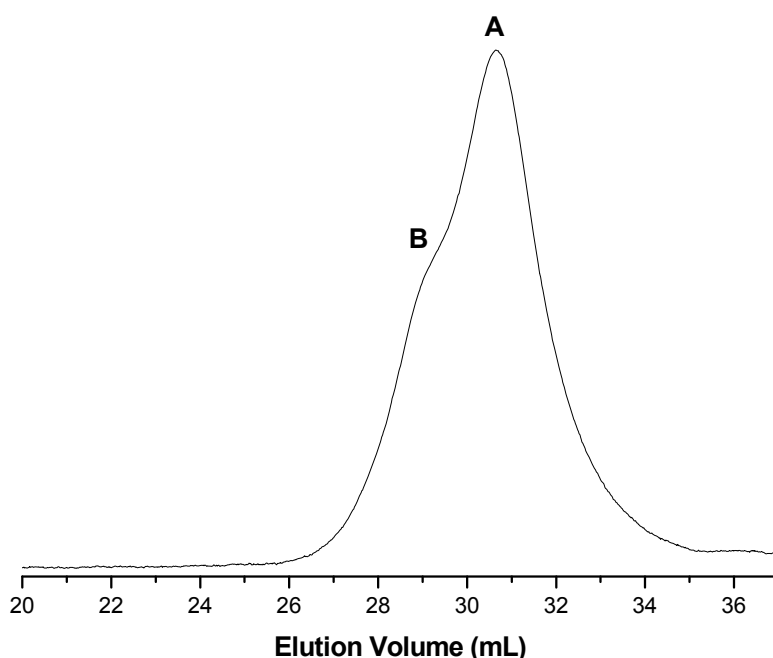


Figure 5.6 SEC trace indicating the bimodality of the conjugation reaction with PVP-CHO and the PBLG-*b*-Cys copolymer (2).

Purification using dialysis allowed for the removal of the homopolypeptide. The copolymer was isolated, redissolved in DMF and left under magnetic stirring. Micellization was induced *via* the slow addition of water, dialyzed against reverse-osmosis water and isolated *via* freeze-drying. SEC indicated no increase in the molar mass. The MW after purification (showed no increased in molar mass) indicated the unlikelihood that the core (which now contains 2 – 3 free thiols) would crosslink without some external oxidizable bridge.

### 5.5.3 Conjugation of $\omega$ -aldehyde PVP and PBLG-Cys (1)

The 1:1 molar reaction was repeated with PBLG 1 using the same conditions as described for PBLG 2. Figure 5.7 shows the SEC trace for the PVP starting material (B) as well as the amphiphilic block copolymer (A) formed during the conjugation reaction. Trace A is a monomodal peak indicating no starting material is present. The removal of high molar mass PVP is not possible when using SnakeSkin® pleated dialysis tubing with a MWCO of 7000 g/mol (dialysis generally only removes impurities with a MW 10 times lower than the MWCO). It could therefore be concluded that quantitative conjugation did take place for the  $\omega$ -aldehyde material, as all the starting material was consumed in the reaction.

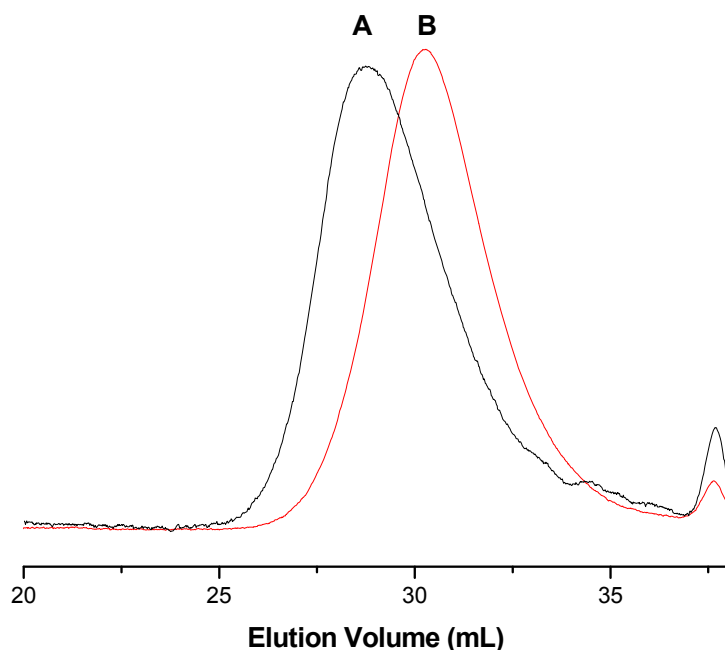


Figure 5.7 SEC trace of PVP<sub>90</sub>-*b*-PBLG<sub>54</sub> indicating quantitative conjugation of the PVP and PBLG chains.

A similar reaction was attempted using a dialdehyde functional PVP chain (Section 3.4.1.1.2). It was thought that the PBLG-*b*-PVP-*b*-PBLG triblock copolymer would be able to assume unique three-dimensional structures in solution. More specifically, that it would adopt a flower-like assembly in aqueous solution with the PBLG blocks in the core and PVP block as the shell (Figure 5.8).

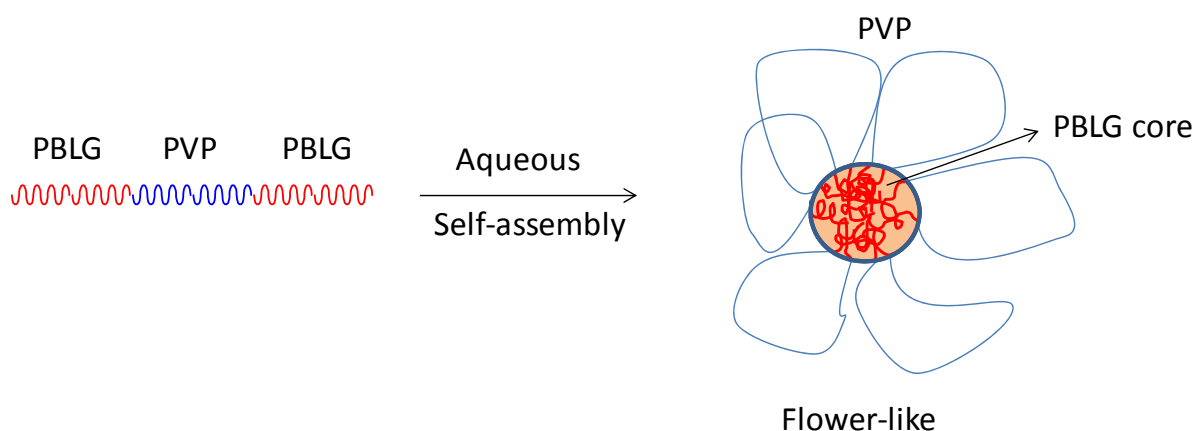


Figure 5.8 Schematic diagram depicting the self-assembly concept of PBLG-*b*-PVP-*b*-PBLG into a flower-like conformation.

## Chapter 5: PVP and PBLG hybrid block copolymers

The SEC trace indicated a broad bimodal distribution which indicated that the triblock copolymer was not solely formed (results not shown). The fraction fronting the main distribution represents the triblock copolymer (referred to as PBLG<sub>54</sub>-*b*-PVP<sub>62</sub>-*b*-PBLG<sub>54</sub>).

This combination of products illustrates the difficulty in obtaining quantitative conjugation using the modular approach. This is attributed to the low concentration of functional end-groups present in the reaction mixture. The conjugation further decreases upon the initial diblock formation as reactive chain-ends decrease along with reduced chain mobility. The characterization of the sample in aqueous solution should therefore be interesting as it is effectively a combination of PVP<sub>62</sub>-*b*-PBLG<sub>54</sub> and PBLG<sub>54</sub>-*b*-PVP<sub>62</sub>-*b*-PBLG<sub>54</sub>.

A comparative summary of the conjugation reactions using both PBLG **1** and PBLG **2** is described in table 5.4.

**Table 5.4** Summary of reaction conditions and results after the conjugation of PBLG (1) and PBLG (2) with  $\omega$ -aldehyde functional PVP.

PVP-CHO (g/mol)	$\bar{D}$	PBLG-Cys (g/mol)	<sup>a</sup> Structure	$\bar{D}$	PVP:PBLG	<sup>b</sup> Remarks
3300	1.23	8000	1	1.11	4:1	Excess PVP
5500	1.29	9200	*2	1.12	1:4	Excess PVP and PBLG
10 200	1.31	9200	2	1.12	1:1	Excess PVP and PBLG
8900	1.33	7800	1	1.12	1:1	Quantitative ( $\bar{D}$ = 1.37)
10 200	1.32	11 200	1	1.13	1:1	Quantitative ( $\bar{D}$ = 1.35)
10 200	1.32	14 300	1	1.13	1:1	Quantitative ( $\bar{D}$ = 1.39)
23 600	1.33	11 200	1	1.12	1:1	Excess PVP and PBLG
23 600	1.33	9200	2	1.12	1:1	Excess PVP and PBLG

<sup>a</sup>Structure 1 refers to PBLG-Cys and structure 2 refers to P(BLG<sub>40</sub>-*b*-Cys) (see Figure 5.2).

<sup>b</sup>Excess PVP and PBLG refers to unreacted homopolymer isolated after the conjugation reaction.

\*This was a *in situ* deprotection and conjugation reaction.

The conjugation reactions involving PBLG-*b*-Cys could not be obtained in quantitative yield. Even in a 4:1 excess of PVP-CHO, it was not possible to fully consume the PBLG block. This was evident in the SEC trace as well as from precipitation of PBLG during the dialysis step.

Conjugation reactions with certain combinations of  $\omega$ -aldehyde PVP and cysteine end-functional PBLG did result the full consumption of both the starting blocks. The

most successful combinations were those where the molecular weight blocks were below 15 000 g/mol, while the conjugation of PVP<sub>30</sub>-*b*-PBGL<sub>37</sub> is expected to be quantitative when run in a 1:1 fashion. The conjugation system which incorporated the 23 600 g/mol PVP block suffers from extremely low functional group concentrations, which increases the necessary reaction time.

### 5.5.3 Secondary structure identification

It is possible to characterize the secondary structure of the polypeptide *via* ATR-FTIR spectroscopy. The amide absorption of PBLG shifts depending on the conformational environment. For a polypeptide, the  $\alpha$ -helical conformation can be confirmed *via* the amide I band and the amide II band which are located near 1653 cm<sup>-1</sup> and 1548 cm<sup>-1</sup>, respectively.<sup>23,24</sup> ATR-FTIR spectroscopy was used to characterize the structural conformation of the PVP-*b*-PBLG copolymer after micellization. Figure 5.9 exhibits these bands, which verifies that PBLG is in a rigid  $\alpha$ -helical conformation in aqueous solution. The PBLG block behaves as a rigid segment and PVP-*b*-PBLG therefore behaves as a rod-coil block copolymer in water.

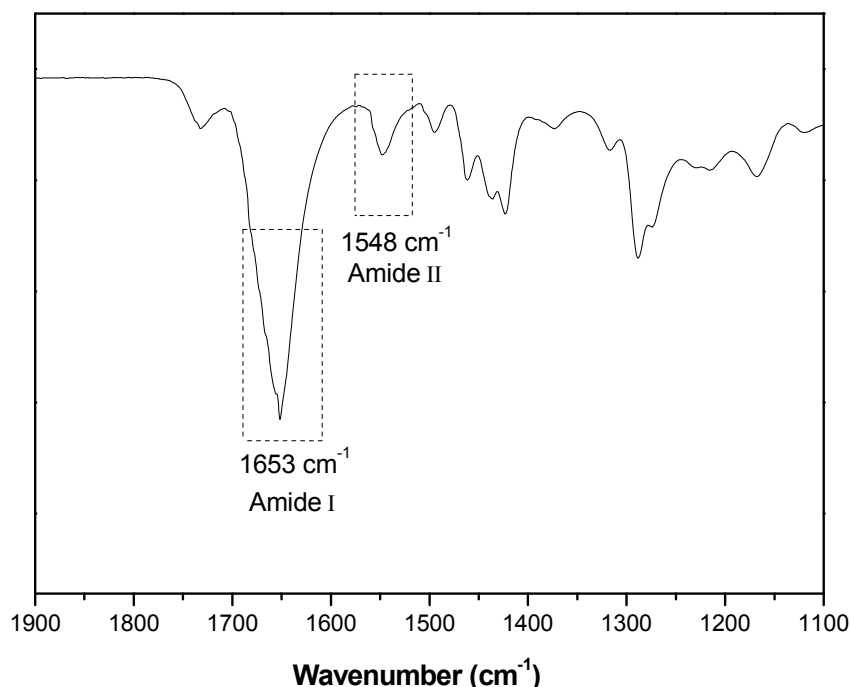


Figure 5.9 A typical ATR-FTIR spectrum for a PVP-*b*-PBLG copolymer is shown. The amide I band and amide II band is shown which is indicative of  $\alpha$ -helical conformation.

### 5.5.4 CMC of PVP-*b*-PBGL

The CMC was determined for PVP<sub>90</sub>-*b*-PBLG<sub>54</sub> via fluorescence spectroscopy with NR as probe. This copolymer was formed quantitatively *i.e.* no starting material was present to influence the CMC calculation. The CMC was determined by plotting the maximum emission wavelength against the negative Log function of the micelle concentration. This was determined *via* the intersection of the extrapolated curves below and above the CMC (Figure 5.10).

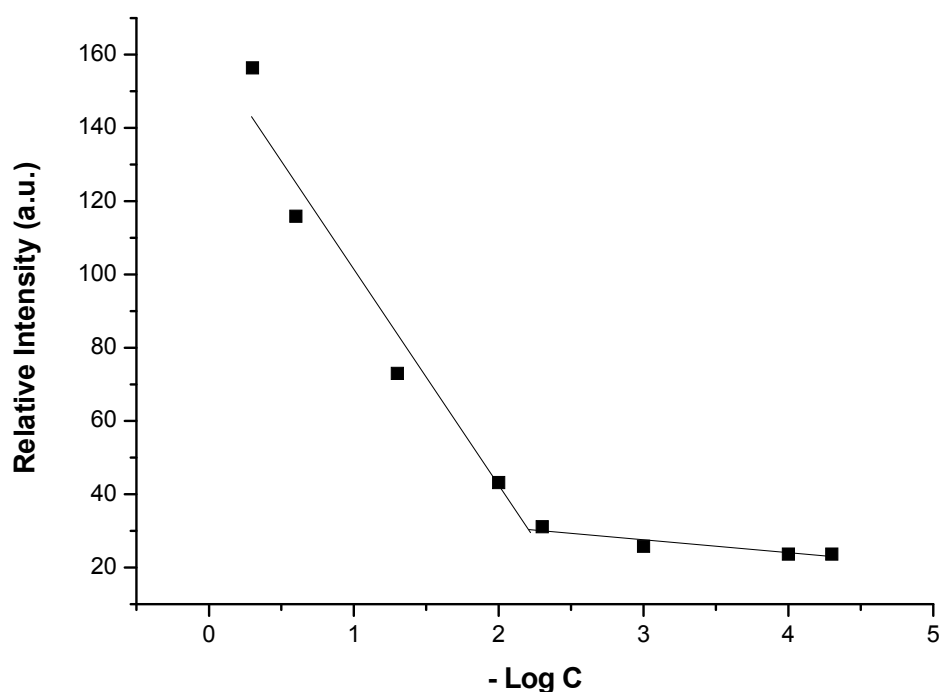


Figure 5.10 The CMC determination for PVP<sub>90</sub>-*b*-PBLG<sub>54</sub> using fluorescence spectroscopy with Nile Red as probe.

The CMC for PVP<sub>90</sub>-*b*-PBLG<sub>54</sub> was determined to be 6  $\mu\text{g}/\text{mL}$ . This compared well with CMCs determined for poly(ethylene glycol)-*b*-poly( $\gamma$ -benzyl-L-glutamate) block copolymers determined by Du *et al.*<sup>25</sup> which ranged from 1.37 – 2.14  $\mu\text{g}/\text{mL}$ .

### 5.5.5 Particle size and morphology determination with TEM and DLS

The PVP-*b*-PBLG block copolymers were initially dissolved in DMSO, a solvent that solubilizes both the hydrophilic and hydrophobic blocks. Water, a non-solvent for PBLG, was slowly introduced *via* dialysis to induce micellization. The resulting micelle solutions were analyzed by dynamic light scattering (DLS) and transmission electron microscopy (TEM) (Table 5.5).

The copolymers formed nanoparticles with a unimodal size distribution according to DLS, and the TEM images indicated that the nanoparticles were spherical in shape. The mean diameter of nanoparticles were in the range of 20 - 130 nm, depending on the PBLG block length of the copolymer as well as the PVP/PBLG molar ratio (Figure 5.11). The mean diameter of the nanoparticles did not significantly change over the course of a week when subjected to a pH of 7.2. This indicates that the micelles are stable in aqueous solution of pH 7.2.

## Chapter 5: PVP and PBLG hybrid block copolymers

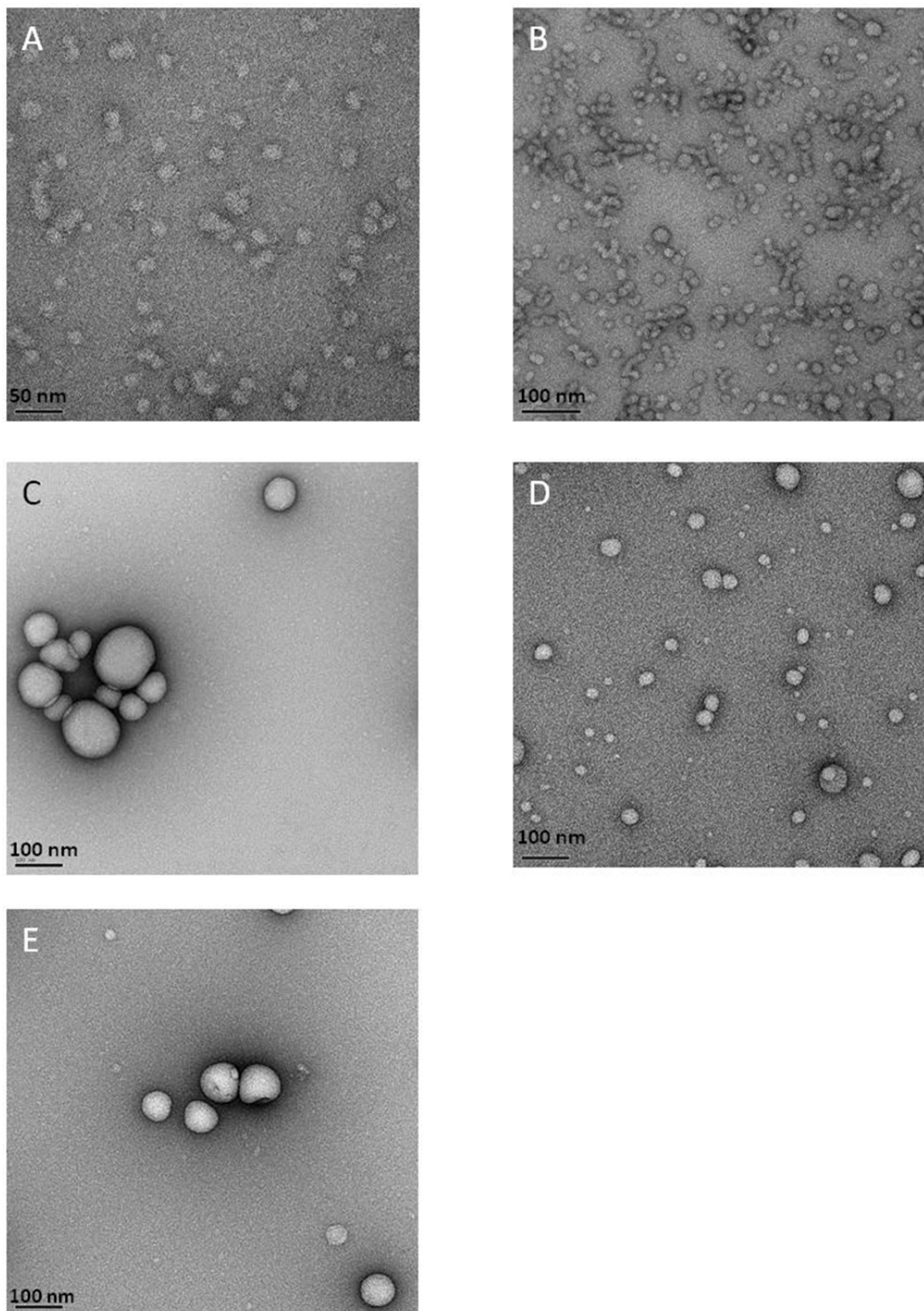


Figure 5.11 TEM images indicating particle sizes of PVP<sub>90</sub>-*b*-PBLG<sub>41</sub> (A), PVP<sub>90</sub>-*b*-PBLG<sub>54</sub> (B), PVP<sub>27</sub>-*b*-PBLG<sub>54</sub> (C), PVP<sub>225</sub>-*b*-PBLG<sub>54</sub> (D) and PBLG<sub>54</sub>-*b*-PVP<sub>62</sub>-*b*-PBLG<sub>54</sub> (E).



## Chapter 5: PVP and PBLG hybrid block copolymers

The TEM images (Figure 5.11) indicated a distribution of sizes for the nanoparticles in all cases except for PVP<sub>90</sub>-*b*-PBLG<sub>41</sub> (**A**) and PVP<sub>90</sub>-*b*-PBLG<sub>54</sub> (**B**) which were quite narrow. The latter, however, showed a combination of spherical particles and wormlike structures which appear as coalesced spherical particles. The particle sizes for both PVP<sub>90</sub>-*b*-PBLG<sub>41</sub> and PVP<sub>90</sub>-*b*-PBLG<sub>54</sub> were between 20 – 40 nm.

Generally, smaller particle diameters are observed with TEM (in comparison to DLS) as micelles are fully hydrated in solution during the DLS measurement but dried under TEM conditions. DLS measurements in the present study showed a larger particle size (compared to TEM) which could not solely be attributed to hydration effects. This was due to a large increase in the particle size as well as the dispersity which would seem to indicate aggregation of individual nanoparticles. The aggregation could result in discrepancies for the size determination by DLS.

Table 5.5 TEM and DLS results for the self-assembled PVP-*b*-PBLG copolymers.

Block copolymer	DLS			TEM
	Size <sub>Intensity</sub> (d.nm)	Size <sub>Number</sub> (d.nm)	<sup>a</sup> PDI	Diameter
	pH 7.2	pH 7.2		pH 7.2 (nm)
PVP <sub>90</sub> - <i>b</i> -PBLG <sub>41</sub>	123.1	51	0.25	24 - 40
PVP <sub>90</sub> - <i>b</i> -PBLG <sub>54</sub>	95.8	24.1	0.27	20 - 35
PVP <sub>27</sub> - <i>b</i> -PBLG <sub>54</sub>	193.9	101.7	0.09	35 - 100
PVP <sub>225</sub> - <i>b</i> -PBLG <sub>54</sub>	122.3	87.7	0.13	30 - 90
<sup>b</sup> PBLG <sub>54</sub> - <i>b</i> -PVP <sub>62</sub> - <i>b</i> -PBLG <sub>54</sub>	212.2	174.1	0.04	60 - 130

<sup>a</sup>The PDI values are based on the intensity distribution determined with DLS.

<sup>b</sup>The triblock copolymer sample is a combination of PBLG<sub>54</sub>-*b*-PVP<sub>62</sub>-*b*-PBLG<sub>54</sub> and PVP<sub>62</sub>-*b*-PBLG<sub>54</sub>.

For three of the copolymers, the PBLG block length was kept constant and the hydrophilic PVP block was varied. Two factors seemed to affect the particle size. The PVP<sub>27</sub>-*b*-PBLG<sub>54</sub> copolymer has a large diameter due to less stabilization from the hydrophilic block and thus a larger aggregation number ( $N_{agg}$ ) was required. PVP<sub>225</sub>-*b*-PBLG<sub>54</sub> is better stabilized by the hydrophilic block, but has a significantly larger outer shell due to a ten-fold increase in the DP of PVP.

The combination of PBLG<sub>54</sub>-*b*-PVP<sub>62</sub>-*b*-PBLG<sub>54</sub> and PVP<sub>62</sub>-*b*-PBLG<sub>54</sub> resulted in larger nanoparticles when compared to diblocks such as PVP<sub>27</sub>-*b*-PBLG<sub>54</sub> and PVP<sub>90</sub>-*b*-PBLG<sub>54</sub> (which is comparable to PVP<sub>62</sub>-*b*-PBLG<sub>54</sub>). This was expected to be due to the increased outer hydrophobic segments which needed to be stabilized by the middle block.



## Chapter 5: PVP and PBLG hybrid block copolymers

It was expected that the triblock would have a larger core as well as a larger  $N_{agg}$  when compared to diblock copolymers of similar hydrophilic/hydrophobic block length ratios. The increased particle size however does not have a trivial explanation as a single ABA chain is not limited to a particular structure and thus the outer PBLG blocks can be in different micellar cores. This is however outside the scope of this study.<sup>26</sup>

### 5.5.6 Effect of pH on particle size

The pH dependence on the particle size was investigated for PVP<sub>27</sub>-*b*-PBLG<sub>54</sub> and PBLG<sub>54</sub>-*b*-PVP<sub>62</sub>-*b*-PBLG<sub>54</sub> due to their narrow particle size distributions obtained from DLS. The micelles were dialyzed against a sodium acetate buffer system, pH 5.4 for 48 hours and 168 hours. The diameters were measured with DLS (Table 5.6, Figure 5.12 – 5.13) after 48 hours and TEM (Figure 5.14 and Figure 5.15) after 7 days.

Table 5.6 reports the number distribution of the particle sizes after the initial 48 hour period in the pH 5.4 buffer system. The diameters are representative of what is observed in the TEM results as the size of individual particles determine the distribution size. It was evident that the increased acidic environment affected the particle size of both PVP<sub>27</sub>-*b*-PBLG<sub>54</sub> and PBLG<sub>54</sub>-*b*-PVP<sub>62</sub>-*b*-PBLG<sub>54</sub>. Relevant also is the increase in the number of larger particle after only 48 hours in the acidic environment (see Table 5.6).

**Table 5.6** DLS (Number distribution) and TEM results for the self-assembled PVP-*b*-PBLG copolymers after being subjected to aqueous conditions of pH 5.4 and pH 7.2 for 48 hours.

Block copolymer	DLS						TEM	
	<sup>a</sup> Z-average (d.nm)		<sup>a</sup> SizeNumber (d.nm)		<sup>a</sup> PDI		<sup>b</sup> Diameter	
	pH 7.2	pH 5.4	pH 7.2	pH 5.4	pH 7.2	pH 5.4	pH 7.2 (nm)	pH 5.4 (nm)
PVP <sub>27</sub> - <i>b</i> -PBLG <sub>54</sub>	168	346.6	101.7	276.9	0.091	0.278	30 – 65	250 - 550
<sup>c</sup> PBLG <sub>54</sub> - <i>b</i> -PVP <sub>62</sub> - <i>b</i> -PBLG <sub>54</sub>	201.9	273.8	174.1	243.3	0.036	0.097	60 – 130	700 - 1200

<sup>a</sup>The particle size and particle size distribution were determined *via* DLS after 48 hours.

<sup>b</sup>The particle size was determined *via* TEM after 7 days.

<sup>c</sup>The triblock copolymer sample is a combination of PBLG<sub>54</sub>-*b*-PVP<sub>62</sub>-*b*-PBLG<sub>54</sub> and PVP<sub>62</sub>-*b*-PBLG<sub>54</sub>.

## Chapter 5: PVP and PBLG hybrid block copolymers

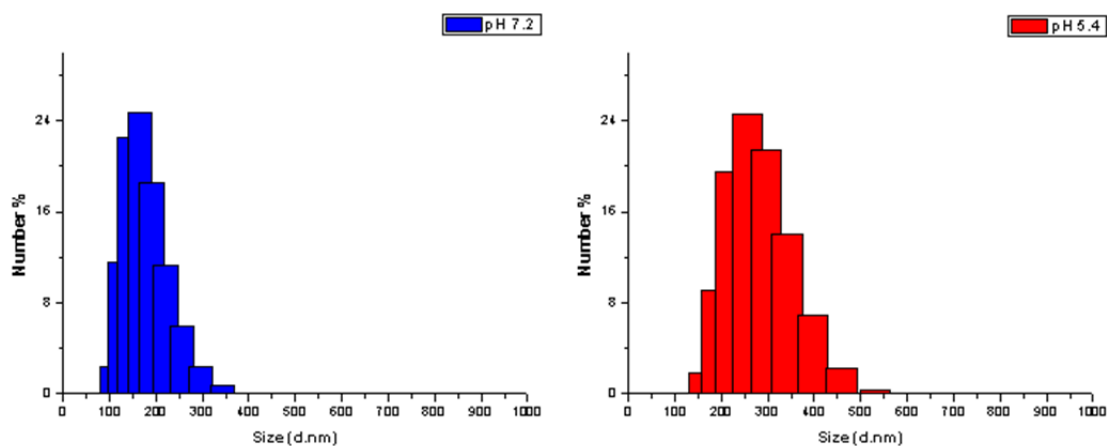


Figure 5.12 Particle size distribution by number for PVP<sub>27</sub>-*b*-PBLG<sub>54</sub> as determined by DLS. The micelles were subjected to a buffer system of pH 7.2 and pH 5.4 for 48 hours.

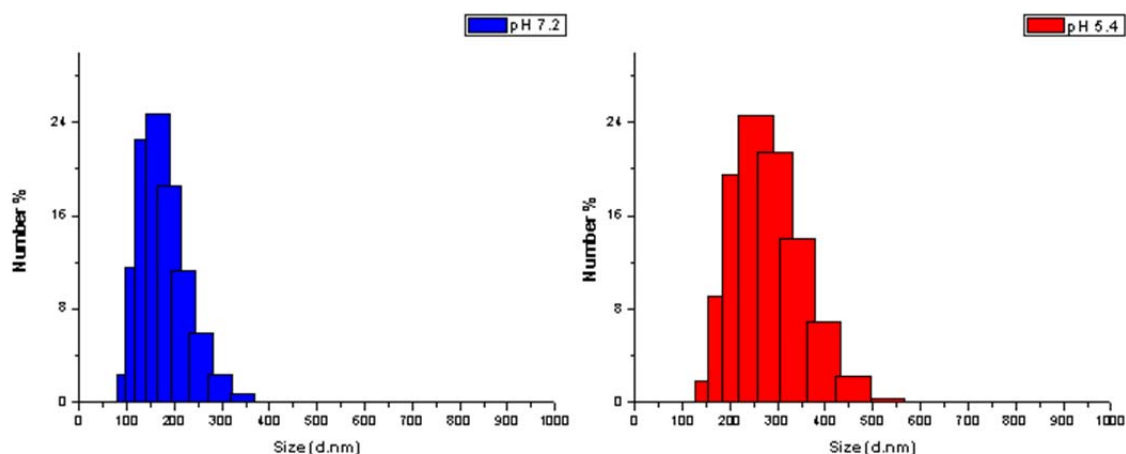


Figure 5.13 Particle size distribution by number for PBLG<sub>54</sub>-*b*-PVP<sub>62</sub>-*b*-PBLG<sub>54</sub> as determined by DLS. The micelles were subjected to a buffer system of pH 7.2 and pH 5.4 for 48 hours.

After the initial DLS results, the micelles were left under magnetic stirring for a week at pH 5.4. This was done to investigate the increase in particle size with time as well as to verify with TEM that the initial increase was not due to the aggregation of individual nanoparticles.

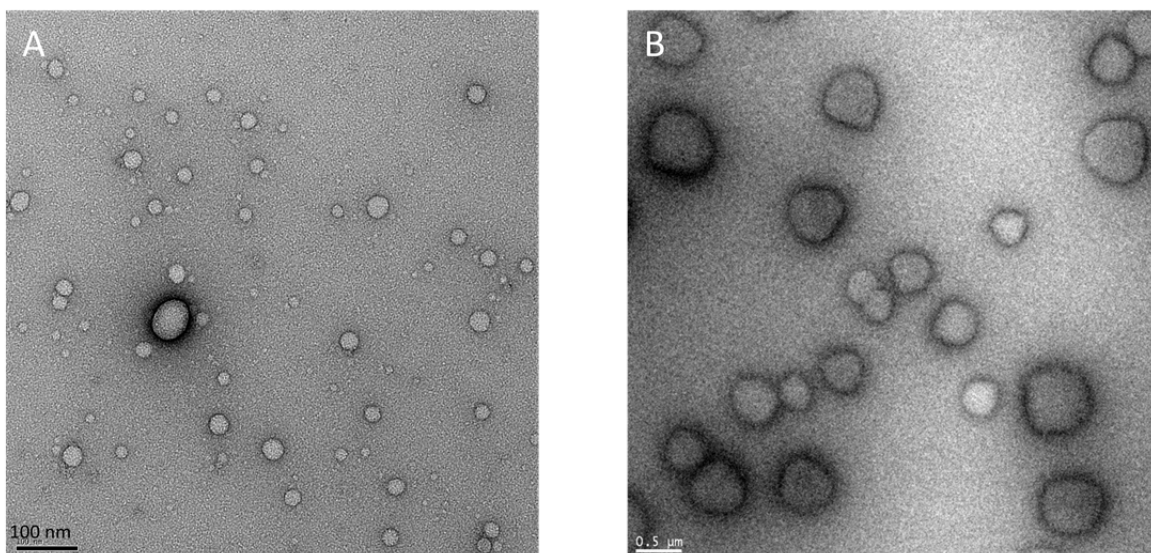


Figure 5.14 TEM images of PVP<sub>27</sub>-*b*-PBLG<sub>59</sub> before (A) and after (B) being subjected to a sodium acetate buffer system (pH 5.4) for 7 days.

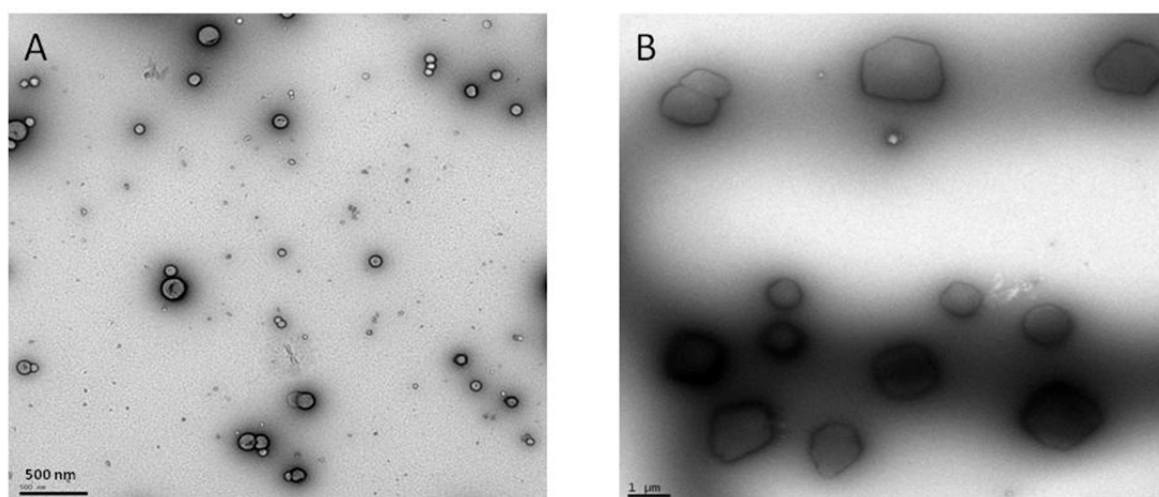


Figure 5.15 TEM images of PBLG<sub>59</sub>-*b*-PVP<sub>101</sub>-*b*-PBLG<sub>59</sub> before (A) and after (B) subjected subjected to a sodium acetate buffer system (pH 5.4) for 7 days.

The increase in the micellar size is quite significant after 7 days of exposure to the acidic environment. Both samples indicate a 10-fold increase in diameter during this time with no apparent aggregation of smaller individual particles. The increase in the size of the nanoparticles was suspected to be due to the acidic hydrolysis of the labile ester linkages. The nanoparticles were analyzed with ATR-FTIR spectroscopy to determine whether hydrolysis had indeed taken place (Figure 5.16).

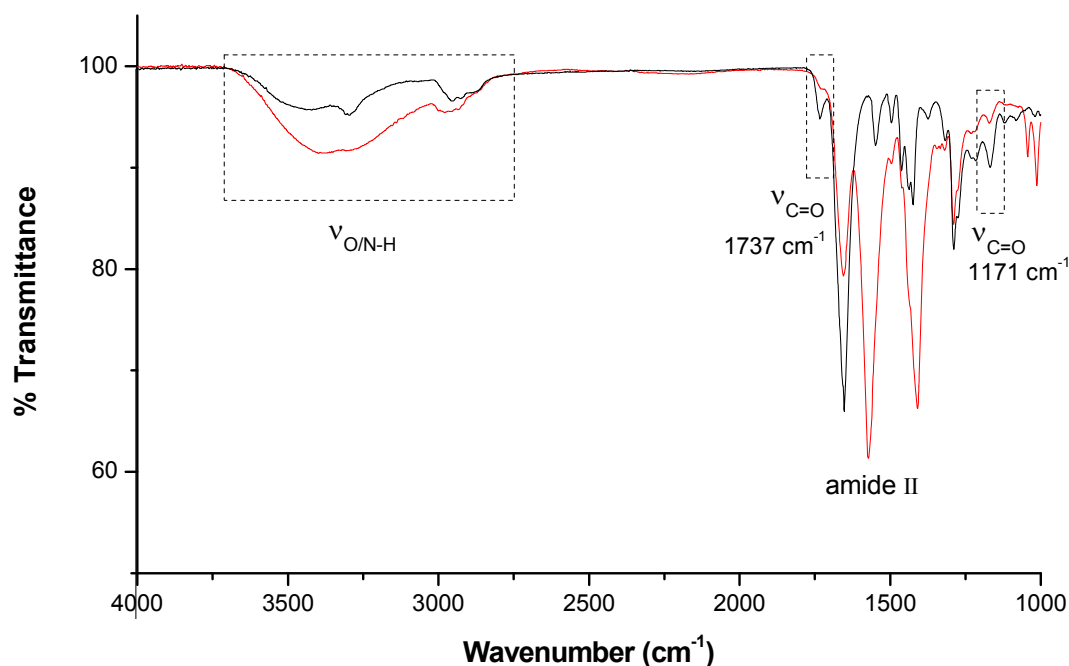
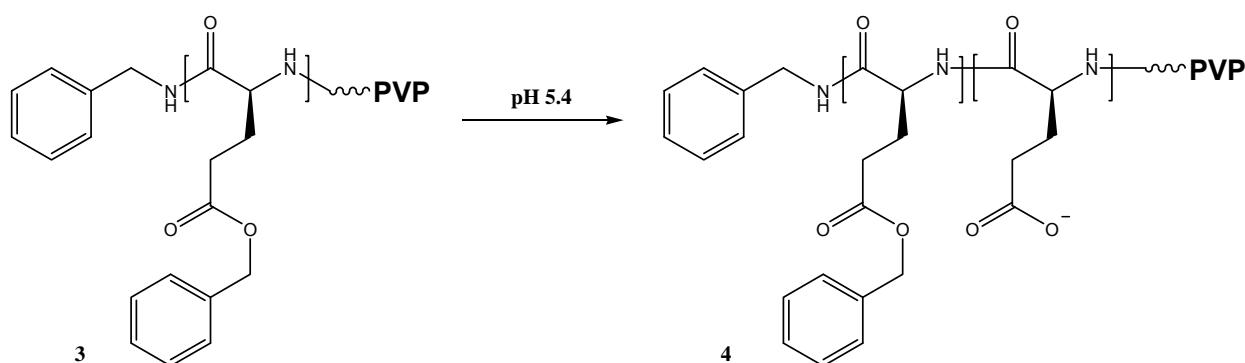


Figure 5.16 ATR FT-IR spectrum comparing PVP-*b*-PBLG before (black) and after (red) exposure to pH 5.4 environment for 7 days.

The ATR FT-IR spectra confirmed that hydrolysis had taken place by the reduction of the ester carbonyl stretches at  $1737\text{ cm}^{-1}$  and  $1171\text{ cm}^{-1}$ . Furthermore, a shift in the amide II band (indicative of  $\alpha$ -helical conformation) indicated a change in the conformational structure of the polypeptide block. This could be the result of cleaving the benzyl ester linkages and thus decreasing the hydrophobicity. The result of this is a random copolypeptide consisting of  $\gamma$ -glutamic acid and  $\gamma$ -benzyl glutamate repeat units (Scheme 5.4).



Scheme 5.4 Hydrolysis of the labile benzyl ester groups resulting in a random copolypeptide comprising of  $\gamma$ -glutamic acid and  $\gamma$ -benzyl glutamate repeat units.

## Chapter 5: PVP and PBLG hybrid block copolymers

The  $^1\text{H-NMR}$  spectra in Figure 5.17 further illustrate the extent of the benzyl ester hydrolysis. Peaks **A** and **B** represent the aromatic benzyl protons and the benzylic methylene protons on the PBLG backbone, respectively. Peaks **C** represent the backbone protons of the PVP repeat unit (peaks **F** and **G** in Figure 3.2). The bottom spectrum represents the PVP-*b*-PBLG copolymer after being hydrolyzed in a sodium acetate buffer system of pH 5.4 for 48 hours.

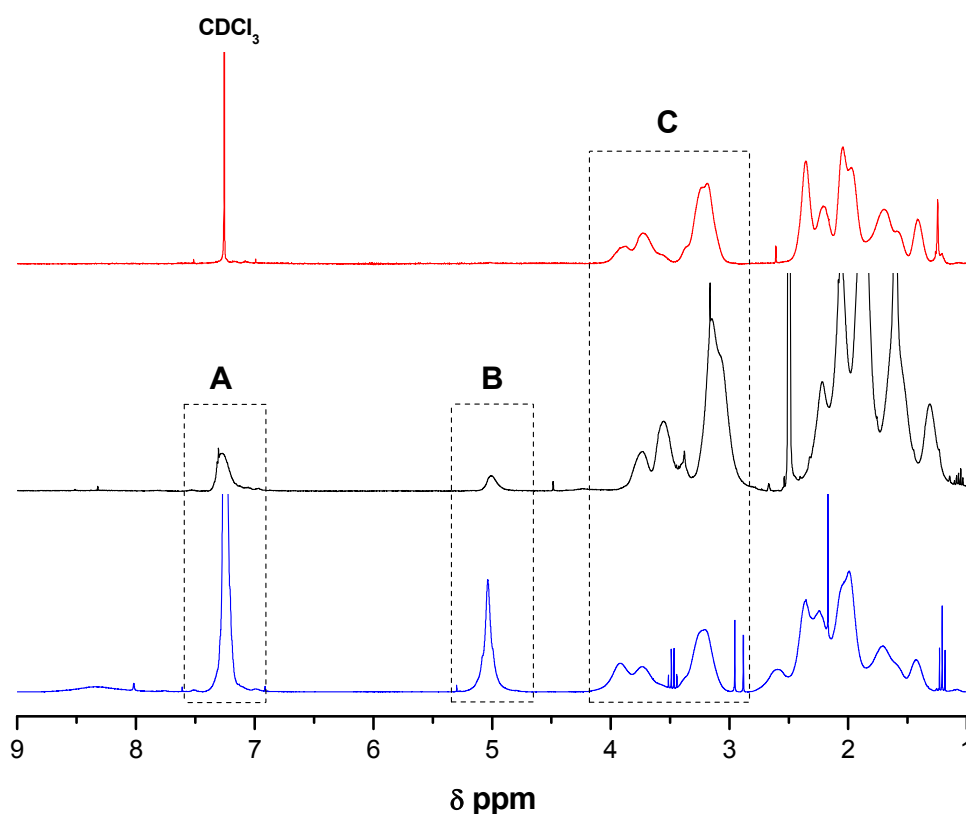


Figure 5.17  $^1\text{H-NMR}$  spectra comparing PVP-*b*-PBLG in  $\text{CDCl}_3$  before (bottom) and after (top) hydrolysis of the benzyl ester groups. The middle  $^1\text{H-NMR}$  spectrum is the copolymer after hydrolysis in  $\text{DMSO-d}_6$ .

The disappearance of peaks **A** and **B** in the top spectrum as well as the significant decrease in the middle spectrum is a clear indication of the hydrolysis of the benzyl ester groups.

The top and middle spectra are identical samples, but in different solvents. It is interesting to note the complete disappearance of the benzylic protons in  $\text{CDCl}_3$ . This is most likely due to phase separation in the system, causing the hydrolyzed copolymer to self-assemble in  $\text{CDCl}_3$ . The driving force for the self-assembly is most likely due to polar interaction of the deprotonated glutamic acid in  $\text{CDCl}_3$ .<sup>27</sup> The self-

assembly of the copolymer inhibits the mobility of the remaining benzylic protons in the hydrophobic core and suppresses the signals.

It is known that the  $pK_a$  value for poly( $\gamma$ -glutamic acid) is 2.9.<sup>28</sup> Thus, as mentioned before, at pH 5.4 the hydrolyzed PBLG is fully ionized, acting like a charged coil in solution. Aggregation still occurs, but due to the electrostatic repulsion, the hydrophobic core itself is swollen. The increase in the hydrophilicity of the hydrophobic core could lead to an increased aggregation number as more unimers are needed to effectively stabilize the micelle. The combination of the electrostatic interactions along with the decreased hydrophobicity would lead to the formation of these large structures seen in figures 5.14 **B** and 5.15 **B**. The large increase in diameter as well as the particles morphology leads us to conclude that the hydrolysis reaction leads to the transformation of micellar nanoparticles to vesicular structures.

The increase in the particle size due to the pH variation is interesting for future pH-regulated drug release research. The possibility of engineering pH responsive micelles which dissociate in acidic conditions holds a lot of promise. This is due to the pH variations found in the human body. Blood has a pH of 7.4, which is contrary to the pH value in tumorous tissue. The extracellular pH value in tumorous tissues is determined to be around 6.5 – 7.0 while the intracellular environment (endosome, lysosomes) is typically more acidic (pH 5.0 – 6.0). Thus, ideally a drug delivery vehicle should be able to retain the drug at pH 7.4 and quickly release it at a lower pH.<sup>9</sup>

### **5.5.7 Cell viability**

For biomedical purposes, especially *in vivo* applications like DDS, toxicity is a critical factor which ultimately determines their *viability*. It is thus critical to ensure that these polymeric modifiers do not cause any adverse effects.

The toxicity is indicated through cell death, which causes either a rupture in the cell membrane (necrotic cell death) or the condensation of the nucleus (apoptotic cell death). Both, apoptotic and necrotic cell death provide detailed information regarding cell *viability* and potential cytotoxic effects.

The block copolymer toxicity was tested at two concentrations, 0.5 mg/mL and 0.9 mg/mL. Both of which are high concentrations for micelles, seeing as the CMC was determined as 6  $\mu$ g/mL.



## Chapter 5: PVP and PBLG hybrid block copolymers

Exposure to certain cytotoxic agents can compromise the cell membrane which would lead to the uptake of the membrane-impermeable fluorochrome, propidium iodide, which shows as a bright red nucleus. As a positive control, the cells were treated with a known membrane permeabilizer (1:1 methanol/acetone reagent). This served as a positive control for cell death identification where all the nuclei are stained red (Figure 5.18 **A**). In figure 5.19 **A** however, this was not evident which indicated that the cell membranes were still intact.

The membrane-permeable fluorochrome, Hoechst 33342, is able to permeate both healthy and dead cells. It serves as an indication for nuclear condensation and appears as bright blue spots and fragments. Neither is seen in the presence of the PVP-*b*-PBLG micelles (Figure 5.18 and Figure 5.19, **B**).

Images **C** and **D** in figures 5.18 and 5.19 are an overlay of images **A** and **B** where nuclei stained pink indicate cell death. Images **C** and **D** only differ in that the background of image **D** allows for the identification of individual heart cells. The absence of these pink stains in figure 5.19 **D** indicates that no apparent cell death was visible. Thus, the *in vitro* test demonstrates good cell compatibility of the block copolymer micelles, even at high concentrations (0.9 mg/mL).

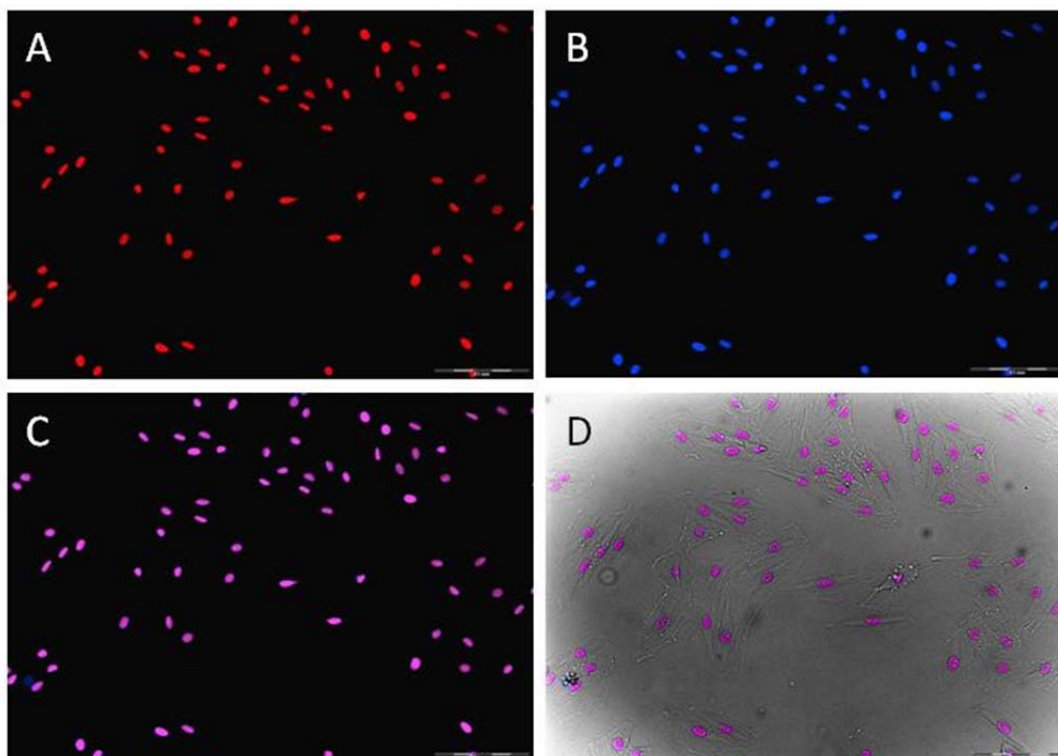


Figure 5.18 Copolymer cytotoxicity test results for a known membrane permeabilizer to indicate positive cell death.

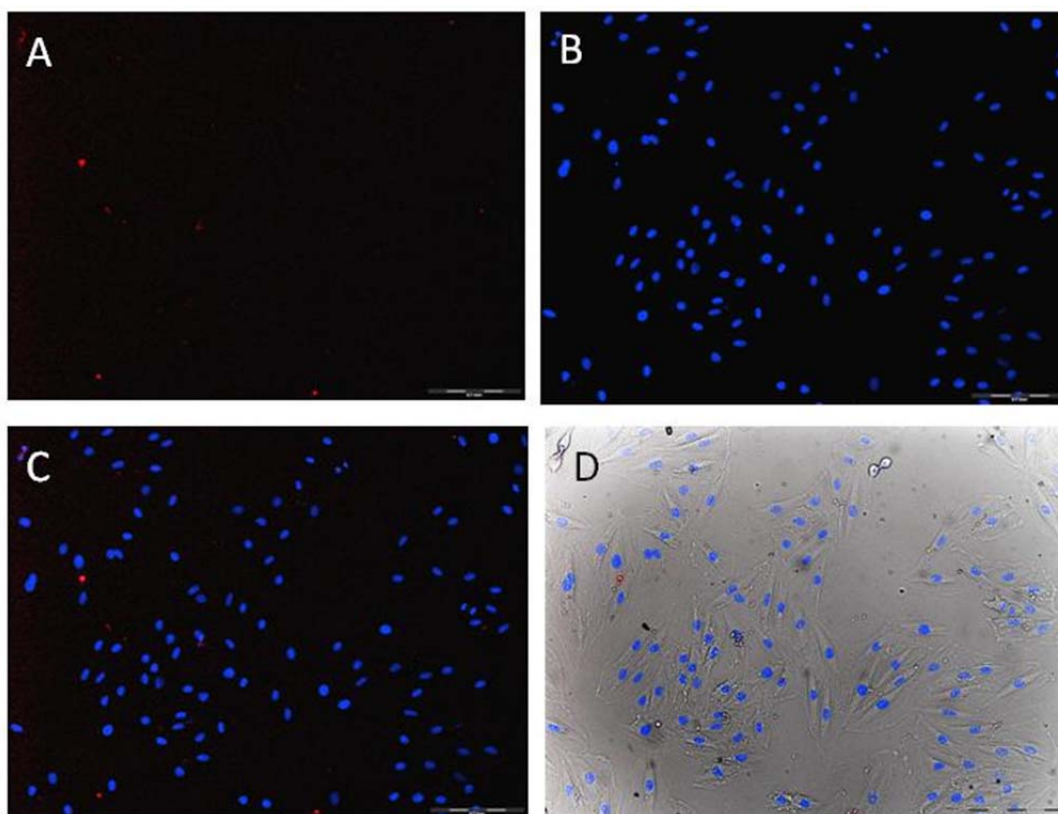


Figure 5.19 Copolymer cytotoxicity test results for PVP<sub>90</sub>-*b*-PBLG<sub>54</sub> at a concentration of 0.9 mg/mL.

### 5.5.8 Pyrene loading of micelles

Preliminary studies have been done to investigate the *viability* of using the PVP-*b*-PBLG as drug delivery vehicles. It is known that hydrophobic drugs can be physically encapsulated inside the hydrophobic core of amphiphilic block copolymers. This is the first step in assessing a possible DDS; subsequent investigation then includes drug loading, drug retention and drug release characteristics to better evaluate the system's drug delivering potential.

The preliminary studies indicated that the micelles could successfully be loaded with hydrophobic compounds, pyrene (results no shown). However, further research in this direction is necessary to explore the scope and limitations of the PVP-*b*-PBLG copolymers as DDS.



## 5.6 Conclusions

Through variation of the conditions for the ligation reaction, a solvent system was determined in which conjugation reactions could take place. The water-miscible solvent DMF compared well with the aqueous system at pH 4.5 to the extent that it was preferred. Furthermore, the presence of a reducing agent (DTT or TCEP) showed no notion of inhibiting the thiazolidine formation.

The thiazolidine linkage could not be identified by any one traditional characterization method, but was instead confirmed *via* a sequence of techniques in a deductive manner.

*In situ* deprotection and conjugation of P(BLG<sub>40</sub>-*b*-tBMLC<sub>3</sub>) and  $\omega$ -aldehyde PVP resulted in very low conjugation efficiency. Independent deprotection and then conjugation of the PBLG copolymer and PVP resulted in an increased conjugation efficiency, but still not quantitative. The cysteine end-functional PBLG (**2**) resulted in quantitative conjugation with PVP for systems where each of the two blocks were below 15 000 g/mol.

Furthermore, the amphiphilic block copolymer and its inherent self-assembling properties were investigated. The CMC for PVP<sub>90</sub>-*b*-PBLG<sub>54</sub> was determined to be 6  $\mu$ g/mL. This was found to be comparable to a PEG-*b*-PBLG system as determined by Du *et al.*<sup>25</sup>

The nanoparticles were analyzed with TEM and DLS which revealed that particle aggregation did occur in some instances. The particle sizes ranged from 25 nm to 120 nm depending on the polymer block lengths as well as hydrophobic/hydrophilic block length ratios.

Furthermore, when the micelles were subjected to an increased acidic environment, the labile benzyl ester bonds were hydrolyzed which subsequently decreased the hydrophobicity. This was observed with TEM where the particle sizes increased 10-fold to form vesicular structures. Hydrolysis was further confirmed with ATR-FTIR and <sup>1</sup>H-NMR spectroscopy. Cytotoxicity tests confirmed that the copolymer micelles had excellent cell compatibility even at high concentrations such as 0.9 mg/mL.

Preliminary work was done on the drug loading capability of the micelles. It was found that pyrene could successfully be encapsulated as a hydrophobic model drug

compound. This, along with the hydrolysis at pH 5.4 verified the potential as a responsive DDS.

## 5.7 References

- (1) Duncan, R. *Nat. Rev. Drug Discovery* **2003**, *2*, 347.
- (2) Dhal, P. K.; Holmes-Farley, S. R.; Mandeville, W. H.; Neenan, T. X. *Polymeric Drugs*; John Wiley & Sons, Inc., 2002.
- (3) Pasut, G.; Veronese, F. M. *Prog. Polym. Sci.* **2007**, *32*, 933-961.
- (4) Heredia, K. L.; Maynard, H. D. *Org. Biomol. Chem.* **2007**, *5*, 45-53.
- (5) Nicolas, J.; Mantovani, G.; Haddleton, D. M. *Macromol. Rapid Commun.* **2007**, *28*, 1083-1111.
- (6) Croy, S. R.; Kwon, G. S. *Curr. Pharm. Des.* **2006**, *12*, 4669-4684.
- (7) Pasut, G.; Sergi, M.; Veronese, F. M. *Adv. Drug Delivery Rev.* **2008**, *60*, 69-78.
- (8) Yi, J.; Zhou, X.; Hu, G.; Wang, B. *Polymer Science Series B*, *52*, 35-40.
- (9) Lin, J.; Zhu, J.; Chen, T.; Lin, S.; Cai, C.; Zhang, L.; Zhuang, Y.; Wang, X.-S. *Biomaterials* **2009**, *30*, 108-117.
- (10) Tang, D.; Lin, J.; Lin, S.; Zhang, S.; Chen, T.; Tian, X. *Macromol. Rapid Commun.* **2004**, *25*, 1241-1246.
- (11) Chow, D.; Nunalee, M. L.; Lim, D. W.; Simnick, A. J.; Chilkoti, A. *Mater. Sci. Eng., R* **2008**, *62*, 125-155.
- (12) Habraken, G. J. M.; Peeters, M.; Dietz, C. H. J. T.; Koning, C. E.; Heise, A. *Polymer Chemistry* **2010**, *1*, 514-524.
- (13) Carlson, J. S.; Hill, M. R.; Young, T.; Costanzo, P. J. *Polymer Chemistry*, *1*, 1423-1426.
- (14) Shao, J.; Tam, J. P. *J. Am. Chem. Soc.* **1995**, *117*, 3893-3899.
- (15) Wathier, M.; Johnson, C. S.; Kim, T.; Grinstaff, M. W. *Bioconjugate Chem.* **2006**, *17*, 873-876.
- (16) Saiz, C.; Wipf, P.; Manta, E.; Mahler, G. *Org. Lett.* **2009**, *11*, 3170-3173.

## Chapter 5: PVP and PBLG hybrid block copolymers

- (17) Habraken, G. J. M.; Koning, C. E.; Heuts, J. P. A.; Heise, A. *Chem. Commun. (Cambridge, U. K.)* **2009**, 3612-3614.
- (18) Bi, X.; Hartono, D.; Yang, K.-L. *Langmuir* **2008**, *24*, 5238-5240.
- (19) Ellman, G. L. *Arch. Biochem. Biophys.* **1959**, *82*, 70-77.
- (20) Li, Y.-J.; Rothwarf, D. M.; Scheraga, H. A. *J. Am. Chem. Soc.* **1998**, *120*, 2668-2669.
- (21) Pound, G.; Eksteen, Z.; Pfukwa, R.; McKenzie, J. M.; Lange, R. F. M.; Klumperman, B. *J. Polym. Sci., Part A: Polym. Chem.* **2008**, *46*, 6575-6593.
- (22) Villain, M.; Vizzavona, J.; Rose, K. *Chemistry & Biology* **2001**, *8*, 673-679.
- (23) Segura-Sánchez, F.; Montembault, V. r.; Fontaine, L.; Martínez-Barbosa, M. E.; Bouchemal, K.; Ponchel, G. *Int. J. Pharm.*, *387*, 244-252.
- (24) Barbosa, M. E. M.; Montembault, V.; Cammas-Marion, S.; Ponchel, G.; Fontaine, L. *Polym. Int.* **2007**, *56*, 317-324.
- (25) Du, Z.; Pan, S.; Yu, Q.; Li, Y.; Wen, Y.; Zhang, W.; Feng, M.; Wu, C. *Colloids Surf. A* **2009**, *353*, 140-148.
- (26) Kong, W.; Li, B.; Jin, Q.; Ding, D.; Shi, A.-C. *Langmuir* **2009**, *26*, 4226-4232.
- (27) Rodríguez-Hernández, J.; Lecommandoux, S. *J. Am. Chem. Soc.* **2005**, *127*, 2026-2027.
- (28) Lin, Y.-H.; Chung, C.-K.; Chen, C.-T.; Liang, H.-F.; Chen, S.-C.; Sung, H.-W. *Biomacromolecules* **2005**, *6*, 1104-1112.

## Epilogue

### 6.1 Introduction

The goal of this study was to synthesize hybrid amphiphilic block copolymers from poly(*N*-vinylpyrrolidone) (PVP) and poly( $\gamma$ -benzyl-L-glutamate) (PBLG) using thiazolidine chemistry. Furthermore, the assembly properties along with the cytotoxicity of the conjugates were to be investigated.

In Chapter three, an optimized method on work previously done in our group was introduced for the preparation of  $\omega$ -aldehyde end-functional PVP via facile post-polymerization modification reactions.<sup>1</sup> PVP was synthesized by the RAFT-mediated polymerization of NVP using two different xanthate CTAs. The two polymers synthesized had different end-functionalities which included a fluorescent tag at the alpha chain-end and xanthate functionality at the omega chain-end (via CTA X21) as well as two xanthate functionalities at the alpha and omega chain-end respectively (via CTA X16). Chain-end functionality ratios were determined with <sup>1</sup>H-NMR spectroscopy and confirmed that only a small fraction of the labile xanthate moiety was not present for PVP<sub>X21</sub>. The reactivity of the *N*-vinylpyrrolidone repeat unit allows for a unique modification of the end-functional xanthate moiety. The optimized conditions entailed hydrolysis at a pH of 1 and subsequent thermolysis, which resulted in quantitative conversion of the xanthate moiety to an aldehyde functionality. Hydrolysis at an elevated temperature shows promise to decrease the initial hydrolysis reaction time, but possible side reactions need to be investigated. This modification reaction allowed for the synthesis of telechelic aldehyde-functional PVP as well as  $\omega$ -aldehyde functional PVP with a fluorescent tag on the  $\alpha$ -chain-end.

In Chapter four, the hydrophobic polypeptide, poly( $\gamma$ -benzyl-L-glutamate) was synthesized via the ring-opening polymerization of *N*-carboxyanhydrides. The conditions used promoted polymerization via the normal amine mechanism to produce well-defined and narrowly distributed polypeptides.<sup>2</sup> These conditions allow for decreased cyclization of the terminal  $\gamma$ -benzyl glutamate repeat unit, which results in chain termination. The primary amine is also necessary for post-polymerization conjugation reactions and was subsequently end-capped with a protected cysteine end-functionality, Fmoc-L-Cys(Acm)-OPfp. MALDI-ToF-MS and <sup>1</sup>H-NMR spectroscopy confirmed the successful attachment of the activated ester as well as the deprotection of the Fmoc group to produce the primary amine. The deprotection

## Chapter 6: Conclusions and Outlook

of the AcM group to produce the free thiol was initially a major setback. A modified procedure using excess TFA under oxidizing conditions effectively removed the AcM group. The hydrolysis of the labile benzyl ester group was inhibited by creating a competitive system where ester exchange reactions effectively inhibited the hydrolysis.<sup>3</sup>

In Chapter five, the work done in the previous two chapters were brought together. This entailed the conjugation of the hydrophilic PVP and the hydrophobic PBLG via a thiazolidine linkage to produce a hybrid amphiphilic block copolymer. Initial work was done to find conditions that favoured the formation of the thiazolidine linkage, these conditions were then applied during the subsequent conjugation reactions. A PBLG-*b*-Cys copolymer and cysteine end-functional PBLG were conjugated to PVP and compared to each other. *In situ* deprotection and conjugation of the copolymer and PVP resulted in very low conjugation efficiency. Independent deprotection and then conjugation of the copolymer and PVP resulted in an increased conjugation efficiency, but still not quantitative as purification steps revealed unreacted PBLG even with excess PVP present. The cysteine end-functional PBLG resulted in near quantitative conjugation with PVP.

Furthermore, the amphiphilic block copolymer and its inherent self-assembling properties were investigated. The CMC was determined for PVP<sub>90</sub>-*b*-PBLG<sub>54</sub> and found that it was comparable to the value for PEG-*b*-PBLG as determined by Du *et al.*<sup>4</sup> The nanoparticles were analyzed with TEM and DLS which revealed that particle aggregation did occur in some instances. The particle sizes ranged from 25 nm to 120 nm depending on the polymer block lengths as well as hydrophobic/hydrophilic block length ratios. It was found that when the micelles were subjected to an increased acidic environment, the labile benzyl ester bonds were hydrolyzed, which led to a decrease in the hydrophobicity of the PBLG block. This was observed with TEM where the particle sizes increased 10-fold to form vesicular structures. Hydrolysis was further confirmed with ATR-FTIR and <sup>1</sup>H-NMR spectroscopy. Cytotoxicity tests confirmed that the copolymer micelles had excellent cell compatibility even at high concentrations such as 0.9 mg/mL.

Preliminary work was done on the drug loading capability of the micelles. It was found that pyrene could successfully be encapsulated as a hydrophobic model drug compound. This, along with the hydrolysis at pH 5.4 verified the potential as a responsive DDS.

## 6.2 Outlook

The PVP-*b*-PBLG self-assembling system showed that it has potential as a DDS. The conjugation reactions need to be stream-lined to reproducibly obtain near quantitative results. This will allow for more conclusive results regarding the relationship of the PVP and PBLG chain lengths on CMCs, particle sizes and particle size distributions. Furthermore, investigation is necessary in regards to drug loading, drug retention and drug release to better evaluate this system's drug delivering potential.

The modified polymers need to be further analyzed with liquid chromatographic techniques to provide more quantitative data to complement the structural information provided by NMR, MALDI-ToF-MS and TEM. This is necessary for both the end-group modification and conjugation reactions.

## 6.3 References

- (1) Pound, G.; McKenzie, J. M.; Lange, R. F. M.; Klumperman, B. *Chem. Commun. (Cambridge, U. K.)* **2008**, 3193-3195.
- (2) Habraken, G. J. M.; Wilsens, K. H. R. M.; Koning, C. E.; Heise, A. *Polymer Chemistry*, **2**, 1322-1330.
- (3) Guo, J.; Huang, Y.; Jing, X.; Chen, X. *Polymer* **2009**, *50*, 2847-2855.
- (4) Du, Z.; Pan, S.; Yu, Q.; Li, Y.; Wen, Y.; Zhang, W.; Feng, M.; Wu, C. *Colloids Surf. A* **2009**, *353*, 140-148.